Athens Journal of Sciences

Quarterly Academic Periodical, Volume 13, Issue 1
Published by the Athens Institute
URL: https://www.athensjournals.gr/ajs Email: journals@atiner.gr
e-ISSN: 2241-8466 DOI: 10.30958/ajs

March 2026

Athens Journal of Sciences

Quarterly Academic Periodical, Volume 13, Issue 1, March 2026
Published by the Athens Institute
URL: https://www.athensjournals.gr/ajs Email: journals@atiner.gr
e-ISSN: 2241-8466 DOI: 10.30958/ajs

Front Pages

Athens Journal of Sciences

Published by the Athens Institute

Athens Institute is an Athens-based World Association of Academics and Researchers based in Athens. Athens Institute is an independent and non-profit Association with a Mission to become a forum where Academics and Researchers from all over the world can meet in Athens, exchange ideas on their research and discuss future developments in their disciplines, as well as engage with professionals from other fields. Athens was chosen because of its long history of academic gatherings, which go back thousands of years to Plato's Academy and Aristotle's Lyceum. Both these historic places are within walking distance from Athens Institute's downtown offices. Since antiquity, Athens was an open city. In the words of Pericles, Athens"…is open to the world, we never expel a foreigner from learning or seeing". ("Pericles' Funeral Oration", in Thucydides, The History of the Peloponnesian War). It is Athens Institute's mission to revive the glory of Ancient Athens by inviting the World Academic Community to the city, to learn from each other in an environment of freedom and respect for other people's opinions and beliefs. After all, the free expression of one's opinion formed the basis for the development of democracy, and Athens was its cradle. As it turned out, the Golden Age of Athens was in fact, the Golden Age of the Western Civilization. Education and (Re)searching for the 'truth' are the pillars of any free (democratic) society. This is the reason why Education and Research are the two core words in Athens Institute's name.

The Athens Journal of Sciences (AJS) is an Open Access quarterly double-blind peer reviewed journal and considers papers from all areas of Natural & Formal Sciences, including papers on agriculture, computer science, environmental science, materials science, transportation science, chemistry, physics, mathematics and statistics, biology, geography, and earth science (geology, oceanography, astronomy, meteorology). Many of the papers published in this journal have been presented at the various conferences sponsored by the Natural & Formal Sciences Division of the Athens Institute. All papers are subject to Athens Institute's Publication Ethical Policy and Statement.

Athens Journal of Sciences
ISSN NUMBER: 2241-8466 - DOI: 10.30958/ajs
Volume 13, Issue 1, March 2026
Download the entire issue (PDF)

Athens Journal of Sciences
Editorial and Reviewers' Board

President's Message

All Athens Institute's publications including its e-journals are open access without any costs (submission, processing, publishing, open access paid by authors, open access paid by readers etc.) and is independent of presentations at any of the many small events (conferences, symposiums, forums, colloquiums, courses, roundtable discussions) organized by Athens Institute throughout the year and entail significant costs of participating. The intellectual property rights of the submitting papers remain with the author. Before you submit, please make sure your paper meets the basic academic standards, which includes proper English. Some articles will be selected from the numerous papers that have been presented at the various annual international academic conferences organized by the different divisions and units of the Athens Institute for Education and Research. The plethora of papers presented every year will enable the editorial board of each journal to select the best, and in so doing produce a top-quality academic journal. In addition to papers presented, Athens Institute will encourage the independent submission of papers to be evaluated for publication.

The current issue is the first of the thirteenth volume of the *Athens Journal of Sciences (AJS)*, published by Natural & Formal Sciences Division of Athens Institute.

Gregory T. Papanikos
President
Athens Institute

14th Annual International Conference on Chemistry
20-24 July 2026, Athens, Greece

The Natural Sciences Unit of Athens Institute, will hold its **14th Annual International Conference on Chemistry, 20-24 July 2026, Athens, Greece** sponsored by the Athens Journal of Sciences. The aim of the conference is to bring together academics and researchers of all areas of chemistry and other related disciplines. You may participate as stream organizer, presenter of one paper, chair a session or observer. Please submit a proposal using the form available (https://www.atiner.gr/2026/FORM-CHE.doc).

Academic Members Responsible for the Conference

- **Dr. Haiduke Sarafian**, Head, Natural Sciences Unit, ATINER & Professor of Physics and Endowed Chair of John T. and Paige S. Smith Professor of Science, Pennsylvania State University, USA.

Important Dates

- Abstract Submission: **31 March 2026**
- Acceptance of Abstract: 4 Weeks after Submission
- Submission of Paper: **22 June 2026**

Social and Educational Program

The Social Program Emphasizes the Educational Aspect of the Academic Meetings of Athens Institute.

- Greek Night Entertainment (This is the official dinner of the conference)
- Athens Sightseeing: Old and New-An Educational Urban Walk
- Social Dinner
- Mycenae Visit
- Exploration of the Aegean Islands
- Delphi Visit

Conference Fees

Conference fees vary from 400€ to 2000€
Details can be found at: https://www.atiner.gr/fees

14th Annual International Conference on Physics
20-24 July 2026, Athens, Greece

The Natural Sciences Unit of Athens Institute, will hold its **14th Annual International Conference on Physics, 20-24 July 2026, Athens, Greece** sponsored by the Athens Journal of Sciences. The aim of the conference is to bring together academics and researchers of all areas of physics and other related disciplines. Please submit a proposal using the form available (https://www.atiner.gr/2026/FORM-PHY.doc).

Important Dates

- Abstract Submission: **31 March 2026**
- Acceptance of Abstract: 4 Weeks after Submission
- Submission of Paper: **22 June 2026**

Academic Member Responsible for the Conference

- **Dr. Haiduke Sarafian**, Head, Natural Sciences Unit, ATINER & Professor of Physics and Endowed Chair of John T. and Paige S. Smith Professor of Science, Pennsylvania State University, USA.

Social and Educational Program

The Social Program Emphasizes the Educational Aspect of the Academic Meetings of Athens Institute.

- Greek Night Entertainment (This is the official dinner of the conference)
- Athens Sightseeing: Old and New-An Educational Urban Walk
- Social Dinner
- Mycenae Visit
- Exploration of the Aegean Islands
- Delphi Visit
- Ancient Corinth and Cape Sounion

More information can be found here: https://www.atiner.gr/social-program

Conference Fees

Conference fees vary from 400€ to 2000€
Details can be found at: https://www.atiner.gr/fees

Athens Journal of Sciences - Volume 13, Issue 1, March 2026 – Pages 9-24

Two-Dimensional Hydrodynamic Simulations in Urban Water Systems

*By Marcell Knolmar**

In the studies presented here, we demonstrate the latest simulation capabilities of two-dimensional (2D) free-surface flow modeling through specific case studies. In hydrodynamic investigations, it is often necessary to use coupled one-dimensional (1D) and two-dimensional (2D) modeling. For the unsteady 1D–2D tasks at hand, we employed the widely accepted HEC-RAS (Hydrologic Engineering Center's River Analysis System) and HEC-HMS (Hydrologic Modeling System) simulation software. In one case study, a one-kilometer urban reach of a stream flowing through the outskirts of a major city was analyzed in connection with plans to improve water quality in recreationally impounded lakes. The hydrodynamic assessment of the planned lake conditions was carried out using 2D modeling. The spatial resolution of the model enabled the identification of potential sediment deposition zones and the verification of the proper operation of the weir and outlet structures. In another case, we analyzed surface runoff generated by precipitation falling on the site of a planned solar power plant located within a small riverside town. The results helped assess the need for and potential design of a stormwater drainage system. The spatial resolution of the 2D model allowed for an accurate determination of both the quantity and extent of surface runoff accumulation.

Keywords: *HEC-HMS, HEC-RAS, hydrodynamic, runoff, distributed model*

Introduction

In the study of urban stormwater management, one-dimensional (1D) hydraulic models are often sufficient. The assessment of sewer network capacity is fundamentally a 1D task. Surface flooding occurs when the stormwater network cannot accommodate the runoff generated within contributing sub-catchments connected to inlet manholes. Such overflows can also develop at downstream points in the network where the channel capacity is lower than the incoming discharge. Insufficient capacity may result from a combination of factors such as slope, conduit cross-section size, sediment deposition, and pipe roughness. Additionally, due to backwater effects, surface flooding may occur even upstream of the actual capacity restriction.

While 1D models can be used to calculate the volume of inundation, determining the spatial extent of flooding is inherently a two-dimensional (2D) problem. This is because even shallow water depths can result in widespread overland flow across urban surfaces.

In smaller watercourses, flow dynamics can often be modeled adequately using 1D techniques. However, when cross-sectional complexity or significant lateral flow expansion exists — such as in shallow impoundments or floodplains

*Assistant Professor, Budapest University of Technology and Economics, Hungary.

— a 1D model may no longer be sufficient. In such cases, a 2D model becomes necessary to simulate the flow conditions accurately. These hydrodynamic processes are typically unsteady and temporally variable, with discharges potentially fluctuating by orders of magnitude during flood events.

High-flow events may coincide with peak discharges in both receiving watercourses and urban runoff systems. In such scenarios, the performance of gravity-based stormwater systems or combined sewer overflows (CSOs) becomes critical. Backwater effects can lead to upstream flooding and surface ponding. To simulate these conditions accurately, coupled 1D–2D modeling is required, which integrates detailed channel flow with surface flow dynamics.

In urban settings, the spatial resolution of sub-catchment delineation generally aligns with the location of inlets in the sewer network. For stormwater runoff modeling, more detailed delineation is typically unnecessary, as average hydrologic responses within each sub-catchment provide adequate representation. However, in larger or undeveloped catchments, the spatial resolution of a lumped 1D hydrologic-hydraulic model may be insufficient to yield accurate spatial results. In such cases, 2D modeling enables the identification of runoff and ponding zones, as well as the estimation of water accumulation volume and depth.

In the first case study, we conducted a 2D hydrodynamic analysis along a 1-kilometer urban section of the Hosszúréti Stream, which flows through the southern districts of Budapest. This section includes artificially impounded recreational lakes, such as Kána Lake. As part of plans to improve water quality, we examined flow conditions under low, medium, and high streamflow scenarios. The spatial resolution of the 2D model allowed for the evaluation of sediment transport, deposition zones, and the performance of weir and outlet structures.

The second case study focused on surface runoff generated by rainfall over a proposed solar park site within a riverside town (Tiszaújváros). Due to local topography, fluvial flooding was not a concern. The objective of the analysis was to provide foundational calculations for the design of a stormwater drainage system. The 2D runoff model was constructed with sufficient spatial resolution to accurately determine the volume, depth, and extent of accumulated surface runoff.

Urban hydrology faces increasing challenges due to the intensification of rainfall events, rapid urbanization, and the growing complexity of drainage systems. Traditional one-dimensional (1D) modeling approaches often fall short in representing the spatial variability of urban runoff, especially in complex topographies and densely built environments. The aim of this paper is to explore modern two-dimensional (2D) hydrodynamic modeling techniques and demonstrate their applicability to solving key urban runoff problems. Through case studies, the paper presents practical examples of how state-of-the-art 2D tools can be applied in real-world scenarios, illustrating the current capabilities, methods, and solution approaches available to practitioners and researchers. The scope includes simulations of both urban creek overflow and stormwater runoff on a solar park site, showcasing the versatility and limitations of 2D methods. The central research question addressed is: How effectively can current 2D hydrodynamic models capture and represent urban stormwater processes? This paper is structured as follows: after this introductory section, Section 2 details the case study areas and the modeling setup. Section 3 discusses the simulation results and

evaluates model performance. Section 4 offers conclusions drawn from the findings and suggests future research directions.

The modeling of open-channel and surface water flows has long been a central concern in hydraulic and hydrological engineering. Traditional one-dimensional (1D) models have proven effective in simulating flows within confined channels where lateral flow variations are negligible (Chow 1959). However, with the increasing complexity of urban landscapes and the growing need for detailed flood risk assessments (Perera 2024), two-dimensional (2D) modeling has gained prominence due to its ability to capture lateral flow dynamics, especially in floodplains, surface runoff zones, and shallow impoundments (Hunter et al. 2007, Horritt & Bates 2002).

The integration of 1D and 2D modeling approaches has become standard practice in simulating urban water systems. In combined 1D–2D frameworks, 1D models represent in-channel flows, while 2D models are used to simulate out-of-bank flows or surface runoff, providing a more holistic view of hydrodynamic behavior under unsteady, gradually varied flow conditions (Fread 1992, Lin 2006). This hybrid approach is particularly important in urban flood modeling, where infrastructure such as culverts, weirs, and detention basins interacts with terrain-driven surface processes.

HEC-RAS and HEC-HMS, developed by the U.S. Army Corps of Engineers, are widely used in both research and practical applications for hydrodynamic and hydrological modeling, respectively. HEC-RAS has evolved to support 2D unsteady flow modeling using a finite volume solution of the shallow water equations, enabling detailed simulation of floodplain dynamics and urban drainage systems (Brunner 2024). Likewise, HEC-HMS supports the simulation of precipitation-runoff processes and can be integrated with HEC-RAS for comprehensive watershed analysis (USACE 2024). The synergy of these tools allows for detailed spatial and temporal analysis of flow patterns, flood extents, and runoff accumulation, which are essential in modern urban water infrastructure planning.

Several studies have successfully applied these tools in urban settings. For instance, Madhuri et al. (2021) demonstrated the advantages of 2D modeling in assessing flood hazards in highly urbanized areas with complex topographies. Similarly, Thakur et al. (2017) used coupled HEC-HMS/HEC-RAS simulations to evaluate drainage system performance under extreme rainfall events. These case studies underscore the increasing demand for high-resolution hydrodynamic modeling in response to climate change, urbanization, and infrastructure development.

Recent studies have focused on enhancing the accuracy and stability of coupled 1D–2D models. For instance, Xiang et al. (2024) developed a two-dimensional hydrodynamic urban flood model based on equivalent drainage of manholes, providing a more accurate representation of urban flood dynamics. This model accounts for the complex interactions between surface runoff and subsurface drainage systems, which are critical in densely populated urban areas. Ata et al. (2023) utilized HEC-HMS and HEC-RAS for flood hazard mapping at the Junjung River catchment, demonstrating the effectiveness of integrating hydrological and hydraulic models in flood risk assessment. Their approach highlighted the importance of combining different modeling tools to capture the multifaceted nature of urban flooding. Miremad et al. (2025) applied also HEC-RAS and HEC-HMS for Sustainable Urban

Drainage Systems such as green roofs and permeable pavement comparing the results with previous situation.

In the context of water quality and sediment transport, 2D models also provide valuable insights into spatial patterns of deposition and scouring, particularly in shallow, slow-moving zones (Wu 2007). Accurate prediction of such dynamics (Mohammad et al. 2016, Raji et al. 2024) is critical in planning recreational water bodies and stormwater retention basins, where sediment management and hydraulic structure performance are closely linked. The sediment yield of a river upstream of a reservoir can be estimated using Geographic Information Systems (GIS) (Sabri et al. 2017).

The integration of hydrodynamic models with GIS has enhanced the spatial analysis capabilities of flood modeling. By incorporating high-resolution topographic data and land use information, models can more accurately predict flood extents and identify vulnerable areas. For example, the integration of HEC-RAS and HEC-HMS with GIS has been utilized to develop flood hazard and risk maps, aiding in urban planning and disaster management (Peker et al. 2024).

Several studies have been published on the application of HEC-HMS and HEC-RAS software for urban flood simulations (El Alfy 2016, Rangari et al. 2019a, Rangari et al. 2019b, Sahu et al. 2023, Alshammari et al. 2024). While numerous works focus on fluvial flood modeling, the application of HEC software to pluvial flood events remains relatively scarce.

Overall, the transition from purely 1D to integrated 1D–2D modeling reflects a broader trend toward spatially distributed, data-driven, and scenario-based analysis in urban hydrology. The present study builds upon this foundation by applying 2D hydrodynamic simulations to evaluate design and operational challenges in contemporary urban water systems, using real-world case studies to highlight the practical utility of high-resolution models.

Methodology/Materials and Methods

Case Study 1

For hydrodynamic modeling, we selected the Hydrologic Engineering Center's River Analysis System (HEC-RAS), due to its widespread acceptance and its capability to simulate gradually varied, unsteady 1D–2D flow conditions. HEC-RAS also includes comprehensive GIS-based visualization tools. HEC-RAS solves the system of partial differential equations governing open-channel flow using the finite difference method for 1D flow and the more numerically stable finite volume method for 2D flow.

The digital terrain model (DTM) of the study area represented the future configuration of the Kána lakes, bounded by embankments (Figure 1). The DTM was imported into HEC-RAS in GeoTIFF format, with a resolution set to 0.25 m, matching the 0.5 m sampling of the original topographic survey. The 2D Flow Area mesh was created using an average cell spacing of 0.25 m, resulting in approximately one million mesh elements, each with an average area of about 0.06 m^2.

Figure 1. *Digital Terrain Model*

In the hydrodynamic model, the upstream and downstream reaches of the stream were linked with the 2D flow area representing the lakes. The upstream and downstream boundaries of the lake matched the cross sections of the respective river reaches. The terrain model included the internal embankments separating the three impounded lakes, but we refined the DTM further by implementing weir structures within HEC-RAS.

The Manning roughness coefficient for the streambed was set to 0.06 $s/m^{1/3}$, corresponding to a partially vegetated channel. For the lakebed, we performed a sensitivity analysis with roughness values ranging around n = 0.03 ± 50%. The flow velocities within the lakes remained in the same order of magnitude across this range. The observed differences in flow patterns were attributed more to numerical instability—especially with higher n values (e.g., 0.06)—than to changes in hydraulic resistance. Ultimately, we selected a stable and realistic value of n = 0.03 $s/m^{1/3}$, representing a coarse sandy or gravel bed.

The upstream boundary condition in the model was defined by a flow hydrograph applied at the top cross section of the upstream river reach. At the downstream end, a normal depth condition was specified at the lower cross section of the river reach. The initial conditions included a predefined water surface elevation across the entire 2D flow area. The computational time step for the unsteady simulations was set to 1 minute, with a total simulation duration of 24 hours. To ensure numerical stability at the beginning of the simulation, a 60-minute steady inflow period was introduced along the 1D reaches, followed by a 60-minute gradual ramp-up of inflow at the interfaces between the 1D and 2D domains.

We performed three separate simulations representing low (100 L/s), average (500 L/s), and high (29.7 m^3/s) flow conditions. A large flood simulation was performed using a synthetic flood wave characterized by a rapid rising limb followed by a slowly receding limb, representing a peak flow scenario.

The HEC-RAS "particle tracking" feature was used to visualize the flow patterns, helping to assess directional flow behavior and relative velocities. For a more quantitative depiction, we applied a color-coded visualization of velocity magnitudes across the 2D domain.

The sediment transport module of HEC-RAS was not utilized in this study due to the significant uncertainties associated with several model parameters, and the lack of sediment transport measurements required for proper calibration. Since the sediment transport formulations in HEC-RAS are primarily based on shear stress at the water-sediment interface and the derived stream power—defined as the product of shear stress and flow velocity—we instead calculated the stream power values for each cell of the lake areas under various streamflow scenarios. This approach provided a spatial representation of potential sediment transport capacity without relying on the full sediment transport model.

Case Study 2

For the approximately 1.5 km² design area, a TIN surface was created based on a LIDAR survey, consisting of over 4 million points and more than 8 million triangles. The design boundaries were determined by the cadastral parcel boundaries.

Soil investigation data were available from 12 borehole sections, which included the composition of sand–silt–clay soil layers, infiltration coefficients, and moisture content.

As precipitation input, we used the 10-minute interval aggregated data from the nearest automatic weather station of the national meteorological service, located approximately 15 km away. Data is available from 2005 onward, providing 20 years of records, which reflect climate change well over this period. For surface flooding assessments, longer-duration rainfall events can be more critical. We selected the ~60 mm, 24-hour rainfall event from April 19–20, 2005 for runoff analysis.

The delineation of subcatchments was carried out using HEC-HMS 4.12 software. To do this, we exported the TIN surface into DTM format, setting a 1 m × 1 m grid size. Using HEC-HMS's GIS functions, we first filled shallow terrain depressions (< 0.25 m) to avoid numerous small internally draining areas. Roads were raised a few meters above the terrain (visible as lighter lines) so that flow paths would adjust accordingly. We clipped terrain areas outside the design boundary to match the cadastral parcel lines. The main flow paths were then identified (

Figure **2**). The green–yellow–red shading and increasingly thicker lines indicate the direction and concentration of water accumulation. Based on the flow paths, we delineated 17 subcatchments (Figure 3) for further detailed runoff calculations.

Figure 2. *Flow Paths and Digital Terrain Model*

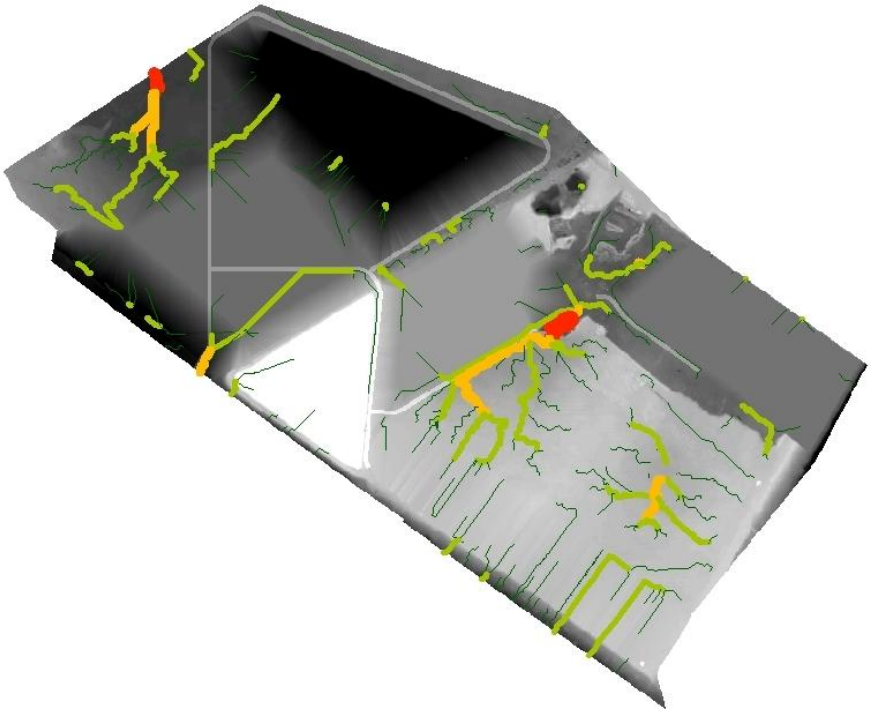

Figure 3. *Flow Paths and Subcatchments*

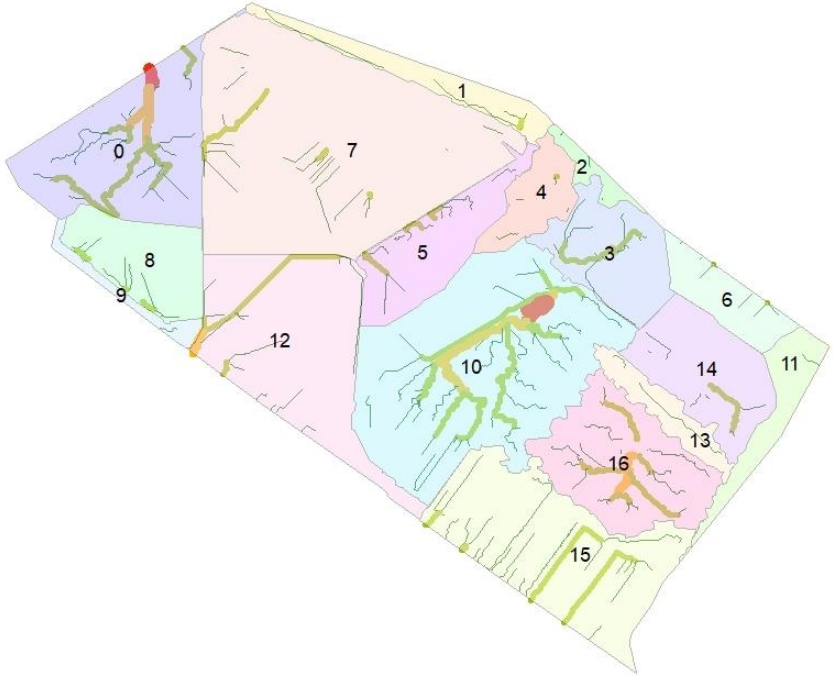

To calculate surface runoff and infiltration, we used the HEC-RAS 6.6 simulation software. The HEC-RAS 2D runoff model applies the finite volume method to numerically solve the Saint-Venant equations. Given the nature of the task (slowly varying flow), we chose the diffusion wave model to solve the momentum equations.

A computational mesh had to be created for the 2D flow domain. We generated 2D flow areas from the catchment regions, using 1 m × 1 m (in some cases 2 m × 2 m) grids composed of unstructured polygons.

For infiltration modeling, we used the Green-Ampt model, as it fit well with the available soil parameters. This model assumes a downward-moving, horizontally flat-bottomed saturated zone (wetting front), homogeneous soil, constant infiltration rate, and constant suction head. Total infiltration is calculated by solving the corresponding ordinary differential equation. For each subcatchment, we interpolated infiltration parameters (saturated hydraulic conductivity, suction head, initial and saturated moisture content) from the borehole section data. In HEC-RAS, infiltration is calculated by directly subtracting it from the precipitation depth. It does not consider any additional infiltration due to the depth of surface water that accumulates on the terrain.

To perform the runoff simulation in HEC-RAS, we developed an unsteady flow model, specifying the geometric layout, precipitation loading, and other parameters necessary for the simulation.

Results

Case Study 1

Under low-flow conditions, a steady-state flow regime is established within 24 hours (

Figure **4**). The water surface elevations are primarily determined by the crest levels of the transverse weirs. Flow velocities remain in the order of 1/1000 m/s in all three lakes (

Figure **5**). Flow directions and relative velocities are shown in more detail for the middle lake (

Figure **6**).

Figure 4. *Steady-state Water Surface Elevations under Low-flow Conditions across the Entire Lake System*

Figure 5. *Steady-state Velocities under Low-flow Conditions across the Entire Lake System*

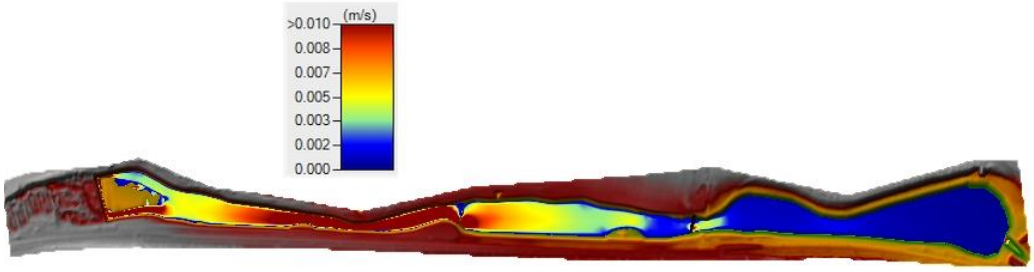

Figure 6. *Flow Directions and Relative Velocities in the Middle Lake under Low-flow Conditions*

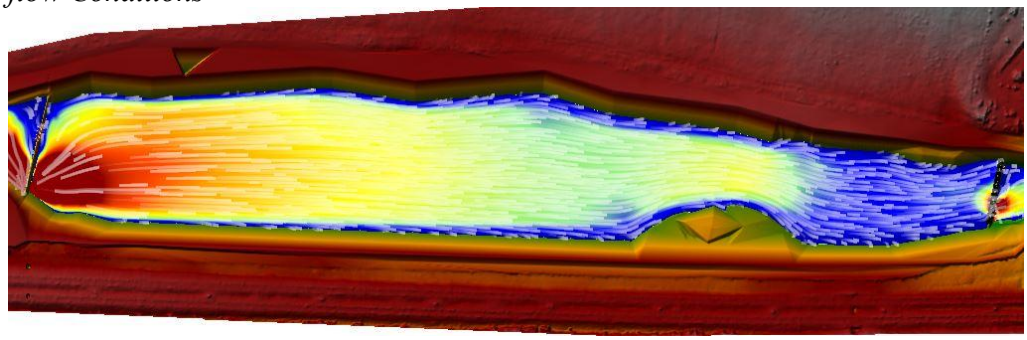

Under medium-flow conditions, water levels similar to those in the low-flow scenario are reached within 24 hours, but with flow velocities an order of magnitude higher.

In the case of a high-flow flood wave, water levels exceed the crest levels of the transverse weirs in all three lakes. The boundary between the lower and middle lakes becomes nearly indistinguishable (

Figure **7**), while a higher water level develops in the upper lake. Maximum velocities in all three lakes range from 0.1 to 2.0 m/s (Figure 8 and Figure 9).

Figure 7. *Maximum Water Surface Elevations in the Lakes under High-Flow Flood Conditions*

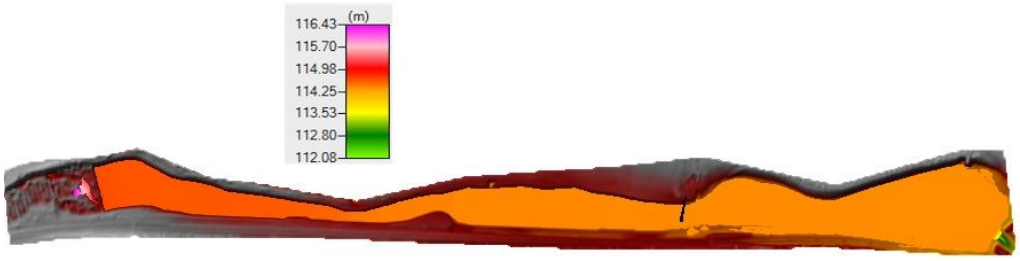

Figure 8. *Maximum Velocities in the Lakes under High-flow Flood Conditions*

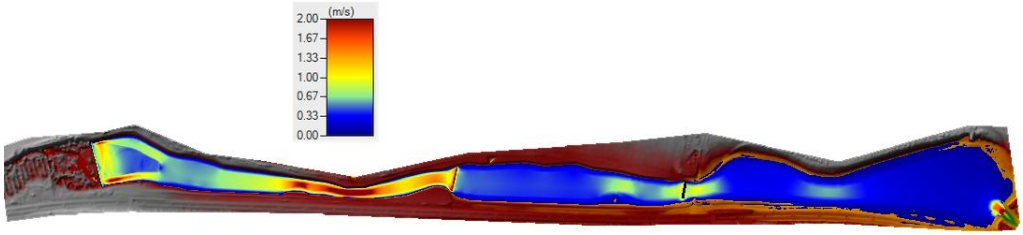

Figure 9. *Flow Directions and Relative Velocities in the Middle Lake under High-flow Conditions*

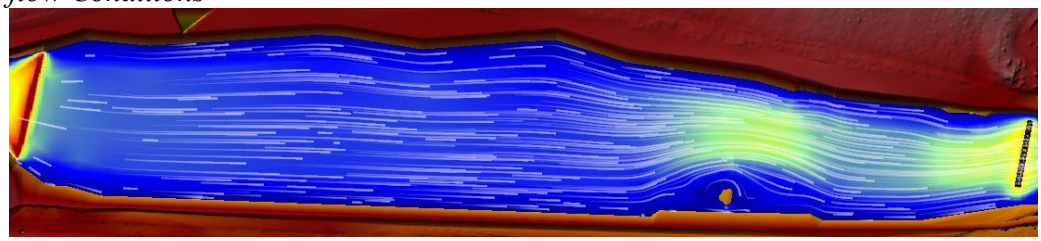

Under both medium- and high-flow stream conditions, the sediment transport capacity of the lakes is characterized by calculated "stream power" values for each grid cell (

Figure **10** and Figure 11).

Figure 10. *Stream Power Under Medium-flow Conditions*

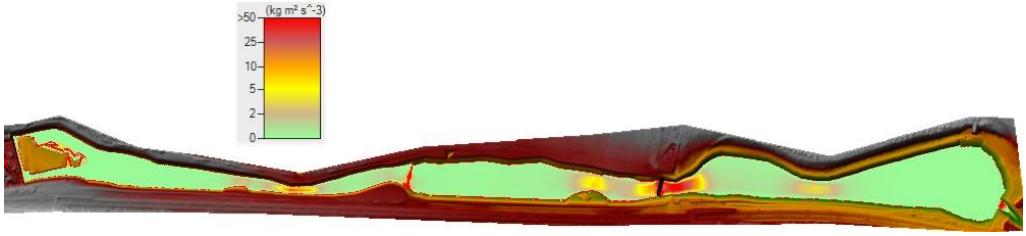

Figure 11. *Stream Power Under High-flow Conditions*

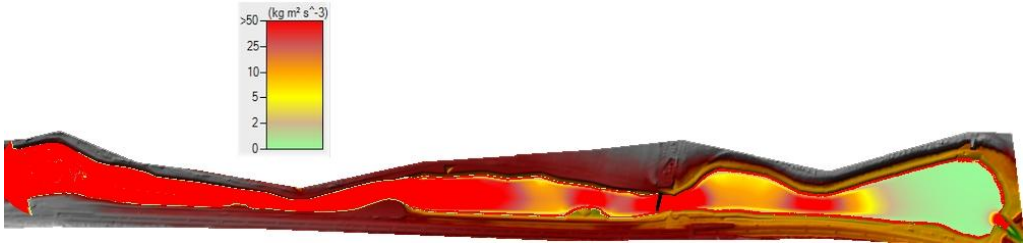

Case Study 2

As a result of the runoff simulation, key hydrodynamic parameters—water depth, flow velocity, and water surface elevation—were calculated and stored for each computational cell at the defined time steps (Figure 12).

Additionally, the maximum and minimum values of these parameters over the entire simulation period can be visualized (Figure 13 and Figure 14).

Figure 12. *Simulated Water Depths after 24 Hours*

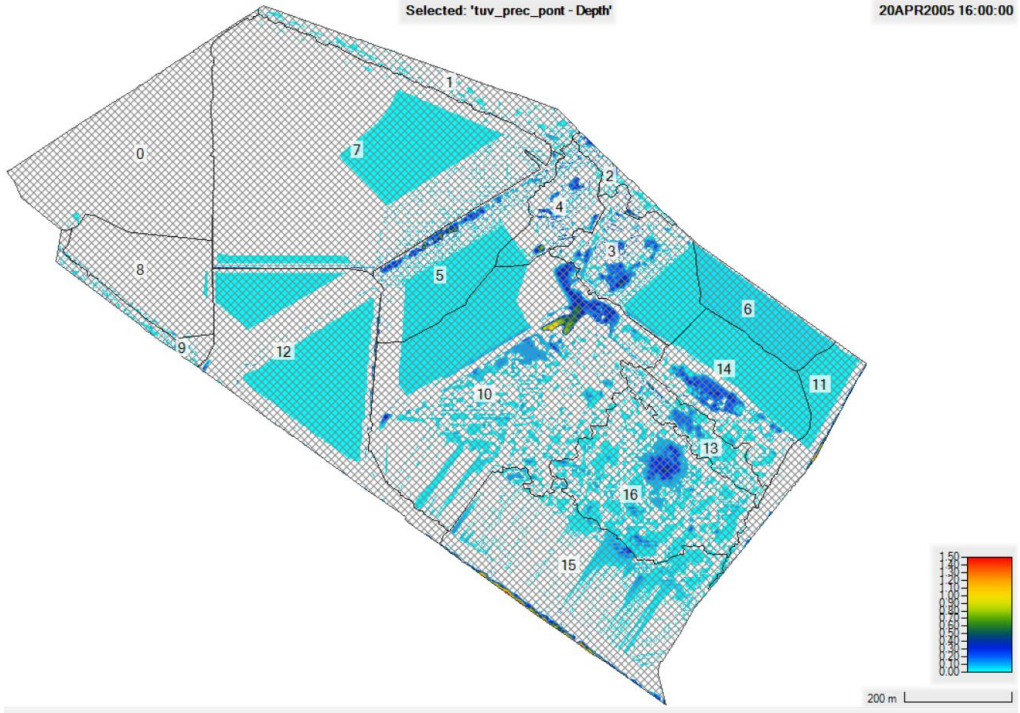

Figure 13. *Maximum Water Depths during the Simulation*

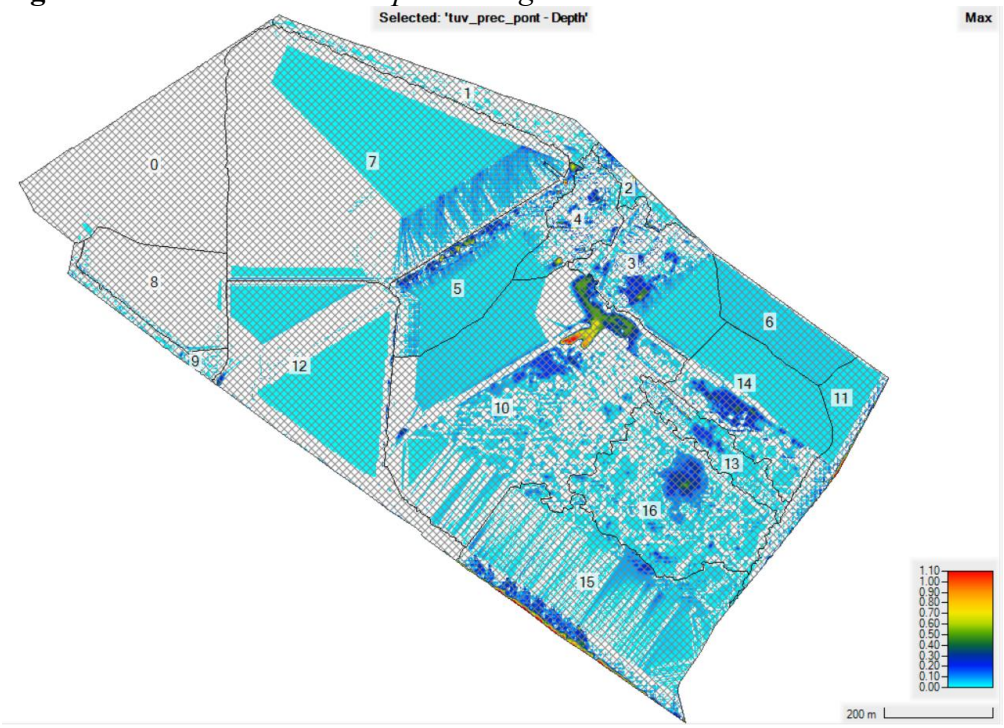

Figure 14. *Maximum Flow Velocities during the Simulation*

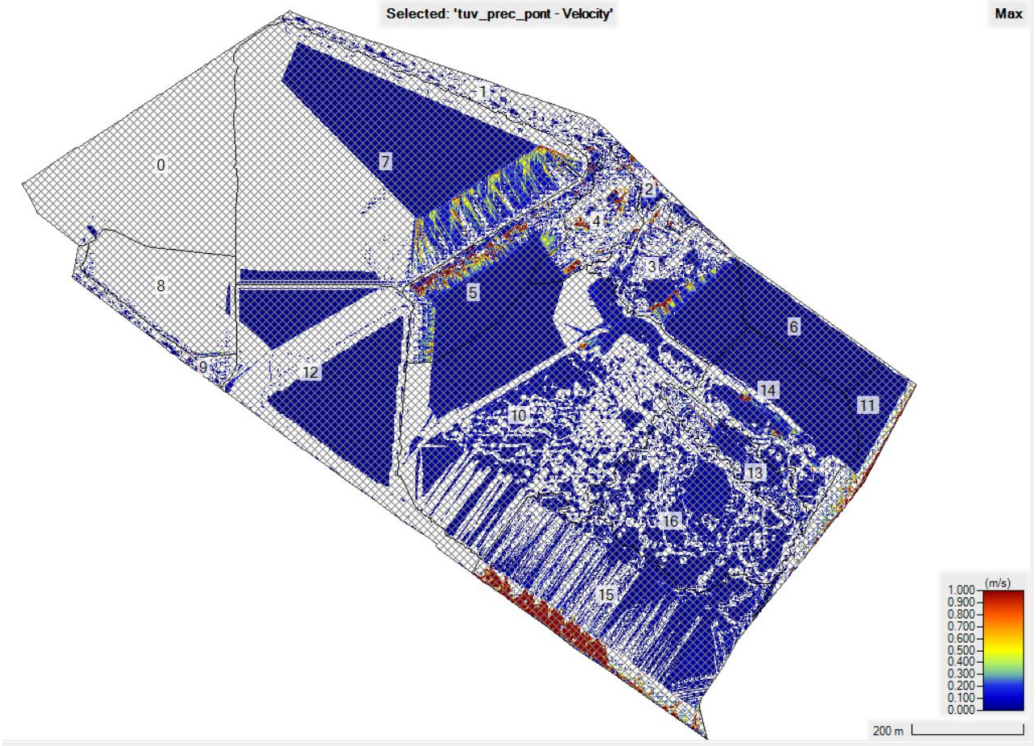

After 24 hours of simulation time (by April 20, 2005, at 16:00), the water levels had generally stabilized across the domain. Figure 15 shows the time series of water depth at the lowest elevation point within the terrain.

Figure 15. *Time Series of Water Depth at the Lowest Terrain Elevation Point*

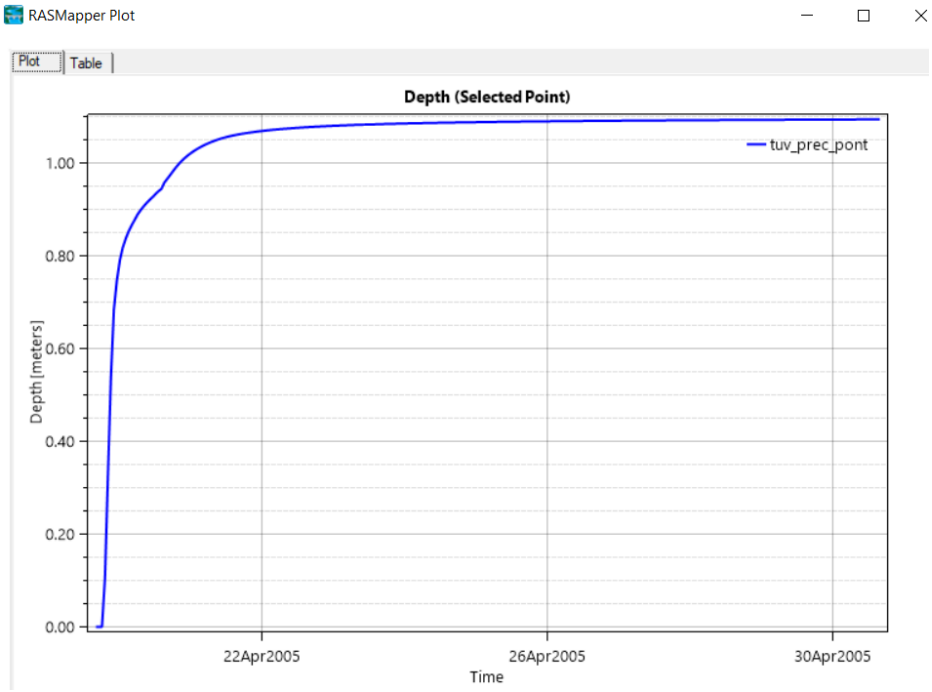

Discussion

Case Study 1

Based on the steady-state velocities, the calculated residence time of water within the lake system is approximately 56 hours under low-flow and 35 hours under medium-flow conditions. The peak of the high-flow flood wave passes through the system from the upstream to the downstream end in about 40 minutes.

According to the flow maps, velocity distributions are uniform. Flow is nearly parallel throughout the lakes in all characteristic flow conditions, without eddies or dead zones. Flow becomes constricted near the transverse weirs, which were represented as DTM surfaces in the model. Due to the resolution of the DTM, the weirs are not perfectly level; however, a few meters downstream from each weir, flow once again becomes uniform.

Simulation results suggest that under low- and medium-flow conditions, sediment movement is not expected within the lakes themselves, but may occur at the weirs. From approximately 2 m^3/s flow rate (corresponding to return periods of 2 to 5 years, i.e., 20%–50%), sediment erosion is likely to begin in the lower lake. However, even under flood conditions, sediment is not expected to be mobilized from the upper lake. Therefore, periodic dredging will likely be necessary in the upper lake.

Case Study 2

Thanks to the high-resolution terrain model and the corresponding mesh grid, the HEC-RAS model was able to accurately simulate surface runoff across the area. Due to the existing terrain conditions, rainfall runoff flows outward from the outer sub-catchments of the planning area. In contrast, within the internal sub-catchments, all rainfall accumulates, as any water that cannot infiltrate at the point of precipitation remains within these enclosed areas.

The majority of the flow velocities (Figure 14) remain below 0.2 m/s across the site, with only very short sections of a few meters experiencing higher velocities. As such, erosion-related issues are not expected.

Infiltration is only partially accounted for in the model — by subtracting it directly from the precipitation depth based on predefined values. However, the simulation does not consider additional infiltration during surface flow or in inundated areas, which may lead to an overestimation of flow depths and inundation extents.

Conclusions

This study demonstrates that two-dimensional (2D) hydrodynamic models, particularly those implemented in HEC-RAS, are highly effective tools for simulating both fluvial and pluvial flood events in urban environments. Through two case studies—one involving stream channel modifications near recreational lakes and the other addressing rainfall runoff in a planned solar park—the paper highlights how 2D simulations provide detailed insights into water depth distributions, flow velocities, and potential sediment transport. Based on our simulation results, rehabilitation work around the lakes has already commenced (Figure 16), focusing on eliminating critical sedimentation zones and reconstructing dam structures.

Figure 16. *Ongoing Excavation and Drying of Sediment from the Lakes as Part of the Rehabilitation Process*

In situations characterized by shallow but widespread surface flow, 2D models prove especially valuable for delineating flood extents, assessing hydraulic structure performance, and informing sediment management strategies. The case studies confirm that while 1D lumped models such as HEC-HMS are useful for subcatchment-level hydrologic processes (e.g., infiltration, depression storage, and evapotranspiration), they lack the spatial resolution required for precise hydraulic analysis. By coupling HEC-HMS and HEC-RAS, it is possible to leverage the strengths of both tools for integrated hydrologic-hydraulic modeling.

A key conclusion is that modern 2D modeling techniques are not only technically feasible but also necessary for capturing the spatial complexity of urban runoff, particularly under changing climate conditions. The findings also underscore the importance of high-resolution terrain data and appropriate mesh design in achieving accurate simulation outcomes.

Future research should focus on improving model calibration methods, enhancing the integration of real-time data, and developing user-friendly tools to make these advanced models more accessible to engineers and decision-makers. In doing so, urban water systems can be designed and managed with greater resilience and precision.

Acknowledgments

The research presented in this article was carried out with the support of the RRF-2.3.1-21-2022-00008 project, by the National Research, Development and Innovation Office.

References

Alshammari E, Rahman AA, Ranis R, Seri NA, Ahmad F (2024) Investigation of Runoff and Flooding in Urban Areas based on Hydrology Models: A Literature Review. *International Journal of Geoinformatics* 20(1): 99–119.

Ata FM, Toriman ME, Desa SM, San LY, Kamarudin MKA (2023) Development of hydrological modelling using HEC-HMS and HEC-RAS for flood hazard mapping at Junjung River Catchment. *Planning Malaysia* 21.

Brunner GW (2024) *HEC-RAS 2D User's Manual* (Version 6.6). Hydrologic Engineering Center, U.S. Army Corps of Engineers.

Chow VT (1959) *Open-channel hydraulics*. McGraw-Hill.

El Alfy M (2016) Assessing the impact of arid area urbanization on flash floods using GIS, remote sensing, and HEC-HMS rainfall–runoff modeling. *Hydrology Research* 47(6): 1142–1160.

Fread DL (1992) Flow Routing. In *Handbook of Hydrology*, Chapter 10, pp. 10.1–10.36. New York: McGraw-Hill.

Horritt MS, Bates PD (2002) Evaluation of 1D and 2D numerical models for predicting river flood inundation. *Journal of Hydrology* 268(1–4): 87–99.

Hunter NM, Bates PD, Horritt MS, Wilson MD (2007) Simple spatially-distributed models for predicting flood inundation: A review. *Geomorphology* 90(3–4): 208–225.

Lin B, Wicks JM, Falconer RA, Adams K (2006) Integrating 1D and 2D hydrodynamic models for flood simulation. In *Proceedings of the institution of civil engineers-water management* (Vol. 159, No. 1, 19–25). Thomas Telford Ltd.

Madhuri R, Raja YS, Raju KS, Punith BS, Manoj K (2021) Urban flood risk analysis of buildings using HEC-RAS 2D in climate change framework. *H2Open Journal* 4(1): 262–275.

Miremad S, Concilio G, Azzellino A (2025) Sustainable Urban Drainage Systems for reducing Flood Risk at the Catchment Scale: The Seveso River Basin Case Study. *Athens Journal of Technology & Engineering* (forthcoming).

Mohammad ME, Al-Ansari N, Issa IE, Knutsson S (2016) Sediment in Mosul Dam reservoir using the HEC-RAS model. *Lakes & Reservoirs: Research & Management* 21(3): 235–244.

Peker İ B, Gülbaz S, Demir V, Orhan O, Beden N (2024) Integration of HEC-RAS and HEC-HMS with GIS in flood modeling and flood hazard mapping. *Sustainability* 16(3): 1226.

Perera KKE (2024) An analysis of stream flow and flood frequency: A case study from downstream of Kelani river basin, Sri Lanka. *Athens Journal of Sciences* 11(1): 55–74.

Raji BM, Turabi H, Nasimi MN (2024) Sedimentation Analysis of Kabul River by Using HEC-RAS. *Journal of the Institution of Engineers (India): Series A* 105(1): 229–238.

Rangari VA, Sridhar V, Umamahesh NV, Patel AK (2019a) Rainfall runoff modelling of urban area using HEC-HMS: a case study of Hyderabad City. In *Advances in Water Resources Engineering and Management: Select Proceedings of TRACE* 2018, 113–125.

Rangari VA, Sridhar V, Umamahesh NV, Patel, AK (2019b) Floodplain mapping and management of urban catchment using HEC-RAS: a case study of Hyderabad City. *Journal of the Institution of Engineers (India): Series A* 100(1): 49–63.

Sabri E, Boukdir A, El Meslouhi R, Mabrouki M, El Mahboul A, Ekouele Mbaki VR, et al. (2017) Predicting soil erosion and sediment yield in Oued El Abid watershed, Morocco. *Athens Journal of Sciences* 4(3): 225–243.

Sahu MK, Shwetha HR, Dwarakish GS (2023). State-of-the-art hydrological models and application of the HEC-HMS model: a review. *Modeling Earth Systems and Environment* 9(3): 3029–3051.

Thakur B, Parajuli R, Kalra A, Ahmad S, Gupta R (2017) Coupling HEC-RAS and HEC-HMS in precipitation runoff modelling and evaluating flood plain inundation map. In *World Environmental and Water Resources Congress* 2017, 240–251.

U.S. Army Corps of Engineers – USACE (2024) *HEC-HMS Hydrologic Modeling System User's Manual* (Version 4.13.0). Hydrologic Engineering Center.

Wu W (2007) *Computational River dynamics*. Taylor & Francis.

Xiang M, Zhang S, Wu C, Tang C (2024) A two-dimensional hydrodynamic urban flood model based on equivalent drainage of manholes. *Journal of Hydroinformatics* 26(2): 519–533.

Athens Journal of Sciences - Volume 13, Issue 1, March 2026 – Pages 25-64

Valuation of the Environmental Services of an Urban Forest - A Case Study of 'Vetal Tekdi' Pune

By Priti Mastakar[*], Atharva Kulkarni[±], Dhruvika Lakhmani[•], Harsh Uttam[◦], Sibani Singh[•], M.K. Darshan[◦], Robia Kshetrimayum[♠], Srushti Pradhan[♥], Swara Bakshi[♦], Swastik Indalkar[♣], Deboleena Nasker[·], Miheer Karandikar[▽], Munib Ahmad[◠], Padmaja Uttawar[◡] & Rupali Sharma[⊃]

Gross Domestic Product (GDP) remains the measurement of growth and development, and while we struggle to find a more accurate rubric than GDP for an economy's progress, Environmental Economics has developed numerous tools to assess this rubric against a criterion of sustainability. Among these tools is the valuation of environmental services (ES) of an ecosystem in monetary terms. When we protect or sacrifice a certain naturally developed ecosystem that has promoted the health of a population, we are able to assess the value of the ecosystem preserved or destroyed using these tools. The present study conducts the valuation of the ES of Vetal Tekdi, a sixty-five-million-year-old extinct volcano that exists as an urban forest right in the midst of a rapidly growing city of Pune in the state of Maharashtra, India. Named after the temple of the malevolent God of demons 'Vetal', (Nalwalla, 2021), this temple has both heritage and cultural value to add to the ES value besides amenity value, carbon sequestration and the like. Field work for the valuation has been done by young environmental scientists and documented by young economists guided by an expert, and has been presented in this research study. Measurement of value of pristine water of ancient aquifers providing water to the city, carbon sequestration, provision of oxygen, biodiversity, heritage, cultural, and amenity value was conducted and then documented to provide a rubric to assess the benefits as well as the costs of the ES lost if the forest is axed in the name of development. Methodology for this research used, existence value and use value, contingent valuation, hedonic pricing method, expert opinion, and travel cost method. Willingness to Pay was used for the amenity valuation. The study monetises the environmental value of the ES to understand the contribution of ES to the health

[*]Professor, Gokhale Institute of Politics and Economic, India.
[±]Arachnologist, India.
[•]Associate at S&P Global, India.
[◦]Sustainability Consultant at Intertek, India.
[•]JSW Foundation Fellow, India.
[◦]Herpetologist, India.
[♠]Project Associate at NCBS, Bangalore, India.
[♥]Data Analyst at S&P Global, India.
[♦]Associate Partner at Capparis Eco Solutions, India.
[♣]MIT WPU, Coordinator, TERI, India.
[·]GIPE, Research Analyst, India.
[▽]GIPE, India.
[◠]GIPE, India.
[◡]GIPE, Research Analyst, Pune International Centre, India.
[⊃]SSE, currently Green Transition and Climate Change Intern at NITI Aayog, India.

of a population, in an area which is not much researched, namely, urban forests and aquifers. This study, based on primary research, will help further the vital valuation of urban forests which are usually undermined and sacrificed to urbanisation.

Keywords: *urban forest, environmental services, valuation, biodiversity, aquifers, amenity value, heritage value, cultural value.*

Introduction

Pune, in the western state of Maharashtra, India, is a city nestled among the Northwest 'Ghats' (mountains) of India, popularly known as the 'City of Hills'. Some of the hills in Pune include - Taljai Hill, Baner Hill, and the focus of the present study, the well-known Vetal Tekdi, tekdi meaning hill**.** Vetal Tekdi is a sixty-five-million-year-old hill, an urban forest, situated in the heart of Pune city.

The site Vetal Tekdi or Vetal Hill, is an urban forest, a part of 'Bhamburda Van Vihar' (forest department), and is a demarcated forest reserve. Located on the western side of Pune Municipal Corporation within the city limits. Vetal Tekdi is prominent and is visible from and surrounded by residential areas of Pashan, Kothrud, Gokhale Nagar, and Bavdhan. The geographical area is 18º 30' to 18º 32' N and 73º 49' to 73º 52' E covering an area of 10.5 square kilometers (4.1 sq mi) and is 800 meters above sea level. The hill shares the same climatic conditions with that of Pune City. The landscape of Vetal Tekdi is predominantly covered by scrubland species of Casia, and Acacia, along with blooms of the invasive Lantana. Vetal Tekdi, is one of the most well-known landmarks of Pune city. Vetal Tekdi is the highest point inside the city limits from where you can see the horizon and the cityscape. It is an excellent area to spend an early morning or late evening. A beautiful natural oasis in the bustling city of Pune, Vetal Tekdi is home to a variety of birds, trees, and plants and is known as the lungs of the city. It is a major groundwater recharge zone, providing clean and safe water to many of the city's residents. Vetal Tekdi is the pride of Pune, lying in the heart of the city and providing a natural refuge.

Urban forests play a crucial role in city environments, providing ecological, recreational, and cultural advantages to local communities. Vetal Tekdi, a significant reserved green area, exemplifies such an essential urban refuge. Renowned for its biodiversity, tranquil atmosphere, and the spiritual importance of the Vetal Baba Mandir, Mandir meaning temple, the Tekdi is cherished by the people of Pune.

These hills are the green lungs of the city acting as an essential oxygen reservoir. The urban forest, Vetal Tekdi, provides a variety of environmental and ecological services that are vital to the city's sustainability and well-being. As urbanisation pressures increase, it becomes crucial to understand and quantify the value of such ecosystems to ensure their preservation and wise management. This study aims to conduct a comprehensive valuation of the environmental services provided by Vetal Tekdi, utilising multiple methods to assess its economic, environmental, and social benefits.

The Vetal Tekdi urban forest provides multiple environmental services of the wetlands, carbon sequestration, biodiversity, aquifer water, cultural value of the temples, and amenity value for all those who benefit from leisure activities here.

The wetlands were formed out of a quarry when stone was extracted to build Pune's historical buildings, residences, colleges, commercial, and infrastructure of the past. Rainwater accumulation in the quarry over many years now sustains diverse flora, fauna, and even methane-eating bacteria, making it a vital ecological habitat. Today, it serves as a serene recreational and research space, symbolic of sustainable urban renewal, enriching both the environment and community well-being. The diverse tree cover supports varied biodiversity, oxygen production and carbon sequestration. Ancient and new aquifers formed between layers of basalt rock store water that recharges the underground streams and one third of the water supply to the Pune city.

Urban green spaces are essential for the ecological balance and survival of ecosystems, which in turn supports the health, both physical and mental, of a population in cities. Vetal Tekdi, is just one such urban forest, known for its peaceful environment, open spaces for physical fitness activities, other leisure activities, presence of diverse ecosystems, and temples that hold cultural and heritage value. A survey was conducted to assess the amenity value of the urban forest, to estimate the value citizens place on the conservation of the amenities of the urban forest. Citizens were interviewed for their willingness to pay for the protection of this ecosystem and their response was recorded.

The following valuations were conducted for each of the environmental services, valuation of the water, biodiversity and carbon sequestration for the wetlands, carbon sequestration and biodiversity of the tree cover outside the wetlands, valuation of water of the aquifers, assessing the willingness to pay, that is contingent valuation for the heritage and amenity values respectively.

Economic valuation of ecosystem services (EVES) acts as one of the quantification of parameters in environmental risk assessment. Environmental risk refers to the potential adverse effects or harm posed to the environment because of human activities or natural phenomena, the ecological damage, pollution, or degradation of natural resources, and the potential consequences for ecosystems, biodiversity, and human well-being. The assessment and management of environmental risks play a crucial role in ensuring sustainable development and safeguarding the well-being of both present and future generations. Any development activity at Vetal Tekdi will increase this environmental risk, hence assessment and management of risks for the Tekdi will have valuation of its services at its core, the objective of this study. Towards protecting this ecosystem, in the past, several initiatives including the Yellow Ribbon, The Chipko Movement, were undertaken to safeguard the Vetal Tekdi (Prasanthi, 2025)

The valuation of environmental and ecological services refers to the process of assigning economic value to the benefits provided by ecosystems. These services are often undervalued because they do not have direct market prices, but they are essential for maintaining environmental health, biodiversity, and the well-being of local communities.

EVES refers to the assessment of the monetary worth of non-market ecosystem benefits, such as those provided by soils, to demonstrate their significance for human well-being and society. The present study on the valuation of the environmental services of the hill aims at using different valuation to derive EVES of the Vetal Tekdi. A simulator integrates all the values to give the total valuation of the urban forest in monetary terms annually.

One of the primary advantages of using EVES in the environmental realm is its ability to consider a wide range of factors and stakeholders. By assigning a monetary value to environmental impacts, such as reduced air pollution or enhanced ecosystem services, EVES allows for more comprehensive and inclusive decision-making (UN, n.d.). Despite being an immensely effective and viable risk management strategy, EVES has certain shortcomings. One of the biggest issues in the analysis is the inability to assign a monetary value to all the benefits identified, the study thus remains conservative in its valuation of the ES of the urban forest.

The research paper first outlines an extensive and recent literature review, followed by the methodology, findings and results, a simulator collating all the valuations gives the final total valuation followed by the conclusion that includes observations and recommendations.

The flow chart for the presentation of the study is presented below:

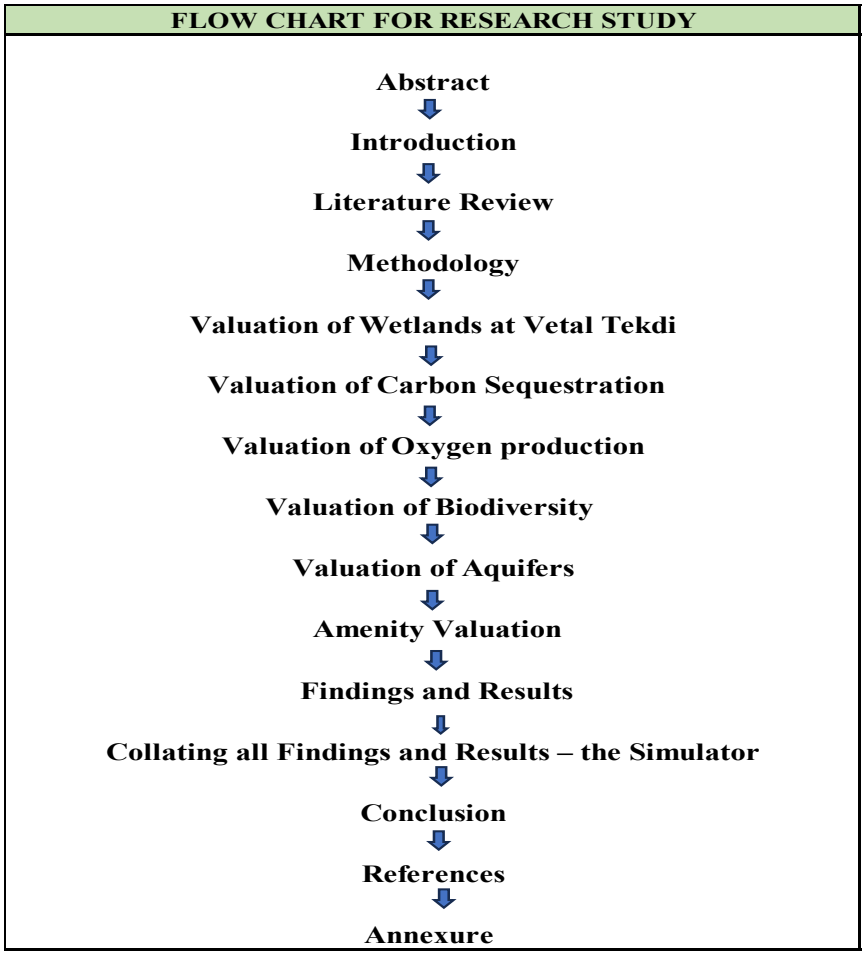

Literature Review

This literature review covers the various environmental services provided by urban forests and the various types of methodologies and perspectives for the valuation of these environmental services. In this, we emphasise the importance of

using different ways of quantifying the economic and non-economic benefits of any environmental/ecological resource to accurately capture the value. First, we begin with a review of the environmental services provided by urban forests and then we move onto the various methodologies that can be used for the valuation of these services.

Ecosystem services (ES) are made up of provisioning, regulating, cultural and supporting services (Meher 2024). Some of these can be directly quantified monetarily, for example, the wood of trees, oxygen production, carbon sequestered can be valued monetarily by using use values, (Callan et al. 2019), however some supporting services like amenity values are difficult to monetise and require to use concepts like willingness to pay, a more abstract concept. Thus, the quantification of the value of the ES is in an area which requires multiple methodologies depending on the nature of the services.

Urban forests provide many provisioning, regulating as well as supporting Ecosystem Services (ES) that contribute to the wellbeing of citizens as well as directly and indirectly to at least nine UN Sustainable Development Goals (SDGs) (Salbitano et. al. 2016). The ES are pollution control, water quality regulation, carbon sequestration, noise reduction, microclimate regulation, recreation, aesthetics and cultural services. People are showing willingness to pay for the associated costs of ecological restoration of natural areas as they realise the direct benefits of urban green spaces (Liu, et al., 2020).

Urban forests provide tree shade that obstructs solar radiation which in turn reduces land and, air temperatures. A 1% increase in tree cover can reduce air temperature by 0.14◦C, and an increase in tree cover from 10% to 25% can bring about a 2.0◦C temperature reduction for 2 meters (Middel et al. 2015).

Urban green spaces can cool land surfaces about two to four times than spaces without tree cover (Schwaab, et al. 2021). Climate change adaptation of local cooling, pollution reduction, and carbon sequestration are other advantages of urban forests and parks (Salbitano et. al. 2016, McPherson et al. 2017, Escobedo et al. 2011, Nowak et al. 2018). Climate regulation through increased tree plantation was observed in California, U.S., (McPherson, et al. 2017).

Cost-benefit Analysis of Urban Forests

Though costs of maintenance of urban forests can be steep, they give more than equal benefits to the population, (Salbitano et. al., 2016). A cost-benefit analysis shows that the benefits to human health far exceed the costs monetarily. For instance, the average annual management cost of USD 19 per tree, gives a benefit of USD 47.83, resulting in a benefit of USD 2.52:1 ratio for 173.2 million trees in California, USA (McPherson et al. 2017).

The regulating services of urban forests include the ‘cooling effect’ due to shade, interception, and evapotranspiration, cooling the micro-climate, building resilience in the eco system by storing and sequestering carbon thereby mitigating climate change, controlling stormwater runoff, and removing air pollutants (McPherson et al. 2017). Large urban forests can bring a cooling effect of up to 8.4◦ C extending up to 883 m during nighttime vis-à-vis comparative urban sites (Peng et al. 2022). Urban forests help prevent/reduce severe respiratory diseases reportedly, 670,000 and thereby save

more than 850 lives annually in the U.S (Novak et al. 2014) through their efficient regulating services of removal of particulate matter (PM10) and ground-level ozone (O_3) air pollutants during summer (Muresan et al. 2022). These climate benefits and avoided expenditures in healthcare are due to urban forests.

Urban forests and its amenities and the interactions therein prevents and restores physical, psychological and emotional health (Taylor et al. 2015). And the restorative benefits associated with regular walking, jogging, strolling, or cycling in urban forest environments with higher tree crown were connected to lesser medicine sales, for cardiovascular problems in people, (Chi et al. 2022). Children get access to green spaces and physical activity thus reducing obesity due to access to urban forests, (Dadvand et al. 2014).

Lessening of clinical depression cases in adults and help with mental health due to urban green spaces was reported, (Frühauf et al. 2016).

There is also evidence of biodiversity of urban forests linkage to mortality rate, (Giacinto et al. 2021). Urban forests with higher levels of biodiversity are associated with a lower mortality rate for heart disease and stroke. Estimates suggest that a 10% increase in urban green space in a community can postpone the average onset of health problems in individuals by up to five years, (Salbitano et. al. 2016).

Increases in urban tree cover and green spaces following extensive tree planting and management that benefits human health and well-being - as well as the spatial expansion of urban settlement - can be better monitored and measured using RS technologies more suitable for larger spatial scales than field survey inventories.

Studies indicate that, (Yang et al. 2024), green viewing, hiking, exercising, biking, and walking, reduced heat due to cooling by shade from tree canopy coverage (74.1%), and, air purification (20.4%), a result of pollution control can extend to a kilometer of the buffer zone.

Urban forests directly and indirectly contribute to the achievement of the UN SDGs by giving many economic benefits, alleviating poverty (SDG 1) of low-income urban residents, improving quality of life and promoting green economies. Food security and nutrition is directly provided through provision of nutritious foods such as fruits and seeds and indirectly by supporting agricultural production by providing wood fuels, high-quality water, and improved soil (SDG2). Forests and other green spaces prevent diseases by removing polluting sources and particulate matter, and ultraviolet radiation and noise pollution, and promoting mental health through amenity value (SDG 3), (Salbitano et al. 2016).

Urban development adversely affects urban forests and associated ecosystem services, these can be minimised with inclusion of urban forests as a non-negotiable part of city planning. ES of urban forests, and access to urban forests are part of basic services for the health of a population that ensure implementation of UN SDGs (Katila et al. 2019) benefiting city and forest dwellers.

Urban forests offer many economic benefits and boost green economies which can raise the quality of life of low-income urban residents and lift them from poverty (SDG1). Urban forests are also sources of pure water as they filter pollutants from water, and reduce the effects of runoff and flooding in urban areas (SDG 6). Urban forests are also a source of affordable energy due to the replacement of fossil fuel with wood fuel which gives heat and power for low-income people (SDG 7).

Entrepreneurship and sustainable employment can be created through investing in urban forests that reduce infrastructure costs and supply ES (SDG 8). Liveable, environmentally sustainable and economically viable cities can be maintained by the presence of urban forests (SDG 11). Carbon sequestration and production of oxygen by trees in urban forests reduce the climate change risk and indirectly save energy and, reduce the effects of urban heat island (SDG 13). Urban forests are sources of biodiversity and, urban wildlife and, they safeguard natural resources (SDG 15), (Ewane et al. 2023).

ES Valuation Methodologies

We first cover some studies that analyse literature on this subject over the years and try to distil findings from them. In (Bockarjova et al., 2020) the authors try to gauge what contingent valuation functions (papers using surveys) look like in different parts of the world to try and create an over-arching function that can be applied everywhere. They then apply it to various cities in Europe. They find decreasing marginal returns based on forest size, income and population density are positively associated. Croci, Lucchitta, and Penati (Croci et al. 2021) define the methods of valuation used for each service and maintain that different types of methods need to be used for valuation to make it more accurate and reflect all the services provided. The study lists the pros and cons of every different valuation methodology for different ecosystem services. In (Söderman et al. 2012), the authors aim to create criteria for measuring, evaluating and assessing various ES in middle-sized urban areas. They use two main databases: the Monitoring System of Spatial Structure (MSSS) and the CORINE Land Cover database. Jim and Chen (Chen et al. 2008) review major studies on ES benefits done in China to evaluate their methodologies and findings. They review the literature on various types of ES across three major cities. They come to a few conclusions and recommendations, mainly on how better studies can be done and how different types of services can be accurately calculated and assessed.

Contingent Valuation (CV) is a method in which surveys are used to find out how much people value a particular environmental resource. (Bernath et al. 2008) do a contingent valuation survey for forests in Zurich using two different methods: bid levels and protest votes for different models of valuation and revenue collection. They integrate a social attitude-behaviour framework because generally, contingent valuation models have large unexplained variation. Messrs del Saz (Salazar et al. 2007) conducted a survey-based study in Valencia to determine the willingness to pay (WTP) for a park replacing a defunct train station. They find that the WTP is higher in the neighbourhoods close to the park than those away. (Tyrväinen et al. 1998) conducted a study to try and estimate the value of urban forests in a city in Finland. The purpose of evaluating these benefits is to stimulate public awareness regarding the potential of urban forests benefits, to apply the cost-benefit analysis for decision making, and to justify decisions related to urban land use planning and policy making. (Yang et al. 2019) use CV valuations to estimate the relationships between ecosystem services of urban and rural forest areas and the human well-being associated with them. They also attempt to study the differences in this perception between urban and

rural areas. (Zegeye et al. 2023) focus on trying to calculate the benefits that citizens would get based on their valuations of urban forest parks (UFP) in the city of Hawassa in Ethiopia. They study the effect of various factors like education level, marital status, number of children, home ownership and others.

Cost-benefit analysis is done by aggregating the monetary value of all the ES in the area based on a central database and the costs of any proposed project to be done on it. (Chen et al. 2008) try to quantify the benefits of a few urban greening projects in Zhuhai City, China. They found that the average perceived benefit would be RMB 161.84 per household per year and evaluated that the greening project would succeed.

Hedonic Pricing Models use market prices of properties differing in access to ES to find out how much people value them. Sander, Polasky, and Haight (Sander et al. 2010) try to estimate the positive externalities caused by afforestation by estimating the changes in house prices as a function of various environmental variables including tree cover. They find that a 10% increase in tree cover within 100 m increases the average home sale price by $1371 (0.48%) and within 250 m increases the sale price by $836 (0.29%). (Tyrväinen 1997) uses the house price values of apartments in a city in Finland to find out the preferences for proximity to green spaces/urban areas are reflected in the prices. The results say that urban forests are an appreciated environmental characteristic, but the specific increases in the city were difficult to find out because of multiple forest areas in the city.

Service Evaluation is the quantification of various ESS based on their biological and ecological functions. These estimates are used in Cost Benefit Analysis. (Aevermann et al. 2015) try and quantify the monetary value of different ecosystem services provided by a park in Munich, Germany. Comparing that to the maintenance costs of the park, they show that the benefits outweigh the costs and that for the select ES (water purification, flood protection) the benefits were €627,586/yr. (Dennis et al. 2016) conducted a study of various types of urban green spaces in the UK to try and estimate the positive impact of complex urban forest systems. They find that collectively managed spaces lead to more impactful urban spaces and that the value of complex natural ecosystems in urban areas is not always accurately captured in assessments of large-scale land. The study concluded that assessments based on landscapes failed to include the provision of a lot of services like microclimate regulation, preservation of genetic diversity and the therapeutic value of engaged community service. (Elmqvist et al. 2015) use the monetary assessments of ecological services from various cities to try and quantify the benefit of restoration of different ES. They then compile the various studies to find out the benefit-cost ratios of different types of urban green spaces. They conclude that the restoration of any ES leads to massive economic gains and that even cities that don't have massive budgets can gain a lot by doing so. (Langemeyer et al. 2015) assess the monetary and non-monetary benefits of the Montjuïc park in Barcelona. They found that the benefits of a same service differed based on whether it was a monetary or nonmonetary valuation. They also found that people assigned high values to collective experiences and sentiments. Hence, they call for a balanced approach towards valuation techniques and to seriously consider non-monetary benefits as monetary benefits. (Nijhum et al. 2021) use a study of ecosystem services to try and quantify the potential benefits of different scenarios for land use in the future for a lake in Saskatchewan province, Canada. The

authors urge the use of land-use assessments in urban land planning and also account for the previous and potential losses of ecosystem services in different types of land use. (Tammi et al. 2017) argue here that there are many different models and perspectives to look at for the valuation of ecosystem services, but there are many discrepancies in the transfer of such frameworks between different types of ecosystems. They recommend using forward-looking surveys to predict land use types and then valuing ecosystems to reflect in urban and land planning.

In a study of valuation of forest services in Himachal Pradesh, India, (Verma 2000), it is found that the total economic value of forests is 2.61 times the value of the growing stock, 980 times the total expenditure incurred by the forestry sector of Himachal Pradesh and 2607 times the revenue realized by the forests annually. This comparison proves gross underestimation of forestry sector's contribution in the economy of the state. When the Gross State Domestic Product (GSDP) of the state is corrected for total economic value calculated through the current study the contribution of the forestry sector increases from 5.26% of GSDP to 92.40% of corrected GSDP.

While reviewing the various literature on valuation of urban forests, the need for an empirical approach using actual use and existence values for monetising the value of urban forests is seen. This study attempts to design an appropriate, empirical methodology for the valuation of each ES listed for the valuation of the ES of the Tekdi, and to suggest appropriate methods of evaluating the efficacy of urban planning projects.

Purpose of the Present Study

Objectives of the research are to primarily carry out a valuation of seven environmental services provided by the Vetal Tekdi, namely: Carbon Sequestration, Oxygen Production, Biodiversity, Aquifers water, Wetland services, Amenity, and Heritage values, this provides a rubric for decision making on projects related to urban forests, whether a development project should be allowed within the urban forest or not, and what would be the loss if such development is allowed.

The novelty of the research study is its empiricity; it is valuing urban forests, aquifers, amenity value, and heritage value on empirical data, all of these services are scarcely researched or assessed.

The research study is based on complete field work and exhaustive, as it encompasses multiple valuations all in a single body of work, viz., valuation of Carbon Sequestration, Oxygen Production, Biodiversity, Aquifers water, Wetland services, Amenity, and Heritage values, and employing all the following methods of valuation of an intangible asset – urban forest: existence value and use value, contingent valuation, hedonic pricing method, expert opinion, travel cost method, Willingness to Pay, and using a simulator that can repeat the valuation every year. The literature review indicates the scarcity of comprehensive empirical research on the valuation of urban forests, aquifers, amenity, through assessing willingness to pay, and heritage value.

Methodology

The site chosen to carry out the valuation of ES is Vetal Tekdi. It is an urban forest of approximately 10 sq kms in size, at the highest point of the city at 800 meters, in the heart of urban Pune. A sample size of approximately one sq km was selected to conduct the field work, and a simulator was created to apply the sample size of one sq km to the valuation of the entire urban forest of ten sq kms. The aquifers were treated separately as one float, that is the aquifers of the entire urban forest were valued together and hence did not have to be converted.

The methodology for this research was to also create a simulator that will assimilate all the values for each parameter automatically to give us the final result, that is the monetary value of the ES of the Urban Forest, Vetal Tekdi, Pune. The forest is surrounded on four sides by residential/commercial sites Gokhalenagar, Pashan, Bavdhan and Kothrud. Land prices were taken for all sites, averaged and added to the simulator, creating a regression. Each ES valuation forms a variable in an equation to which we separately add the land value based on the average values of land surrounding the forest that forms together the regression, viz., Hedonic pricing.

Five environmental services were identified namely:

1. Economic Valuation of Wetland;
2. Economic Valuation of Carbon Sequestration;
3. Valuation of Biodiversity
4. Valuation of Aquifers
5. Valuation of Heritage
6. Amenity Valuation

This study uses five different approaches to value the key services of Vetal Tekdi, each of the services valuation methodology is presented as under:

1. Valuation of Wetlands

Quantification of Economic Values:

Wetlands are crucial ecosystems that provide a range of services, including water filtration, flood control, and habitat for biodiversity. This method involves estimating the economic worth of these services, considering both direct benefits (e.g., water purification) and indirect benefits (e.g., flood mitigation and recreational value). A second valuation of water by market price, and expert opinion valuation for biodiversity was done.

One of the important roles of wetlands is that they perform functions more cost-effectively than engineering solutions. The economic value of such environmental goods, services, and commodities can be measured by the summation of many individuals' willingness to pay for them. In turn, this willingness-to-pay (WTP) reflects individuals' choice for the goods in question.

The economic value of wetlands includes both tangible and intangible values. Wetland use values are associated with a diverse and complex array of direct and indirect uses. Values provided by the wetland can be derived from outputs

consumed directly, such as food, water supply, recreation, or timber; indirect uses arise from the functions occurring within the ecosystem, such as water quality, flood control, future direct or indirect uses such as biodiversity, and conserved habitats. Table 1. below shows the various values and benefits of wetlands:

Table 1. *Use and Non-Use Benefits of Wetlands*

Use Value/Benefits			**Non-Use Value/Benefits**
Direct Use Benefits	**Indirect Use Benefits**	**Opinion and Quasi-option Benefits**	**Existence Benefits**
Recreation: • Fauna (Birds, Animals, Reptiles, Amphibians, etc.) • Wildlife • Viewing • Walking • Fishing	• Biodiversity Conservation • Flood Regulation • Ground water recharge • Carbon Sequestration • Water purification	• Potential future uses (as per direct and indirect uses) • Future value of information, eg., pharmaceuticals, education.	• Biodiversity • Culture • Heritage

Source: Authors

Using a Geographic Information System (GIS) tool, we calculated the amount of land covered by wetlands at the Tekdi to be 54,750 sq. m. as shown in Figure 1 below. The perimeter of the wetland area is approximately 1390 m (Figure 1), to estimate the depth of the water, we consulted primarily (Ramchandra et al., 2005) and estimated it at 3 feet. the water quantity will be: Area x Depth, that is 49,140,000 litres. Monetary valuation is presented in findings.

Figure 1. *Area of Wetlands*

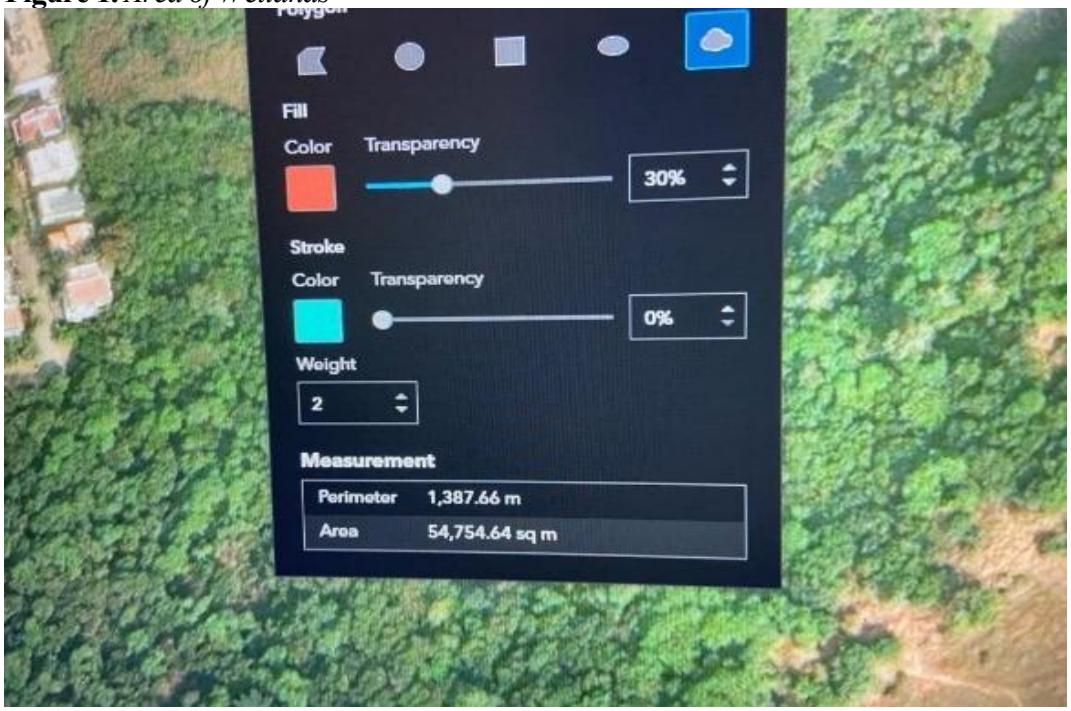

Source: Authors

2. Valuation of Carbon Sequestration:

Vetal Tekdi, like other green spaces, plays an important role in carbon sequestration, helping to mitigate climate change by absorbing atmospheric carbon dioxide. This valuation method assesses the economic value of carbon storage and sequestration by estimating the monetary worth of the carbon captured by the vegetation on Vetal Tekdi. Field work measuring the carbon sequestration was conducted.

To ensure unbiased sampling, the study was conducted across three distinct landscape types within Vetal Tekdi:

- Wetland
- Scrubland
- Slope

From each landscape type, five quadrants measuring 10 x 10 meters were selected for sampling. Within each quadrant, all trees were recorded, and their girth at breast height (GBH) was measured. The species name of each tree was also documented. Monetary value calculations are presented in Findings.

3. Valuation of Biodiversity:

Biodiversity within ecosystems like Vetal Tekdi provides a wide range of services, including pollination, genetic diversity, and resilience against environmental change. This method estimates the value of the biodiversity on the hill by considering the intrinsic worth of species preservation, potential medicinal resources, and the ecosystem's ability to maintain a balanced and resilient environment. Experts of

biodiversity were consulted, and their ranking of species in monetary terms was used for the valuation.

Vetal Tekdi hosts a rich biodiversity of Odonates (damselflies and dragonflies), Lepidopterans (butterflies and moths), and avian species (birds). Understanding the perspectives of experts in conservation is crucial for effective management and preservation of these taxa. In this section, we use conservation valuation questionnaires provided by experts for odonates, butterflies, and avian species (Mrs. Monali Shah) to calculate the economic cost of conservation of these taxa.

First, we scoured through existing literature to identify the species of the three taxa previously recorded on Vetal Tekdi. We then selected experts to give their valuation in monetary terms. We identified and selected Mr Arajush Payra for odonates, Mr Narendra Bhagwat for lepidopterans (butterflies), and Mrs. Monali Shah for avians (birds). They were chosen for their experience/expertise in their respective field as well their familiarity with the species diversity of Vetal Tekdi.

Three questionnaires were then drafted, each specialized to one of the above-mentioned groups, consisting questions highlighting their experience and their opinion on what would the monetary value if it could be evaluated based on their experience. Once the response was collected, it was summarised and analysed, and are presented in the findings and results.

Due to the absence of literature, estimates of the number in any species, and an accurate or standardized tool for measuring the value of conservation, we opted to use expert opinion as one of the prescribed methods for monetary valuation of species. Expert opinion is particularly valuable in this context, given the complexities and nuances involved in estimating the worth of ecological contributions that are difficult to quantify through traditional means.

While the more tangible aspects of the species' value, such as their role in carbon sequestration and nutrient cycling, were considered, these estimates are likely negligible as compared to the value provided by the vegetation. Results are presented in the findings.

4. Valuation of Aquifers:

The aquifers and groundwater recharge services provided by Vetal Tekdi are essential for sustaining the water supply in the region. This method involves calculating the economic value of the ecosystem's role in replenishing aquifers, ensuring water availability for agriculture, human consumption, and industrial use. Market value of water gave a second valuation of the aquifers.

Visualisation and calculating water quantity

The Advanced Centre for Water Resources Development and Management (ACWADAM) provides valuable data about aquifers. This data includes the identification **(**ID**)**, length, area (in various units), and other details about each aquifer present in Pune, the Vetal Tekdi included. We have imported this data into Google Earth Pro software to create a layer from the shared vector file shown in Fig.2. below. This allows us to visualize the aquifers' locations and sizes in a geospatial context. (WC_95_52.pdf).

Figure 2. *View of the Aquifers*

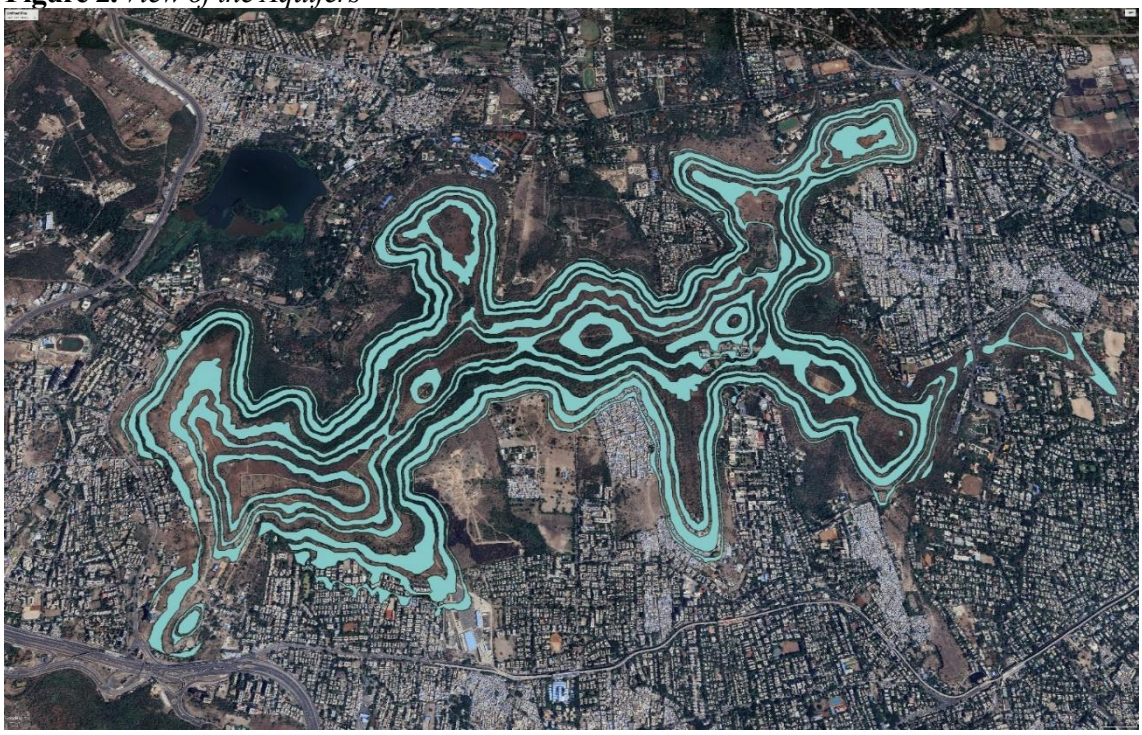

Source: ACWADAM

Next, we have imported this vector information into Excel to further analyse the data. Through this we calculate the potential storage within the effective thickness for each aquifer by multiplying the given area (in square kilometres) by its respective effective thickness. This gives us the potential aquifer storage over the exposed area. We then multiply this value by a specific yield of 0.04 to get the potential storage within the effective thickness. Finally, we convert this value into cubic millimetres (Mm) to obtain the potential aquifer storage in Mm for each aquifer.

5. Amenity Valuation:

Vetal Tekdi is not only a natural ecosystem but also hosts green spaces for health activities like walking, jogging, and is a cultural and historical landmark. This method focuses on estimating the amenity value, which includes heritage value, recreational, aesthetic, and cultural values. Contingent valuation was used here. It involves assessing how the presence of a green space like Vetal Tekdi enhances property values, provides recreational opportunities, and contributes to the overall physical and mental health of citizens. Hedonic pricing was used for the pricing of the land of the urban forest.

Through these valuation methods, the study seeks to provide a holistic understanding of the contributions Vetal Tekdi makes to the environment, and society. The results will offer insights for policymakers and stakeholders to make informed decisions about the conservation and sustainable management of this critical urban ecosystem, and their environmental value estimated in this study.

Urban green spaces are essential for the ecological balance and survival of ecosystems, which in turn supports the health, both physical and mental, of a population in cities. Vetal Tekdi, is one such urban forest, known for its peaceful

environment, open spaces for physical fitness activities, presence of diverse ecosystems, and temples that hold cultural and heritage value.

A survey was conducted to assess the amenity value of the urban forest, to estimate the value citizens place on the conservation of the amenities of the urban forest. Two hundred and fifty citizens were interviewed while they were engaged in various leisure, fitness and study activities.

In the upcoming section, findings and results for the economic valuation of above mentioned five environmental resources have been presented.

Findings and Results

1. Value of Wetlands:

As mentioned in the methodology, we calculated the perimeter of the wetland area as approximately 1390 m, and estimated the depth of the water at 3 feet, using (Ramchandra et al., 2005), the water quantity was assessed at: Area x Depth, to be 49,140,000 litres.

Multiplying the water quantity with the use value defined by the market price of drinking water at Rs. 20 per litre, we got the final value of Rs. 98,28,00,000.

$$Area\ of\ the\ Tekdi = 10{,}50{,}000\ m^2$$
$$Area\ of\ the\ Quarry\ on\ the\ Tekdi = 54{,}000\ m^2$$
$$Estimated\ Average\ Depth\ of\ the\ Water\ present = 3\ feet$$
$$= 0.91\ metres$$
$$\text{Thus, } the\ Volume\ of\ the\ Quarry = 54{,}000\ m^2 \times 0.91\ m$$
$$= 49{,}140\ m^3$$
$$\text{Since, } 1\ cubic\ metre\ of\ Water\ contains\ 1000\ litres\ of\ water,$$
$$49{,}140 m^3\ of\ water\ will\ have = (49{,}140 \times 1000)\ L$$
$$= 4{,}91{,}40{,}000\ Litres\ of\ Water$$
$$According\ to\ the\ current\ market\ rate\ of\ mineral\ water\ at\ INR\ 20\ per\ litre,$$
$$Price\ of\ the\ total\ water\ present\ in\ the\ Quarry = Rs.\ (20 \times 4914000)$$
$$= Rs.\ 98{,}28{,}00{,}000$$
$$= \$\ 11{,}56{,}643.21.\ (Value\ in\ US\$\ as\ of\ 4\ July, 2025)$$

2. Valuation of Carbon Sequestration

Determination of Bio-volume:

Bio-volume (b) was calculated using the following equation:

$$b = 0.4 \times (GBH/\pi)^2 \times H$$

Where,

$D = (GBH/\pi)$, represents diameter calculated of the tree trunk, assuming the trunk to be cylindrical

H = Height of the tree

1. Estimation of Biomass

   Biomass was calculated as:

$$Biomass = Specific\ gravity\ of\ wood \times b$$

The specific gravity (wood density) of each tree species was obtained from publicly available databases:

Bangladesh Forest Information System
World Agroforestry Wood Density Database

2. Carbon Sequestration Rate:

   The carbon sequestration rate was estimated as 1% of the standing biomass.

Results:

Site 1. *Wetland*

Total Carbon Sequestrated (Scrubland):	107434.0095
	118.42 tons

Source: Authors

Figure 3. *Site 2. Grassland*

Source: Authors

Figure 4. *Site 3: Slope*

Source: Authors

Total Carbon Sequestrated (slope):	12551.45508
	13.83 tons

$$Area\ of\ the\ Tekdi = 10{,}50{,}000\ m^2 = 10.50\ Square\ Km \quad (1)$$

$$The\ average\ of\ the\ carbon\ sequestrated\ in\ whole\ Vetal\ Tekdi = 46.86\ ton/Square\ Km \quad (2)$$

$$According\ to\ the\ World\ Bank\ the\ value\ of\ carbon\ is\ \$40/ton \quad (3)$$

$$So, value\ of\ the\ total\ Carbon\ Sequestered = \$\ 40 \times 46.86$$
$$= \$1859.2$$
$$= Rs.\ 161{,}486.99$$
$$or, Rs.\ 161{,}487/year$$
$$or, \$\ 1{,}900.52\ /\boldsymbol{year}$$
$$(Value\ as\ of\ US\$\ as\ of\ 4\ July, 2025)$$

3 Oxygen production:

$$Number\ of\ tress\ in\ all\ five\ quandrants = 302$$

Calculation of oxygen production in tress is as follows:

$$Oxygen\ production\ ability\ of\ prtective\ tress = Number\ of\ tress \times 1.2\ kg/day$$

$$or, 438\ kgs\ per\ year$$

(Kusminingrum, 2008).

$$302 \times 1.2 = 362.4\ kgs/day\ for\ 5m \times 5m\ quadrant/day$$

$$or,$$

$$302 \times 438\ kgs = 132{,}276\ kgs/year\ for\ a\ 5m^2\ quadrant \times 194\ m^2\ for\ the\ entire\ tekdi\ of\ 0.97\ sq\ km$$

$$= 25{,}2661.544/year\ for\ tekdi\ area$$

$$25{,}661.544 \times \$3 = \$\,76{,}984.632/year$$

$$= Rs.\,6{,}694{,}583.59872$$

$$= approximately\ Rs.\,66{,}94{,}584/year$$

$$= about\ \$\,78{,}787.62/year\ (Value\ as\ of\ US\$\ as\ of\ 4\ July, 2025)$$

3. Valuation of Biodiversity

Results of the Biodiversity Expert Opinion survey are presented in Table 2 below.

Table 2. *Expert Valuation of Biodiversity*

Category	Odonates	Butterflies	Birds	Observation
Willingness to Spend on Conservation	₹2000 (damselflies & dragonflies)	₹1000 (butterflies & moths)	More than ₹4000 annually	Variability across taxa; birds have the highest value, indicating differences in perceived value or ecological importance.
Expenditure on Surveys	₹50 on average for surveying	₹200 on average for Lepidopterans	₹250 per visit for bird surveying	Variation in surveying costs; birds and butterflies have higher costs compared to odonates.
Ecosystem Benefits	Habitat quality indicator	Pollination, food chain	Aesthetic value, pollination, seed dispersal, negative economic impact with forest loss	All taxa contribute to ecosystem services; birds are valued aesthetically, while butterflies and odonates are emphasised for ecological roles.
Service Charge for Ecological	₹1,000	₹1,000	More than ₹600	Consistency in willingness to charge; birds show a higher threshold for

Services				service charges.
Monetary Value for Conservation	Not specified	Not specified	>₹20,000 for a significant bird; ₹1000 for migratory species	Birds have a significant monetary value for conservation, highlighting their perceived importance.
Perception of Climate and Habitat Change	Not addressed explicitly	Not addressed explicitly	Negative impact on economic value with forest loss	Only the bird questionnaire explicitly mentions climate and habitat change, indicating variations in how taxa are perceived to be affected.

Source: Authors

We can see from the table that the willingness to spend on conservation varies across taxa, with birds being considered of the highest value. Surveying costs also vary, reflecting the differing methodologies and complexities of studying each taxon. Ecosystem benefits are recognized for all taxa, emphasizing their unique roles in the ecosystem. Service charges for ecological services are generally consistent, showing a recognition of the value of these services. Birds show a higher emphasis on the monetary value of conservation, possibly skewed by a few species. They also are the most prone to habitat damage due to climate change.

Value of Biodiversity: each species valuation was calculated for one representative quadrant, there were ten such quadrants:

a. Odonates & Dragonflies: ₹ 54,000 X 10 = ₹ 5,40,000 (one quadrant multiplied by10)
b. Invertebrates: ₹ 2,46,000 X 10 = ₹ 24,60,000 (one quadrant multiplied by10)
c. Butterflies: ₹ 87,000 X 10 = ₹ 8,70,000 (one quadrant multiplied by10)
d. Birds: ₹10,96,000 X 10 = ₹ 1,09,60,000 (one quadrant multiplied by10)
TOTAL = ₹ 14,830,000 or approximately US $ 173,207 annually.

Valuation of Aquifers

Valuation of Aquifers by Water Treatment Cost

Considering the total water demand for Pune in 2020, (PMC,2014)) which is 1,906,260 cubic meters per day (or 1906.26 MLD, million litres per day). The operation and maintenance cost of the water treatment plant in 2020 is Rs. 2,833,600,000 (or Rs. 283.36 crores).

The cost per cubic meter of water treatment is calculated as follows:

$$Cost\ per\ cubic\ metre = \ Total\ Demand\ /Total\ Cost$$

$$= 1{,}906{,}260\ m^3/day/Rs.\ 2{,}833{,}600{,}000$$

$$\approx Rs.\ 1486.34\ INR/m^3$$

This means that the cost of treating one cubic meter of water is approximately Rs. 1486.34.

Here, we considered the monetary/commercial value of this water. It provides a different perspective on the way we see aquifers as it not only saves the Pune Municipal corporation the water treatment cost. However, it also represents a monetary/commercial value of itself (which we have assumed to be 20rs per litre)

Valuation of Aquifers by Water Market Value

Estimating water quantity in the aquifers:

Table 3. *Water Storage in Aquifers*

Aquifer	Area (Sq. Km)	Area (Sq. m)	Aquifer thickness (m)	Effective thickness at 70% of the mapped thickness (m)	Potential aquifer storage within effective aquifer thickness over exposed area and with a specific yield of 0.04 (Cubic m)	Potential aquifer storage (Cubic mm)
Aquifer-16	0.02435	24,350	11	7.7	7499.8	$7.4998*10^{12}$
Aquifer-17	0.215	2,15,000	6	4.2	36120	$3.6120*10^{16}$
Aquifer-18	0.39686	3,96,860	4	2.8	44448.32	$4.444832*10^{16}$
Aquifer-19	0.6851	6,85,100	4	2.8	76731.2	$7.67312*10^{16}$
Aquifer-20	0.71865	7,18,650	9	6.3	181099.8	$1.810998*10^{17}$
Aquifer-21	0.88302	8,83,020	14	9.8	346143.84	$3.4614384*10^{17}$
Aquifer-22	0.2714	2,71,400	3	2.1	22797.6	$2.27976*10^{16}$
Aquifer-23	0.043	43,000	6	4.2	7224	$7.224*10^{15}$
Aquifer-24	0.00798	7,890	7	4.9	1564.08	$1.56408*10^{15}$
Aquifer-25	0.02324	23,240	12	8.4	7808.64	$7.80864*10^{15}$
Total	**3.2686**	**32,68,600**			**731437.28**	**$7.3143728*10^{17}$**

Source: Authors, derived from ACWADAM report

Where, Potential Aquifer storage = Effective thickness x Area x Specific yield
So, Table 3,

$$\begin{aligned}&Converting\ the\ total\ Potential\ Aquifer\ Storage\ to\ Litres\\&= (7.3143728 \times 10^{17}\ cubic\ millimetres) \times 10^{-6}\\&= 7.3143728 \times 10^{11}\ Litres\\&= 7{,}31{,}43{,}72{,}80{,}000\ Litres\\&or, 73{,}143.728\ Crore\ Litres\end{aligned}$$

Thus, since the value of a bottle of mineral water is Rs 20 per Litre, the value of potential aquifer storage in Rupees (Rs.) is

$$\begin{aligned}&= 7{,}31{,}43{,}72{,}80{,}000 \times Rs.20\\&= Rs.1.4628746 \times 10^{13}\\&= 1{,}46{,}28{,}74{,}60{,}00{,}000\\&0r, Rs.14{,}62{,}874.6\ \ Crores\ or, \$\,172{,}163{,}657{,}762\end{aligned}$$

Results-Discussion

Between 2011 and 2021, Pune's Urban Agglomeration grew by approximately 30%, reaching an estimated total of around 6.57 million residents from 5.05 million (as per the last census data). As of 2025, it is expected to be around 7.4 million. As the population grows, the demand for domestic and non-domestic water usage increases proportionally, so does the total water demand, (PMC 2014).

Hence, aquifers play a key role as they are a natural source of clean water. Expressing the water in terms of litres makes it easier to comprehend their amounts. We then use *table 3*, where we see area, thickness and potential storage within each and every aquifer. We convert the total amount of water present in all aquifers, reaching 7,31,43,72,80,000 Litres or 73,143.728 Crore Litres.

To express this quantity of water in monetary terms, we used the market value of a one litre of drinking water, that is, multiplied the quantity (in litres) with the rate/price of mineral water per litre i.e. Rs 20. Doing that gave us the resultant amount Rs. 1,46,28,74,60,00,000 or Rs. 14,62,874.6 Crores.

The Pune Municipal Corporation receives an annual water supply of 12.8 TMC (Thousand Million Cubic feet) which is around 36,24,55,636,378 Litres (3624 Crore Litres), while they need around 21 TMC to keep up with the demand. 21 TMC equates to 5,94,65,37,78,432 Litres or 59,465 Crore Litres of water, (PMC 2014). This puts into context not only the demand for water but also how indispensable the water storage of the Aquifers in the Vetal Tekdi of Pune truly is.

Data taken from:

- WATER SUPPLY SYSTEM FOR PUNE CITY DETAILED PROJECT REPORT FEBRUARY, 2014
- An economic analysis of groundwater markets and water use efficiency in hard rock area of Hosur union Krishnagiri district of Tamil Nadu.

Data Analysis - Amenity Valuation

Introduction

Urban green spaces are essential for the ecological balance and survival of ecosystems, which in turn supports the health, both physical and mental, of a population in cities. Vetal Tekdi, is one such urban forest, known for its peaceful environment, open spaces for physical fitness activities, presence of diverse ecosystems, and temples that hold cultural and heritage value.

A survey was conducted to assess the amenity value of the urban forest, to estimate the value citizens place on the conservation of the amenities of the urban forest. Two hundred and fifty citizens were interviewed while they were engaged in various leisure, fitness and study activities.

The analysis of the survey is presented in this section, it is divided into four parts: A. demographics, B. the significance of Vetal Tekdi, C. cultural value of Vetal Baba Mandir, and D. access and transportation logistics.

Section A

This section briefly outlines the demographic profile of the survey, majority of respondents were in the 20–50 age group, with limited representation from those over 70. Around 58% of participants identified as male and 41% as female. Most respondents reside in neighbourhoods near Vetal Tekdi, such as Kothrud, Panchavati, and Bavdhan. Income-wise, a large share of respondents reported annual earnings above ₹12 lakhs, indicating a middle- class income group (graphs in annexure 1).

Section B

Section B highlights the diverse significance of Vetal Tekdi, focusing on its recreational use, public benefits, and support for conservation.

Graph 1. *Frequent Use of Vetal Tekdi for various Activities*

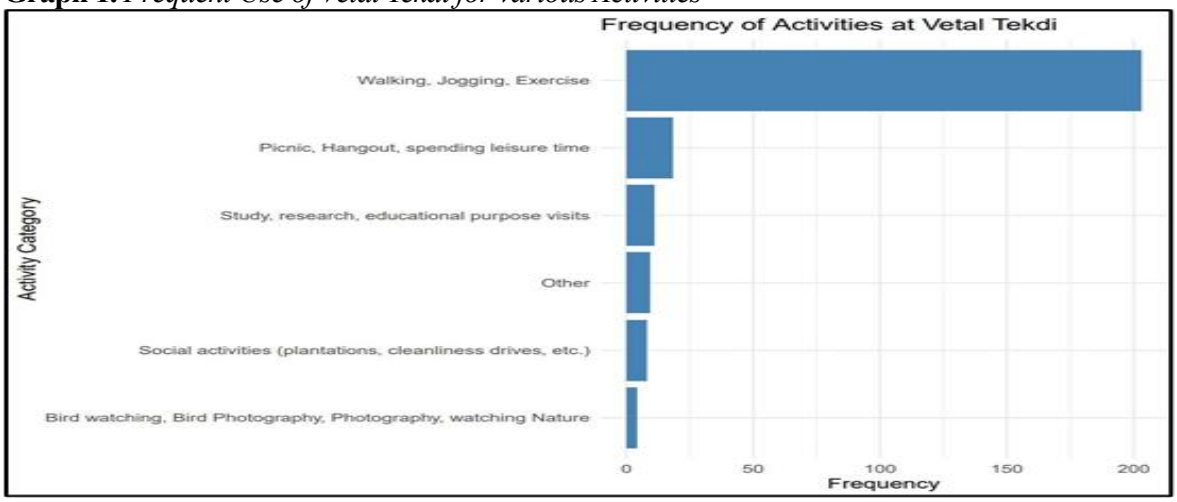

Survey data shows that walking, jogging, and exercising are the most common activities, making the Tekdi a key space for physical fitness. Less frequent uses include various leisure, study, and nature-based visits, indicating that while the Tekdi serves various purposes, its primary role is promoting health and well-being, (Graph.1). Survey shows that a vast majority of respondents, approximately 95% reported visiting Vetal Tekdi indicating a broad public engagement with the Tekdi.

Graph 2. *Pie Chart Indicating Importance of Urban Forest to Citizens*

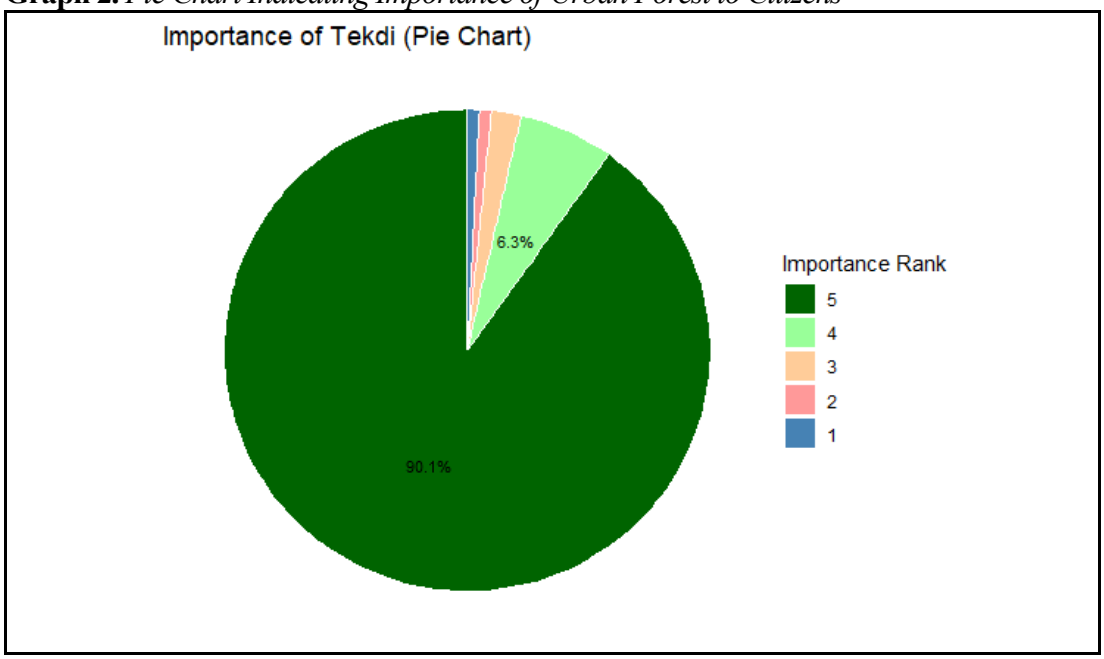

The pie chart (Graph 2) alongside shows that 90.1% of respondents rated Vetal Tekdi as highly important (5 on a 5-point scale), reflecting strong public support for its preservation and consensus on the Tekdi's significance.

Graph 3. Citizens Perceived benefits of Vetal Tekdi

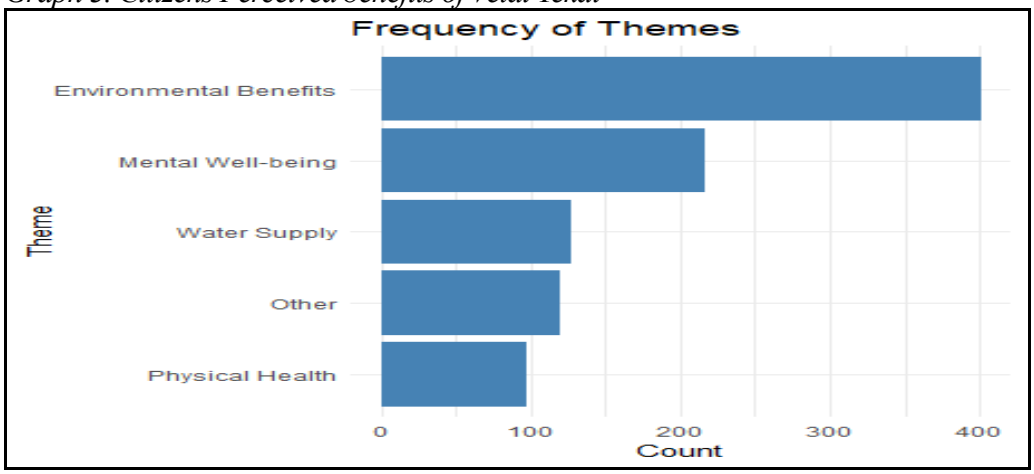

Graph 3 presents citizens perceived benefits of the urban forest - Vetal Tekdi. Grouped into five categories. "Environmental Benefits" was ranked the highest (401 times), followed by "Mental Well-being" (216 times), and "Water Supply" (127). "Others" and "Physical Health" were mentioned less preferred. It was interesting to note that citizens placed more value on environmental benefits and mental well-being, underscoring the Tekdi's ecological and emotional significance to the public.

Graph 4., the bar chart alongside categorises respondents' reasons for supporting the preservation of Vetal Tekdi into 11 themes. The most cited reasons include preserving green cover and biodiversity, followed by reducing air pollution and combating climate change. Mid-tier concerns involve moral duty, overdevelopment, and groundwater preservation, while fewer mentions were made of mental well-being, heritage, and physical health. Overall, the data highlights a strong ecological and environmental motivation behind the public's overwhelming support for preservation. These findings suggest that citizens view the Vetal Tekdi as a vital natural asset integral to the city's environmental health and sustainability.

Graph 4. *Citizens Ranking of Reasons for Preserving Vetal Tekdi*

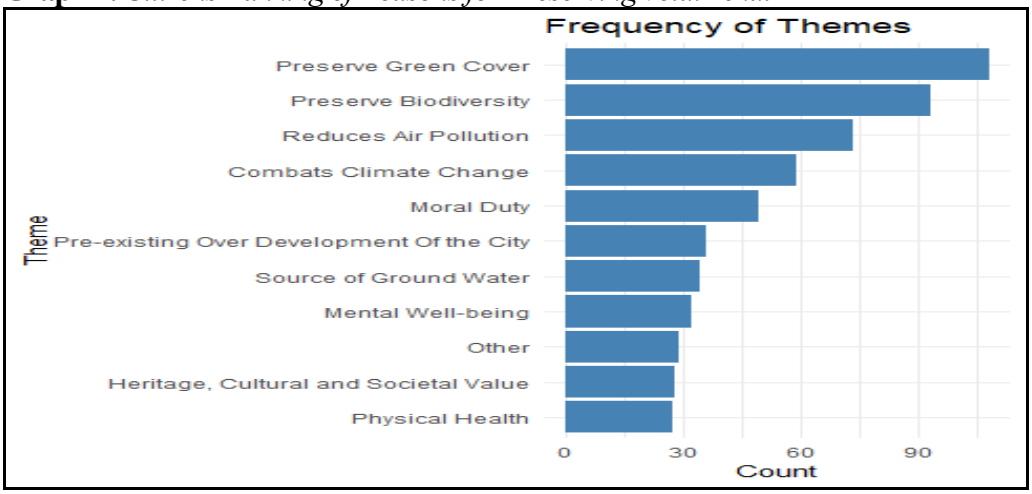

Willingness to pay for Tekdi Conservation

The "willingness to pay" can be considered as the demand price, the value or benefit a consumer expects to receive from consumption of the commodity, it is considered a measure of the marginal benefit, the increase in benefit associated with consuming another unit of the good, (Callan, 2019).

Graph 5. *Willing to pay for Tekdi Conservation*

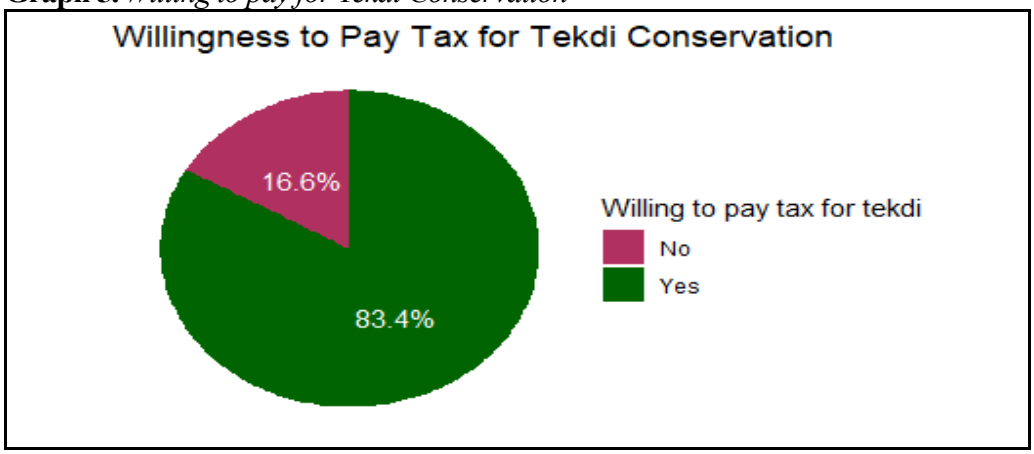

The survey collected data on how much citizens were ready to pay for the conservation of the Urban Forest – Vetal Tekdi. The result is shown in Graph 5.

In Graph 5, 83.4% of the citizens are willing to pay a tax to support the conservation of Vetal Tekdi. This indicates that citizens know they benefit from the presence of the urban forest and are ready to contribute financially to the Tekdi's preservation.

Graph 6. *Amount Citizens will pay for the Urban Forest Vetal Tekdi Conservation*

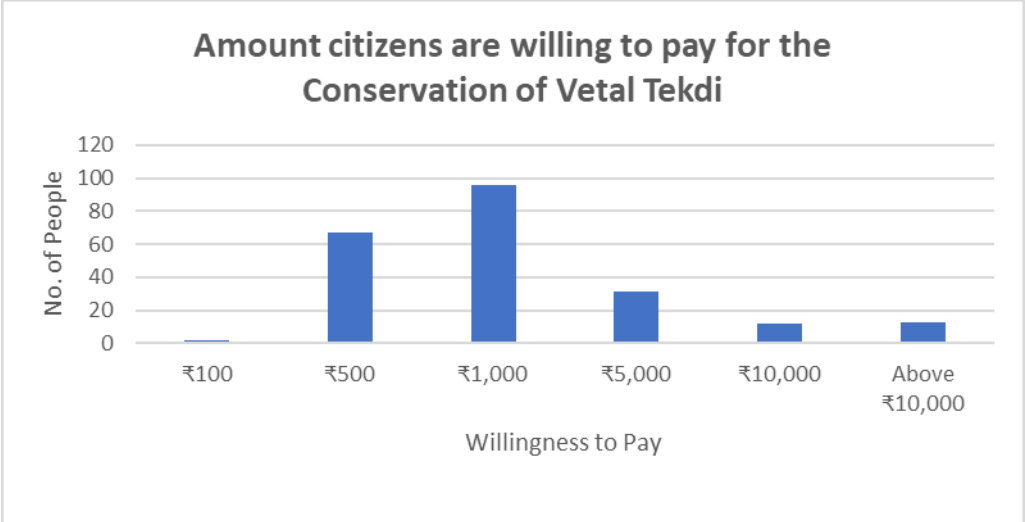

Graph 6 shows the amount citizens are ready to pay for conserving Vetal Tekdi, with most willing to contribute ₹1000 and then ₹ 500, indicating a higher willingness to pay for the conservation of the urban forest. Considering the respondents are from the middle-income group, it is notable that they are ready to pay higher for the conservation of resources. Willingness declines sharply for amounts above ₹1,000 and below ₹500, with very few selecting other amounts. For the purpose of calculation, the average willingness to pay comes to ₹ 3230.435. The willingness to pay increases sharply initially, and then tapers down more gradually at higher amounts indicating a sharp increase in utility of this environmental service, and a decrease in the utility

which can be interpreted as a wide range over which the urban forest has high utility. These insights are useful for designing entry fees for the use of the urban forest, or for realistic fundraising strategies, suggesting that ₹500–₹1,000 is the most acceptable contribution range for the majority.

Section C

Section C focuses on the Vetal Baba Mandir (Temple), analysing its community significance based on visit frequency, perceived importance, preference for preservation over development, and willingness to contribute financially. It combines quantitative and qualitative insights to assess the temple's role in citizens' lives. Further the results show that 69% of respondents reported visiting Vetal Baba Temple, while only 16 respondents said they never visited the site. This indicates a fairly large public engagement with the Mandir, however in varying capacity.

Graph 7 shows that 35.5% of respondents rated the temple as highly important (5), followed by 20% rating it a 4. About 30% gave moderate scores (2 or 3), and 14.1% rated it as least important (1). Overall, most respondents view the temple as important, though opinions vary.

Graph 7. *Preference of Respondents for Preservation of Temple or Housing Development*

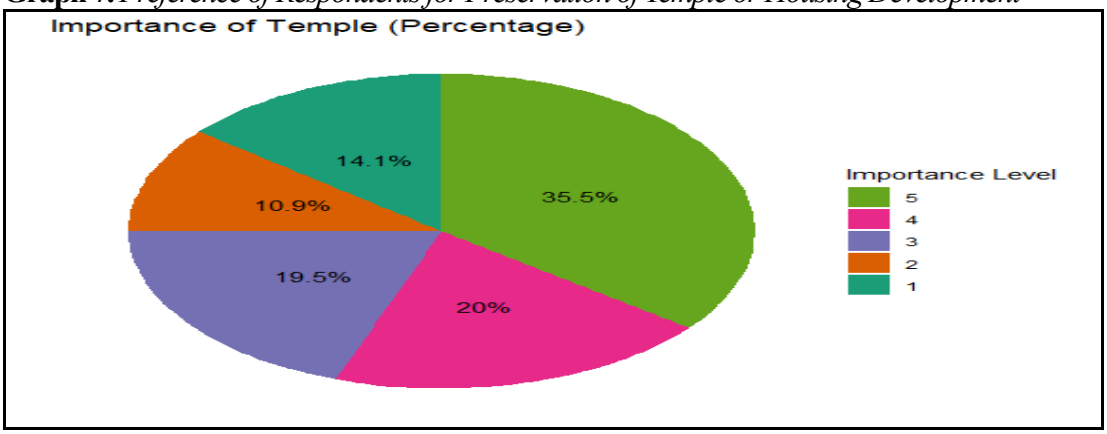

Graph 8 shows that 93.2% of respondents prefer preserving the temple, while only 6.8% support housing development. This reflects strong public consensus for temple preservation.

Graph 8. *Preference of Respondents for Preservation of Temple or Housing Development*

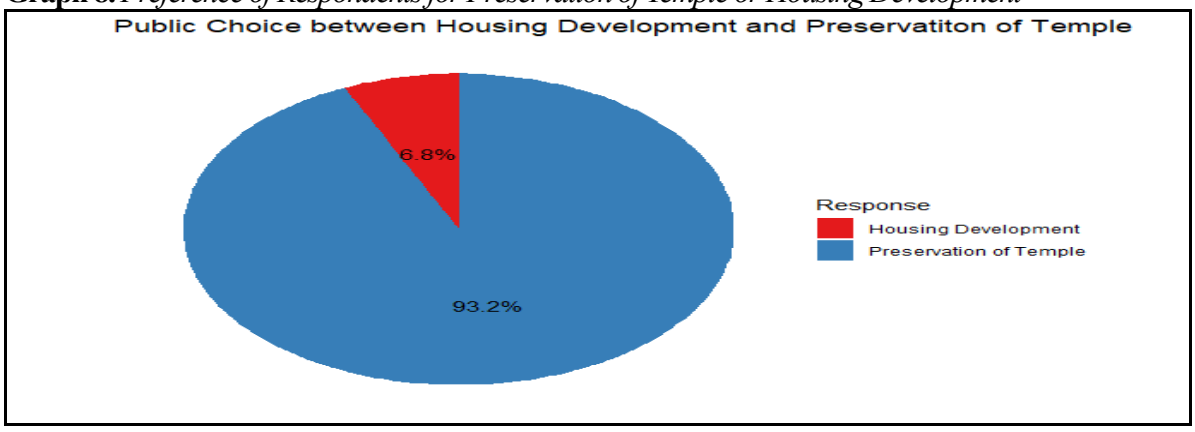

Graph 9 shows a nearly even split in public opinion on financially contributing to temple preservation, with 50.9% willing to pay and 49.1% unwilling. Citizens seem to be divided on their opinion of preserving the temple.

Graph 9. *Willingness to pay for Temple*

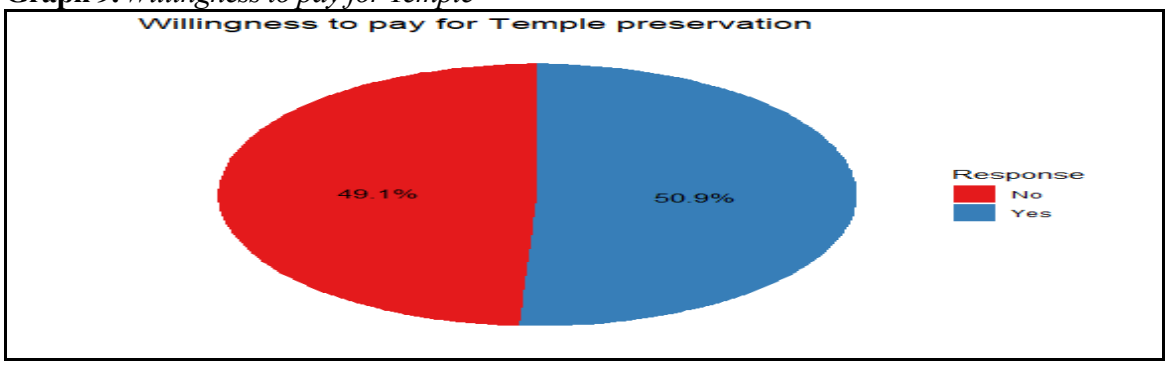

Graph 10. *Willingness to Pay for Temple Conservation*

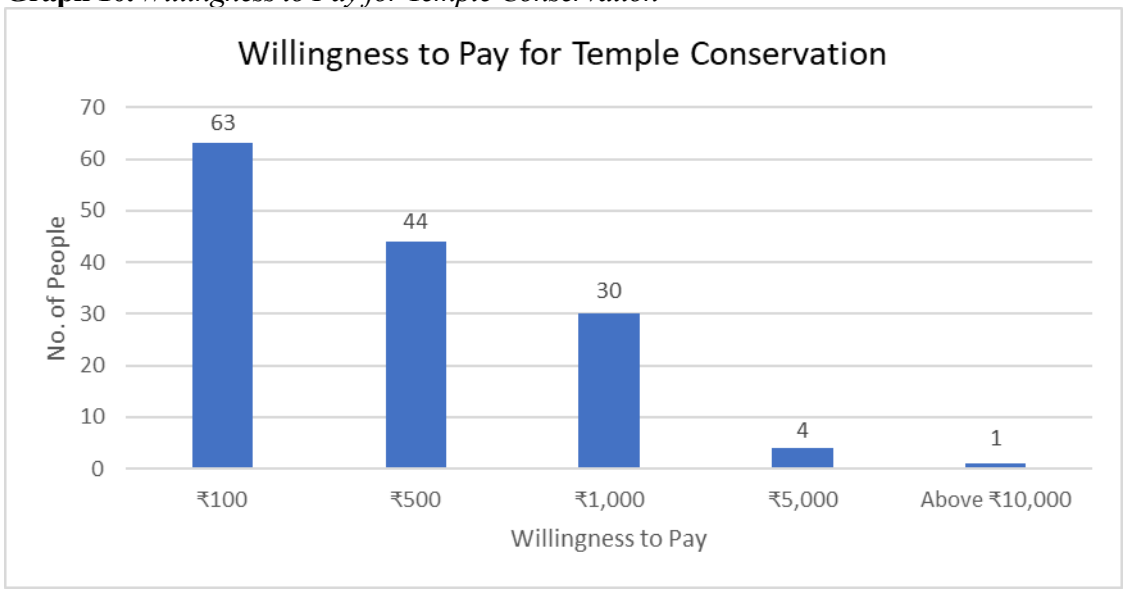

Graph 10 shows respondents' willingness to pay for temple improvement, with most (over 60) preferring to contribute ₹100. The number drops for ₹500 (40–50) and ₹1,000 (30), and significantly fewer opt for ₹5,000 or ₹10,000.

This pattern reflects a typical demand curve—willingness to pay declines as cost increases, indicating diminishing marginal utility. The sharp drop at higher amounts suggests price sensitivity, emphasizing the need to target lower contributions for effective fundraising.

The analysis confirms that perceived importance strongly influences willingness to contribute financially. Understanding public sentiment toward cultural landmarks can help policymakers design more effective, community-aligned conservation strategies.

Section D

This section uses the Travel Cost method to arrive at the Willingness to Pay for the Vetal Tekdi environmental services. It delves into the logistical dynamics of accessing Vetal Tekdi, focusing on the modes of transportation, distances travelled, and associated costs. The section examines the preferences of respondents regarding their choice of transportation, the type of private vehicles used, and the financial implications of using public transport, taxis, or auto-rickshaws.

Graph 11. *Mode of Transport used to reach Vetal Tekdi*

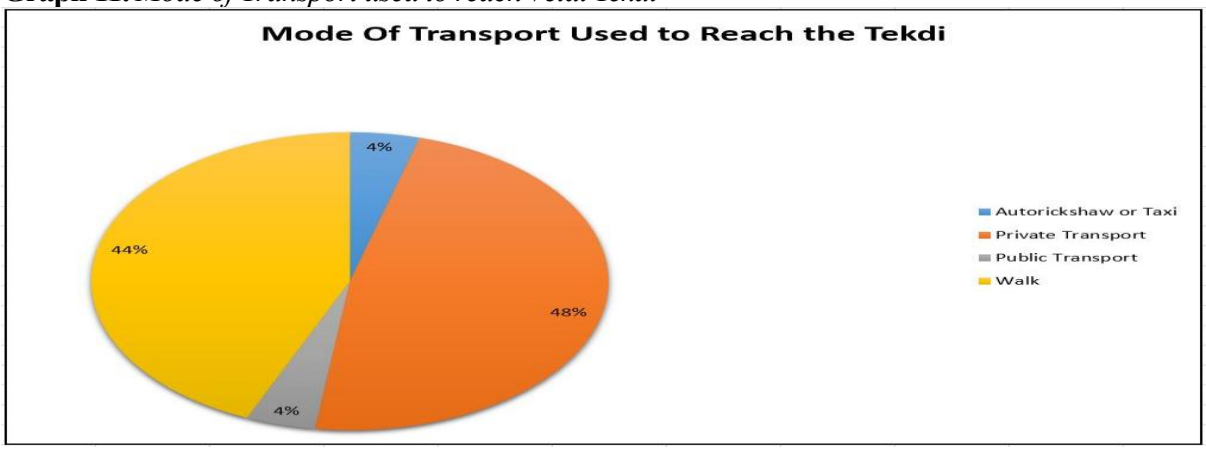

Examining the mode of transport used by citizens to reach Vetal Tekdi shows the following results in the pie chart in Graph11. About 48% of the respondents use private vehicles and 44% walk, highlighting a strong reliance on personal transport or close proximity while only 4% each use public transport or autos/taxis. Among private vehicle users, two-wheelers (50%) are far more common than four-wheelers (20%), indicating that citizens prefer environmentally friendly and less costly modes of reaching the urban forest. Most private vehicle users (20%) live within 1–3 km of the Tekdi, with numbers declining as distance increases, suggesting that proximity influences travel mode.

Graph 12 shows the distribution of bus travel costs to Vetal Tekdi. A majority (143 respondents) reported zero cost, suggesting they either live nearby or use passes/ subsidies. Costs between ₹10–50 were reported by fewer respondents, with only 6

people each in the ₹40–50 and >₹50 categories, indicating limited higher-cost travel. Table 4 shows the total bus travel cost was ₹1,570, with an average cost of ₹24.53 per person. This indicates that while some incur moderate costs, many access Vetal Tekdi at little or no expense.

Graph12. *Total Cost of traveling to the Tekdi via Bus (Public Transportation)*

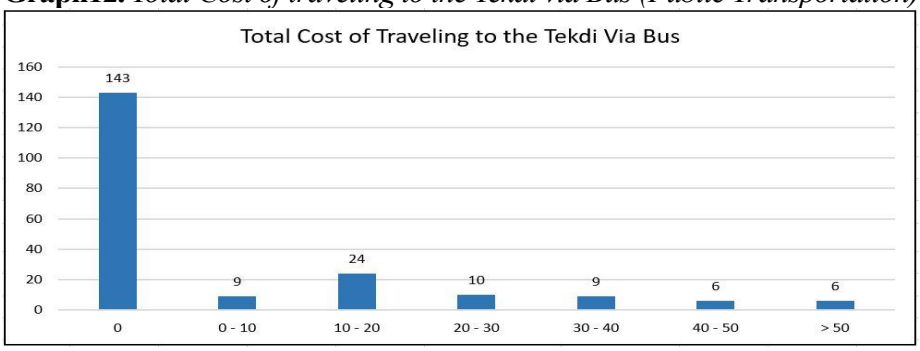

Table 4. *Average Cost of taking Public Transport to the Tekdi*

People who take the Bus	
TC	1570
AC	24.53125

Graph 13. *Total Cost of traveling to the Tekdi via Taxi or Auto*

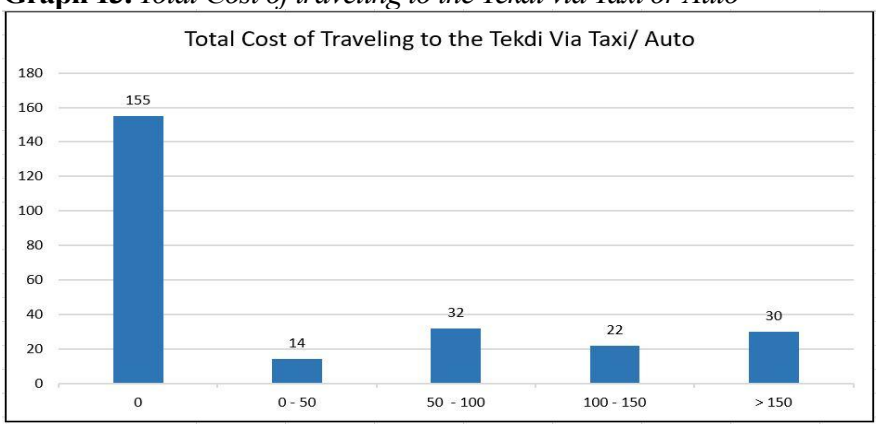

Table 5. *Average Cost of taking Taxi or Auto to Vetal Tekdi*

People Who Take a Taxi/ Auto	
TC	10750
AC	109.6938776

Graph 13 displays the distribution of travel costs for respondents using taxis or auto-rickshaws to reach Vetal Tekdi. About 60% respondents reported zero cost, indicating many live nearby or used free/subsidised transport. As cost increases, the number of respondents declines sharply, with the highest cost category (>₹150) having only 12% respondents. The accompanying table 5 shows the total cost incurred by all users of this transport mode, about ₹10,750, with an average cost of ₹109.69 per

person. This shows higher provides a clear snapshot of the typical financial burden for those using taxis or auto-rickshaws.

It is clear that the travel Cost method used here is more indicative of willingness to use physical exercise to reach and use this urban forest, it is also indicative of the environmental nature of the citizens participating in the survey.

Conclusion

The analysis affirms Vetal Tekdi's vital role as an ecological, recreational, and cultural asset. Urban green spaces like the Tekdi enhance sustainability, mental well-being, and quality of life, with survey findings revealing a strong community connection and overwhelming support for its preservation over urban development.

Final Findings and Results: The Simulator

The methodology for this research was to create a simulator that will assimilate all the values for each parameter automatically to give us the final result, that is the monetary value of the ES of the Urban Forest, Vetal Tekdi, Pune. Table 6 below is one such simulator that can automatically assess the annual value of the urban forest with differing data input each year.

There are seven parameters recorded here, value of the water in the wetlands, value of the carbon sequestration of the different types of trees, value of the oxygen produced, value of the biodiversity of the urban forest including the wetlands, value of the water in the aquifers, heritage value of the Vetal Temple, and the Hanuman temple, the latter part is a part of the amenity value. The biodiversity value covers the value of the following species, namely, odonates, dragonflies, butterflies, invertebrates, and birds. Together these form the valuation of the urban forest, the trees through carbon sequestration and production of oxygen, biodiversity, wetlands, water from the aquifers, and the amenity valuation. We have also added the use value of the land of the urban forest, namely, its market value, this valuation is treated additionally at the end in the simulator.

Willingness to Pay has been treated separately due to lack of data on the number of citizens visiting the urban forest daily/annually, and hence is not a part of the valuation, and will thus reduce the valuation by that extent.

Another important point to note is that this is a very conservative valuation as nature’s services are very intricate, one cannot fathom how each creature, big or small contributes to the efficient functioning of an ecosystem. Willingness to Pay, contingent valuation also could not be added due to lack of data, hence the valuation of the urban forest is a conservative one.

Valuation of the Urban Forest Vetal Tekdi

The annual value of the Environmental Services of the Urban Forest, namely, Vetal Tekdi is presented below in table 6 and is **$ 171.35 Billion**. The value of the water in the aquifers is the highest, a steep Rs. 14.62 trillion, or, $170 billion approximately. Followed by the water in the quarry, Rs. 98,28,00,000, or US $ 11 million approximately. The biodiversity valuation is Rs 1,537,000 or $453,774, carbon sequestration Rs.1,614,870, Oxygen, Rs. 66,945,840, heritage value of Vetal Temple, Rs. 74,368,869, heritage value of Hanuman Temple, is Rs. 10,665,430. Additionally, after we use the market price of the land of the urban forest, the total value goes up to, Rs. 16.5 trillion, or US $ 194.29 billion.

Table 6. *Annual Valuation of the ES of the Urban Forest, Vetal Tekdi, Pune*

Annual Valuation of the Environmental Services of the Urban Forest - Vetal Tekdi, Pune 2024 – 2025				
Parameters for Valuation	**Valuation in Sample Area**	**No. of Samples**	**Valuation of Entire Urban Forest**	
i. Value of Water Present in the Quarry	₹ 98,28,00,000	1	₹ 98,28,00,000	
ii. Value of Carbon Sequestration	₹ 1,61,487	10	₹ 16,14,870	
iii. Value of Oxygen Production	₹ 66,94,584	10	₹ 6,69,45,840	
iv. Value of Biodiversity				
iv.a. Odonates & Dragonflies	₹ 54,000	10	₹ 5,40,000	
iv.b. Invertebrates	₹ 2,46,000	10	₹ 24,60,000	
iv.d. Butterfly	₹ 87,000	10	₹ 8,70,000	
iv.c. Birds	₹ 10,96,000	10	₹ 1,09,60,000	
v. Value of Water in Aquifers	₹ 1,46,28,74,60,00,000	1	₹ 1,46,28,74,60,00,000	
vi. Heritage Value of Vetal Temple	₹ 7,43,68,868.89	1	₹ 7,43,68,869	
vii. Heritage Value of Hanuman Temple	₹ 1,06,65,430.13	1	₹ 1,06,65,430	
Sub-Total Value of Urban Forest			**₹ 1,46,29,89,72,25,009**	**~ ₹ 14.6 Trillion**
			$ 1,71,35,04,00,855*	**~$ 171.35 Billion**
viii. Value of the Tekdi Land (Use Value)	₹ 19,58,65,89,55,939		₹ 19,58,65,89,55,939	
Total Value of Urban Forest			**₹ 1,65,88,55,61,80,948**	**~₹ 16.5 Trillion**
			$ 1,94,29,08,89,915*	**~$ 194.29 Billion**

*US Dollar to Rupee conversion rate of 4 July 2025 was used.

A second valuation of the ES of the Urban Forest was worked out by substituting the India's Supreme valuation of trees in the simulator, the result was approximately the same, proving our tree valuation was accurate. All other valuations remain the same.

Table 7. *Valuation According to Supreme Court of India*

Annual Valuation of the Environmental Services of the Urban Forest - Vetal Tekdi, Pune 2024 – 2025				
Parameters for Valuation	**Valuation of Sample Area**	**No. of Samples**	**Valuation of Entire Urban Forest**	
i. Value of Water Present in the Quarry	₹ 98,28,00,000	1	₹ 98,28,00,000	
ii. Value of Trees (Supreme Court of India**)	₹ 2,24,99,000	10	₹ 22,49,90,000	
iii. Biodiversity				
iii.a. Odonates & Dragonflies	₹ 54,000	10	₹ 5,40,000	
iii.b. Invertebrates	₹ 2,46,000	10	₹ 24,60,000	
iii.c. Birds	₹ 10,96,000	10	₹ 1,09,60,000	
iii.d. Butterfly	₹ 87,000	10	₹ 8,70,000	
iv. Value of Water in Aquifers	₹ 1,46,28,74,60,00,000	1	₹ 1,46,28,74,60,00,000	
v. Heritage Value of Vetal Mandir	₹ 7,43,68,869	1	₹ 7,43,68,869	
vi. Heritage Value of Hanuman Mandir	₹ 1,06,65,430	1	₹ 1,06,65,430	
Sub-Total Value of Urban Forest			**₹ 1,46,30,05,36,54,299**	**~ ₹ 14.6 Trillion**
			$ 1,71,35,22,33,009 *	**~ $ 171.35 Billion**
vii. Value of Tekdi Land (Use Value)	₹ 19,58,65,89,55,939		₹ 19,58,65,89,55,939	
Total Value of Urban Forest			**₹ 1,65,88,71,26,10,238**	**~ ₹ 16.5 Trillion**
			$ 1,94,29,27,22,069 *	**~ $ 194.29 Billion**

*US Dollar to Rupee conversion rate of 4 July 2025 was used.
**Supreme Court has given the value of 1 tree. Is equal to ₹ 74,500.

The annual value of the Environmental Services of the Urban Forest, namely, Vetal Tekdi is presented above in table 6 and is **$ 171.35 Billion**. The value of the water in the aquifers is the highest, a steep Rs. 14.62 trillion, or, $170 billion approximately. Followed by the water in the quarry, Rs. 98,28,00,000, or US $11 million approximately. The biodiversity valuation is Rs 1,537,000 or $453,774, carbon sequestration Rs.1,614,870, Oxygen, Rs. 66,945,840, heritage value of Vetal Temple, Rs. 74,368,869, heritage value of Hanuman Temple, is Rs. 10,665,430. Additionally, after we use the market price of the land of the urban forest, the total value goes up to, Rs. 16.5 trillion, or US $ 194.29

Conclusion

Urban forests provide crucial environmental services, ecological, recreational, cultural, and the urban forest - Vetal Tekdi, Pune has additionally pristine, ancient aquifers, alongside new wetlands formed from previous stone quarries, and very old temples that have cultural and heritage value. The urban forest is part of very old mountain ranges, these mountains are hotspots of biodiversity, there are multiple species of flora and fauna that contribute to the health of the ecosystem. In turn, all these services facilitate good health of the population of the city, both mental and physical, besides providing a robust environment for the flourishing of biodiversity. The aquifers here are the source of clean water to the intricate underground network of streams and ground water. For the aquifers, the rapid population growth in Pune underscores the critical importance of sustainable water management. The aquifers, a gift of nature, emerge as an invaluable resource, holding a staggering 73,143.728 crore litres of water, with a very high monetary value. Protecting and optimizing the utilization of aquifers is not merely a matter of convenience but a necessity to bridge the gap between supply and demand, ensuring Pune's water security for its growing population.

The analysis affirms Vetal Tekdi's vital role as an ecological, recreational, and cultural asset. Urban green spaces like the Tekdi enhance sustainability, mental well-being, and quality of life, with survey findings revealing a strong community connection and overwhelming support for its preservation over urban development. When such urban spaces are protected, they support the health of the population ensuring a healthy and happy life of the citizens while also improving productivity as a result of good health.

This study aimed to do the valuation of the all the services of the Vetal Tekdi, the urban forest at the centre of the city. Multiple valuation methods were used for the purpose, use value, existence value, market value, travel cost method, amenity valuation, expert opinion for the biodiversity, contingent valuation, and hedonic pricing to suit the diverse services of the richly endowed urban forest.

Value of the Wetlands was immense as was that of aquifers, the rain water stored in these newly formed wetlands nestled on top of the hill is not touched by any pollution as it is not exposed to any industrial/commercial human activity. The value of Carbon Sequestration was ₹ 61,487 and of Oxygen Production ₹ 66,94,584. Biodiversity was valued annually at Rs 1,537,000 or $ 453,774, and covered insects, odonates, dragonflies, butterflies and birds. Experts from the field were consulted for their view on the value of these essential species, the species covered were however not exhaustive, hence the valuation is very conservative.

The amenity valuation by citizens in the form of recreational, physical and study activities highlighted near-unanimous support (90.1%) for Tekdi's conservation. It was valued for its environmental benefits and as a space for mental and physical health. A significant majority (83.4%) were willing to contribute financially, especially in the ₹500–₹1,000 range, to note here, the willingness to pay was driven more by values and awareness than by income levels.

The heritage value revealed a nuanced view of the Vetal Baba Temple. While visit frequency was low, 35.5% of respondents rated its importance at the highest level. A dominant 93.2% support preserving the temple over housing development.

Again, perceived importance, not income, was the key factor influencing willingness to pay, indicating the need for value-based fundraising.

The Travel Cost method outlined transportation trends. Walking followed closely behind private vehicles, especially two-wheelers, reflecting a trend for physical fitness and proximity to the urban forest, hence many incurred no travel costs, promoting sustainable, low-cost transport.

The simulator that collated all the resulting values for the various services showed an annual value of the Environmental Services of the Urban Forest, namely, Vetal Tekdi at: $ 171.35 Billion. This included the value of the water in the aquifers, at Rs. 14.62 trillion, or, $170 billion approximately, the water in the quarry at, Rs. 98,28,00,000, or US $ 11 million approximately, the biodiversity valuation at Rs 1,537,000 or $453,774, carbon sequestration at Rs.1,614,870, oxygen at, Rs. 66,945,840, heritage value of Vetal Temple at, Rs. 74,368,869, heritage value of Hanuman Temple, at Rs. 10,665,430, adding the market value of the land at ₹ 19,58,65,89,55,939, gave a total value of Rs. 16.5 trillion, or US $ 194.29 billion to the urban forest Vetal Tekdi.

In conclusion, the six billion old urban forest, Vetal Tekdi is abundantly endowed with multiple environmental services as it is part of a biodiversity hotspot, and while we can conduct only a conservative assessment of its services, it's annual value monetised stands at a huge Rs. 14.6 trillion, or US $ 171.35 Billion. If we add the market value of the land the valuation is Rs. 16.5 trillion, or US $ 194.29 billion annually.

Limitations of the study are that the biodiversity valuation is not exhaustive, the biodiversity valuation is limited to the species of fauna; flora is not considered, the value of the pristine waters of the aquifers is far higher than the market value per litre of drinking water chosen. Also, the Willingness to Pay for the urban forest's services could not be included in the valuation due to the lack of data regarding the number of people using the urban forest. Hence the overall valuation is limited by these shortcomings.

Data paints a clear picture of Vetal Tekdi as an invaluable urban green space that provides wide-ranging benefits extending beyond mere recreation to ecological preservation, community health, and cultural heritage. While urbanization pressures persist, the strong public preference for conservation signals the need for policymakers to prioritize sustainable development strategies. By balancing urban growth with environmental preservation, stakeholders can ensure that essential spaces like Vetal Tekdi remain integral to the city's environmental and cultural fabric. The insights from this report should guide stakeholders in devising informed, community-driven solutions that respect both environmental imperatives and urban development needs. Policy recommendations of this study are that decision makers should use the valuation tools while evaluating projects for implementation. Selection of projects should be on this basis. A cost benefit analysis based on environmental valuation should be used for such decision making.

Strong recommendations of this study are to conduct more such valuations of aquifers and urban forests as both are undermined in their value and often sacrificed in the name of development, hence, both require protection and strong support from empirical research.

More than a green space, the urban forest is a vital part of Pune's ecological, cultural, and community landscape. Strong public support for its conservation calls for sustainable urban planning that protects such spaces. Policymakers must leverage

community values and accessibility insights to craft inclusive, eco-conscious development strategies. This invaluable natural endowment will compromise sustainability and deprive future generations of its valuable services if sacrificed to urbanisation.

Acknowledgements

We are indebted to Dr. Himanshu Kulkarni, previous Founder, Trustee, and Executive Director, ACWADAM, currently, Founder Trustee and Scientist Emeritus for his extensive work on aquifers and groundwater; our aquifer water valuation was based on his guidance and the aquifer details in the ACWADAM Report on groundwater.

References

Aevermann T, Schmude J (2015) Quantification and monetary valuation of urban ecosystem services in Munich, Germany. *Zeitschrift für Wirtschaftsgeographie, 59*(3), 188–200. https://doi.org/10.1515/zfw-2015-0304

Alvarez S, Soto JR, Escobedo FJ, Lai J, Kibria ASMG, Adams DC (2021) Heterogeneous preferences and economic values for urban forest structural and functional attributes. *Landscape and Urban Planning, 215*, 104234. https://doi.org/10.1016/j.landurbplan.2021.104234

Bangladesh Forest Department. (n.d.). *Bangladesh Forest Information System*. https://bfis.Bforest.gov.bd

Bernath K, Roschewitz A (2008). Recreational benefits of urban forests: Explaining visitors' willingness to pay in the context of the theory of planned behavior. *Journal of Environmental Management, 89*(3), 155–166. https://doi.org/10.1016/j.jenvman.2007.01.059

Bockarjova M, Botzen WJW, Koetse MJ (2020. Economic valuation of green and blue nature in cities: A meta-analysis. *Ecological Economics, 169*, 106480. https://doi.org/10.1016/j.ecolecon.2019.106480

Bockarjova M, Botzen WJW, Koetse MJ (2020) Economic valuation of green and blue nature in cities: A meta-analysis. *Ecological Economics, 169*, 106480. https://doi.org/10.1016/j.ecolecon.2019.106480

Callan SJ, Thomas JM (2013) *Environmental economics and management: Theory, policy, and applications* (6th ed.). Cengage Learning.

Chen L, Yao X, Liu Y, Zhu Y, Chen W, Zhao X, Chi T (2020) Measuring impacts of urban environmental elements on housing prices based on multisource data—a case study of Shanghai, China. *ISPRS International Journal of Geo-Information, 9*, 106. https://doi.org/10.3390/ijgi9020106

Chen WY, Jim CY (2008) Cost–benefit analysis of the leisure value of urban greening in the new Chinese city of Zhuhai. *Cities, 25*(5), 298–309. https://doi.org/10.1016/j.cities.2008.06.002

Chen Y, Liu G, Yang Q, Li H, Deng X, Ulgiati S (2022) Valuing regulating services of urban ecosystems towards more comprehensive house pricing. *Journal of Cleaner Production, 357*, 132030. https://doi.org/10.1016/j.jclepro.2022.132030

Chen Y, Liu G, Yang Q, Li H, Deng X, Ulgiati S (2022) Valuing regulating services of urban ecosystems towards more comprehensive house pricing. *Journal of Cleaner Production, 357*, 132030. https://doi.org/10.1016/j.jclepro.2022.132030

Chen Y, Yue W, La Rosa D (2020) Which communities have better accessibility to green space? An investigation into environmental inequality using big data. *Landscape and Urban Planning, 204*, 103919. https://doi.org/10.1016/j.landurbplan.2020.103919

Chi D, Aerts R, Van NA, Bauwelinck M, Demoury C, Plusquin M, Nawrot TS, Casas L, Somers B (2022) Residential exposure to urban trees and medication sales for mood disorders and cardiovascular disease in Brussels, Belgium: An ecological study. *Environmental Health Perspectives, 130*, 057003. https://doi.org/10.1289/EHP9924

Croci E, Lucchitta B, Penati T (2021) Valuing ecosystem services at the urban level: A critical review. *Sustainability, 13*. https://doi.org/10.3390/su13031129

Dadvand P, Villanueva CM, Font-Ribera L, Martinez D, Basaga X, Belmonte J, Vrijheid M, Gražulevičienė R, Kogevinas M, Nieuwenhuijsen MJ (2014) Risks and benefits of green spaces for children: A cross-sectional study of associations with sedentary behavior, obesity, asthma, and allergy. *Environmental Health Perspectives, 122*, 1329–1335. https://doi.org/10.1289/ehp.1308038

del Saz Salazar S, García Menéndez L (2007) Estimating the non-market benefits of an urban park: Does proximity matter? *Land Use Policy, 24*(1), 296–305. https://doi.org/10.1016/j.landusepol.2005.05.011

Dennis M, James P (2016) Considerations in the valuation of urban green space: Accounting for user participation. *Ecosystem Services, 21*, 120–129. https://doi.org/10.1016/j.ecoser.2016.08.003

Elmqvist T, Setälä H, Handel S, van der Ploeg S, Aronson J, Blignaut J, Gómez-Baggethun E, Nowak D, Kronenberg J, de Groot R (2015) Benefits of restoring ecosystem services in urban areas. *Current Opinion in Environmental Sustainability, 14*, 101–108. https://doi.org/10.1016/j.cosust.2015.05.001

Escobedo FJ, Adams DC, Timilsina N (2015) Urban Forest structure effects on property value. *Ecosystem Services, 12*, 209–217. https://doi.org/10.1016/j.ecoser.2014.05.002

Escobedo FJ, Kroeger T, Wagner JE (2011) Urban forests and pollution mitigation: Analyzing ecosystem services and disservices. *Environmental Pollution, 159*, 2078–2087. https://doi.org/10.1016/j.envpol.2011.01.010

Food and Agriculture Organization of the United Nations (2016) *Guidelines on urban and peri-urban forestry* (F. Salbitano, S. Borelli, M. Conigliaro, & Y. Chen, Eds.). https://www.fao.org/3/i6210e/i6210e.pdf

Frühauf A, Niedermeier M, Elliott LR, Ledochowski L, Marksteiner J, Kopp M (2016) Acute effects of outdoor physical activity on affect and psychological well-being in depressed patients – A preliminary study. *Mental Health and Physical Activity, 10*, 4–9. https://doi.org/10.1016/j.mhpa.2016.02.002

Giacinto JJ, Fricker GA, Ritter M, Yost J, Doremus J (2021) Urban forest biodiversity and cardiovascular disease: Potential health benefits from California's street trees. *PLoS ONE, 16*, e0254973. https://doi.org/10.1371/journal.pone.0254973

Goldman RL (2010) Ecosystem services: How people benefit from nature. *Environment, 52*(5), 15–23.

Katila P, Colfer CJP, de Jong W, Galloway G, Pacheco P, Winkel G (2019) *Sustainable development goals: Their impacts on forests and people*. Cambridge University Press. https://doi.org/10.1017/9781108765015

Kusminingrum N (2008) Potensi tanaman dalam menyerap CO_2 dan CO untuk mengurangi dampak pemanasan global [The potential of plants to absorb CO_2 and CO to reduce the impact of global warming]. *Jurnal Permukiman*, *3*(2), 96–105. https://jurnalpermukiman.pu.go.id/index.php/jp/article/view/96

Langemeyer J, Baró F, Roebeling P, Gómez-Baggethun E (2015) Contrasting values of cultural ecosystem services in urban areas: The case of park Montjuïc in Barcelona. *Ecosystem Services, 12*, 178–186. https://doi.org/10.1016/j.ecoser.2014.11.016

Liu Z, Hanley N, Campbell D (2020) Linking urban air pollution with residents' willingness to pay for greenspace: A choice experiment study in Beijing. *Journal of Environmental Economics and Management, 104*, 102383. https://doi.org/10.1016/j.jeem.2020.102383

Maharashtra Jeevan Pradhikaran. (2014) Water supply system for Pune city: Detailed project report. Government of Maharashtra.

McPhearson T, Kremer P, Hamstead ZA (2013) Mapping ecosystem services in New York City: Applying a social–ecological approach in urban vacant land. *Ecosystem Services, 5*, 11–26. https://doi.org/10.1016/j.ecoser.2013.06.005

McPherson EG, Xiao Q, van Doorn NS, de Goede J, Bjorkman J, Hollander A, Boynton RM, Quinn JF, Thorne JH (2017) The structure, function and value of urban forests in California communities. *Urban Forestry & Urban Greening, 28*, 43–53. https://doi.org/10.1016/j.ufug.2017.09.013

Meher M (2024) *Understanding ecosystem services: A comprehensive analysis of importance and implications*. Just Agriculture. https://justagriculture.in/files/newsletter/2024/may/61.%20Understanding%20Ecosystem%20Services-%20A%20Comprehensive%20Analysis%20of%20Importance%20and%20Implications.pdf

Mei Y, Hite D, Sohngen B (2017) Demand for urban tree cover: A two-stage hedonic price analysis in California. *Forest Policy and Economics, 83*, 29–35. https://doi.org/10.1016/j.forpol.2017.05.009

Middel A, Chhetri N, Quay R (2015) Urban forestry and cool roofs: Assessment of heat mitigation strategies in Phoenix residential neighborhoods. *Urban Forestry & Urban Greening, 14*, 178–186. https://doi.org/10.1016/j.ufug.2014.09.010

Nalwalla S (2021) *Know your city: Vetal Tekdi, a 'mini-Sahyadri' named after a malevolent god*. Whatshot.in. https://www.whatshot.in/pune/how-vetal-tekdi-got-its-name-c-32945

Nijhum F, Westbrook C, Noble B, Belcher K, Lloyd-Smith P (2021) Evaluation of alternative land-use scenarios using an ecosystem services-based strategic environmental assessment approach. *Land Use Policy, 108*, 105540. https://doi.org/10.1016/j.landusepol.2021.105540

Nowak DJ, Hirabayashi S, Bodine A, Greenfield E (2014) Tree and forest effects on air quality and human health in the United States. *Environmental Pollution, 193*, 119–129. https://doi.org/10.1016/j.envpol.2014.05.028

Nowak DJ, Hirabayashi S, Doyle M, McGovern M, Pasher J (2018) Air pollution removal by urban forests in Canada and its effect on air quality and human health. *Urban Forestry & Urban Greening, 29*, 40–48. https://doi.org/10.1016/j.ufug.2017.10.019

Nowak DJ, Stein SM, Randler PB, Greenfield EJ, Comas SJ, Carr MA, Alig RJ (2010) *Sustaining America's urban trees and forests: A Forests on the Edge report*. U.S. Forest Service. https://www.fs.fed.us/openspace/fote/reports/nrs-62_sustaining_americas_urban.pdf

Pune Metropolitan Urban Region Population 2011-2025 Census (2025) *Census2011.Co.in.* https://www.census2011.co.in/census/metropolitan/306-pune.html

Prasanthi S (2025) *Chipko Movement, the anti-deforestation tree-hugging protest by rural women in India*. Green Network Asia. https://greennetwork.asia/featured/chipko-movement-the-anti-deforestation-tree-hugging-protest-by-rural-women-in-india/

Söderman T, Kopperoinen L, Shemeikka P, Yli-Pelkonen V (2012) Ecosystem services criteria for sustainable development in urban regions. *Journal of Environmental Assessment Policy and Management, 14*(2), 1250008. https://doi.org/10.1142/S14643 33212500081

Tammi I, Mustajärvi K, Rasinmäki J (2017) Integrating spatial valuation of ecosystem services into regional planning and development. *Ecosystem Services, 26*, 329–344. https://doi.org/10.1016/j.ecoser.2016.11.008

Taylor MS, Wheeler BW, White MP, Economou T, Osborne NJ (2015) Research note: Urban street tree density and antidepressant prescription rates—a cross-sectional study in London, UK. *Landscape and Urban Planning, 136*, 174–179. https://doi.org/10.1016/j.landurbplan.2014.12.005

TNN (2023) Population up, we need more water: PMC to irrigation dept. The Times of India; Times Of India. https://timesofindia.indiatimes.com/city/pune/population-up-we-need-more-water-pmc-to-irrigation-dept/articleshow/104513004.cms

Tyrväinen L (1997) The amenity value of the urban forest: An application of the hedonic pricing method. *Landscape and Urban Planning, 37*(3), 211–222. https://doi.org/10.016/S0169-2046(97)80005-9

Tyrväinen L (2001) Economic valuation of urban forest benefits in Finland. *Journal of Environmental Management, 62*, 75–92. https://doi.org/10.1006/jema.2001.0421

Tyrväinen L, Väänänen H (1998) The economic value of urban forest amenities: An application of the contingent valuation method. *Landscape and Urban Planning, 43*(1–3), 105–118. https://doi.org/10.1016/S0169-2046(98)00103-0

United Nations University (n.d.) *Ecosystems for sustainability*. UNU-EHS. https://unu.edu/ehs/our-work/risk-adaptation/ecosystems-sustainability

United States Department of Agriculture – Natural Resources Conservation Service. (2023) *Environmental markets*. https://nrcs.prod.usda.gov/

Verma M (n.d.) *Economic valuation of forests of Himachal Pradesh*. Indian Institute of Forest Management.

Wang X, Wang Y, Zhou C, Yin L, Feng X (2021) Urban forest monitoring based on multiple features at the single tree scale by UAV. *Urban Forestry & Urban Greening, 58*, 126958. https://doi.org/10.1016/j.ufug.2020.126958

World Bank (2013) *UAV state of play in development – Case studies: Cadastral & community mapping with UAVs in Albania*. https://uav-development.github.io/case-studies.html#albania

Yang S, Zhao W, Pereira P, Liu Y (2019) Socio-cultural valuation of rural and urban perception on ecosystem services and human well-being in Yanhe watershed of China. *Journal of Environmental Management, 251*, 109615. https://doi.org/10.1016/j.jenvman.2019.109615

Yin S, Peng LLH, Feng N, Wen H, Ling Z, Yang X, Dong L (2022) Spatial-temporal pattern in the cooling effect of a large urban forest and the factors driving it. *Building and Environment, 209*, 108676. https://doi.org/10.1016/j.buildenv.2021.1 08676

Appendix

Graph 1. *Age Distribution of Respondents*

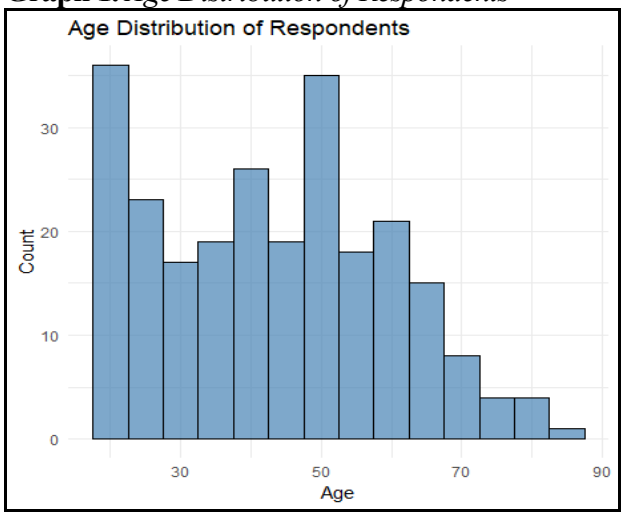

Graph 2. *Gender Distribution of Respondents*

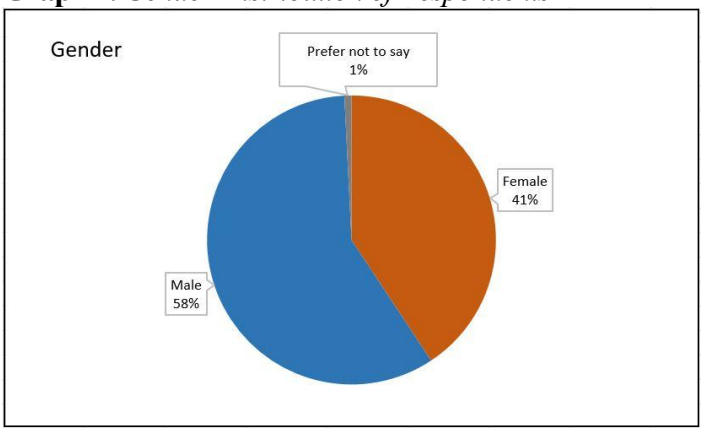

Athens Journal of Sciences - Volume 13, Issue 1, March 2026 – Pages 65-98

Mapping Hydrothermal Alteration Minerals using Landsat 8 and ASTER Data: A Case Study from the Red Sea Hills, NE Sudan

By Mohammed Abdulrauf Mohammed Ibrahim[*] & Evangelos Papadimitriou[±]

Hydrothermal alteration minerals provide key indicators for mineral exploration, particularly in arid and inaccessible regions where field surveys are constrained. This study integrates remote sensing and GIS techniques to map alteration zones in the Red Sea Hills, NE Sudan, using Landsat 8 OLI and ASTER datasets. Preprocessing included FLAASH atmospheric correction and Minimum Noise Fraction (MNF) transformation to enhance spectral integrity. For Landsat 8 diagnostic band ratios and density slicing were applied to highlight ferric/ferrous iron oxides and clay/hydroxyl-bearing minerals, followed by supervised Parallelepiped classification of Sabins band ratios and Crosta transformations to delineate prospective alteration zones. ASTER VNIR-SWIR data enabled higher resolution mapping through Mineral Indices and Spectral Angle Mapper (SAM) classification against USGS spectral library endmembers. These approaches revealed three principal hydrothermal alteration zones: phyllic (muscovite, illite), argillic (kaolinite, alunite), and propylitic (epidote, chlorite). Results demonstrate that Landsat 8 is effective for regional-scale reconnaissance, but ASTER's superior spectral resolution provides more accurate and mineralogically de-tailed alteration mapping. The study underscores the value of ASTER data for early-stage exploration in structurally complex, mineralized terranes such as the Arabian-Nubian Shield.

Keywords: *Hydrothermal alteration; Mineral exploration; ASTER; Landsat 8; Crosta; Band Ratio; Spectral indices; SAM classification; Arabian-Nubian Shield*

Introduction

Remote sensing data from the multispectral Landsat 8 OLI (LC8) and the semi-hyperspectral ASTER (AST) sensors play an important role in locating mineral deposits and in reducing the costs associated with prospecting and exploration (Crósta and Moore 1989, Debba et al. 2005, Carrino et al. 2015, Amer et al. 2016, Alimohammadi et al. 2015). Although commercial mineral deposits are limited in their genetic types and modes of occurrence, a wide range of geological criteria and indicators have been established to support remote sensing techniques in identifying these deposits. These indicators, observable in spaceborne and aerial imagery, include lithological features, rock alteration patterns, structural controls, and geobotanical evidence (Hunt 1979, Hunt and Ashley 1979, Gupta 2017).

Hydrothermal deposits typically form at shallow crustal depths, ranging from approximately 2 to 6 km below the surface. They are usually associated with extensive

[*]Faculty of Petroleum and Minerals, Al Neelain University, Sudan.
[±]Marine Operations Manager, Leaf Global Environmental Services PLC, Saudi Arabia.

hydrothermal alteration (HA), which is zonal in nature. This zonation progresses outward and upward from an inner potassic zone, characterized by intense alteration and dominated by biotite and K-feldspar, into phyllic, argillic, and finally propylitic zones (Mars and Rowan 2006, Berger et al. 2014). The phyllic zone commonly consists of sericite and pyrite-rich rocks, while the ore zone includes disseminated chalcopyrite, molybdenite, pyrite, and other sulfide minerals. Much of the ore is concentrated near the boundary between the potassic and phyllic zones, often forming a cylindrical ore shell. The argillic zone is composed of rocks enriched in alunite and kaolinite, whereas the outer propylitic zone consists of weakly altered rocks with variable mineralogy, including chlorite, epidote, and calcite (Spatz et al. 1995, Seedorff et al. 2005, Mars and Rowan 2006). These successive alteration zones (AZs), rich in characteristic minerals, provide an essential reference for mapping HA using both LC8 and AST data (Pour et al. 2018, Pour et al. 2019).

In Sudan, several studies have successfully applied multispectral data from Landsat TM, ETM+, and LC8 sensors to delineate gossans, gold-bearing zones, and as-sociated sulfide mineralization. These studies have been guided by the distinct spectral signatures of gossans and AZs related to mineral deposits (Zeinelabdein and Albiely 2008, Abdelsalam et al. 2000, El Khidir 2006, El Khidir and Babikir 2013). The Gebeit area was selected as the study site due to the lack of availability of previous information, particularly from remote sensing investigations using LC8 and AST data. In addition, the region holds significant economic importance as an active and prospective mining area.

In this study, LC8 data, processed using various digital image processing algorithms and validated with spectral analysis of AST data, were used to delineate and map the AZs of hydrothermal minerals associated with gold-bearing sulfide deposits.

Geological Setting

The Red Sea Hills (RSHs) of Sudan form part of the Nubian Shield, which belongs to the Arabian-Nubian Shield (ANS) of northeastern Africa and the western Arabian Peninsula. The ANS extends along both sides of the RSHs, from Egypt in the northwest, the Sinai Peninsula in the north, and Saudi Arabia in the northeast, to Ethiopia and Yemen in the southwest and southeast, respectively (Johnsonet al. 2004, Johnson et al. 2011). The ANS is recognized as one of the major orogenic belts formed during the Neoproterozoic assembly of Greater Gondwana. It represents an accretionary orogenic belt composed predominantly of juvenile intra-oceanic island arcs, oceanic islands, and microcontinental fragments (Stern 1994). The ANS evolved between 900 and 550 Ma as a result of the closure of the Mozambique Ocean (800-650 Ma) and the subsequent collision between East and West Gondwana (Stern 1994, Stern 2002). Kröner et al. (1987) divided the RSHs into five geologically distinct terranes, separated from each other by ophiolite-decorated suture zones.

The study area is located within the Gebeit Terrane (Figure 1), which comprises arc-related, low-grade volcano-sedimentary sequences and syn-tectonic igneous complexes in the area north of the Nakasib Suture (Vail 1985, Klemenic and Poole 1988). Whole rock Rb/Sr isochron ages of approximately 720 Ma have been reported

for volcanic and plutonic rocks within the terrane (Fitches et al. 1983, Almond and Ahmed 1987). Regionally, major ductile shearing, faulting, and compressional forces acting from the east to southeast are interpreted to have generated the dominant NE-trending structural fabric of the RSHs, including folds and faults, associated with ophiolite-decorated suture zones such as the Nakasib Suture (Almond and Ahmed 1987, Abdelsalam 2010). Younger NW-trending strike-slip shear zones, including Oko and Keraf shear zones, deform older these earlier structures like Nadasib suture (Abdelsalam 2010).

Figure 17. *Terranes and Suture Zones of the ANS, illustrating the Predominant Ages of Arc Magmatism within each Terrane and the Location of the Study Area*

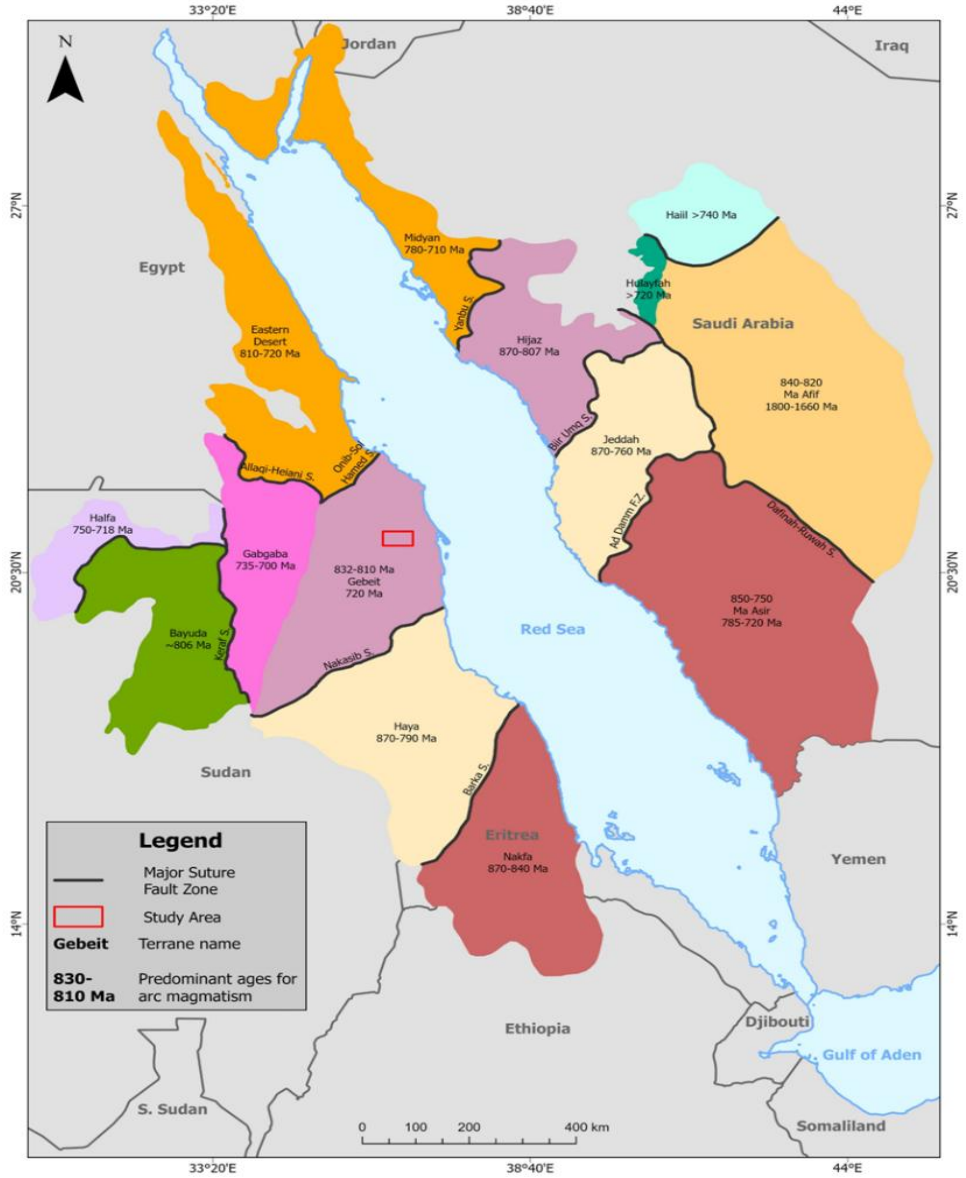

Source: Modified after (Abdelsalam, 2010).

Materials and Methods

Image Data and Data Preprocessing

Landsat 8 OLI Data

LC8 was launched on an Atlas V rocket from Vandenberg Air Force Base, California, USA, on February 11, 2013. It is the eighth satellite in the Landsat program, which has been continuously operated since the 1970s as a joint initiative between the U.S. Geological Survey (USGS) and NASA (Roy et al. 2014, Blondes et al. 2016). LC8 carries two primary instruments: the OLI (Operational Land Imager), which acquires data in nine spectral bands spanning the visible (Table 1), NIR (near-infrared), and SWIR (shortwave infrared) regions (including a panchromatic band and a cirrus band), and the TIRS (Thermal Infrared Sensor), which records two longwave thermal bands (bands 10 and 11) (Wulder et al. 2008, Roy et al. 2014, Blondes et al. 2016).

In this study, a single optical multispectral LC8 scene was used, corresponding to path 172, row 45, acquired on June 5, 2025. The dataset was downloaded from the USGS EROS (Earth Resources Observation and Science) Center website.

ASTER Data

ASTER (Advanced Spaceborne Thermal Emission and Reflection Radiometer) is a multispectral sensor with high spatial, spectral, and radiometric resolution (Abrams, Hook and Ramachandran, 2002). AST data are recorded in 14 spectral bands using three subsystems: the VNIR (Visible and Near Infrared) subsystem, consisting of three bands with wavelengths from (0.52 to 0.86 μm) at 15 m spatial resolution; the SWIR (Shortwave Infrared) subsystem, comprising six bands with wavelengths from (1.6 to 2.43 μm) at 30 m spatial resolution; and the TIR (Thermal Infrared) subsystem, which includes five bands (Bands 10-14) spanning (8.125-11.65 μm) at 90 m spatial resolution (Table 1). The instrument also has a long-track stereo capability, and each AST scene covers an area of 60 × 60 km², making it particularly suitable for regional mapping (Yamaguchi et al., 1999; Abrams, 2000; Yamaguchi et al., 2001; Abrams, Hook and Ramachandran, 2002).

For this research, one AST scene was used. The dataset (Scene ID: 00303032008081257) was acquired on August 12, 2008, and downloaded from the NASA Earthdata Search portal.

Table 1. *Overview of LC8 and AST Imaging Bands*

Satellite	Band No.	Covered Spectrum	Wavelength (μm)	Resolution (m)
LC8	1	Coastal/Aerosol	0.43-0.45	30
LC8	2	Blue	0.45-0.51	30
LC8	3	Green	0.53-0.59	30
LC8	4	Red	0.64-0.67	30
LC8	5	NIR	0.85-0.88	30
LC8	6	SWIR 1	1.57-1.65	30
LC8	7	SWIR 2	2.11-2.29	30
LC8	8	Panchromatic	0.50-0.68	15

LC8	9	Cirrus	1.36-1.38	30
AST	1	VNIR	0.52 - 0.60	15
AST	2	VNIR	0.63 - 0.69	15
AST	3N	VNIR	0.78 - 0.86	15
AST	3B	VNIR	0.78 - 0.86	15
AST	4	SWIR	1.600 - 1.700	30
AST	5	SWIR	2.145 - 2.185	30
AST	6	SWIR	2.185 - 2.225	30
AST	7	SWIR	2.235 - 2.285	30
AST	8	SWIR	2.295 - 2.365	30
AST	9	SWIR	2.360 - 2.430	30
AST	10	TIR	8.125 - 8.475	90
AST	11	TIR	8.475 - 8.825	90
AST	12	TIR	8.925 - 9.275	90
AST	13	TIR	10.25 - 10.95	90
AST	14	TIR	10.95 - 11.65	90

Source: Compiled from USGS Landsat 8 and NASA ASTER specifications

Software

Image processing was performed using ENVI (Environment for Visualizing Images) version 5.3 and ArcGIS version 10.8, installed on a high-performance computer. These software packages provided the necessary tools for preprocessing, spectral analysis, and spatial data integration.

Data Preprocessing

The LC8 data were geometrically corrected and georeferenced by the USGS prior to download. The data are provided in the UTM (Universal Transverse Mercator) coordinate system, zone 36N, based on the WGS84 datum, with all units expressed in meters. Atmospheric correction was carried out using the FLAASH (Fast Line-of-sight Atmospheric Analysis of Spectral Hypercubes) model (Fraser and Green 1987). To improve signal quality and computational efficiency, the MNF (Minimum Noise Fraction) transformation was applied, enabling dimensionality reduction, noise segregation, and optimization for subsequent image analysis (Cooley et al. 2002, Shnain et al. 2024).

Similarly, the AST data underwent atmospheric correction using the FLAASH technique, followed by post-processing band math to remove negative values. To enhance comparability, the six SWIR bands (30 m resolution) were resampled to match the three VNIR bands (15 m resolution), resulting in a nine-band semi-hyperspectral dataset with a uniform spatial resolution of 15 m (Shnain et al., 2024).

Landsat 8 OLI Data for Mineral Prospecting

LC8 data are considered fundamental for mineral prospecting, especially in remote or inaccessible regions. They are extremely useful during the systematic exploration phase of mining and are widely applied to geological mapping and mineral exploration worldwide (Safari et al. 2018, Mwaniki et al. 2015). The LC8 spectral range (0.325–2.5 μm) records solar-reflected light and includes several diagnostic absorption features of alteration minerals. These features are related to

vibrational overtones, electronic transitions, charge transfer, and conduction processes (Sabins and Lulla 1987).

In this study, LC8 data were processed using two complementary approaches: (i) the Band Ratio (BR) technique, and (ii) Supervised Classification applied to Sabins BR and to the Feature Oriented Principal Component Selection (FOPCS) method. Both approaches were used to delineate HA zones (Sabins and Lulla, 1987).

The Band Ratio Process for Mineral Prospecting

BR is one of the most effective techniques for detecting alteration minerals such as ferrous and ferric iron oxides, as well as hydroxyl-bearing minerals (Sabins and Lulla 1987, Zhang et al. 2007). BR images are generated by dividing the digital number (DN) values of one spectral band by those of another (Sabins 1999, Lillesand et al. 2015). These images enhance spectral differences between minerals, minimize the influence of topography and solar illumination, and highlight absorption features associated with alteration. Gray-scale ratio images display pixels with the largest differences in reflectance between two bands. BRs are therefore widely used to emphasize iron oxide and clay or hydroxyl-bearing minerals, which are critical indicators of HA (Gupta 2017). To further enhance interpretation, density slicing was applied, converting the continuous tonal variations of the ratio images into discrete intervals corresponding to specified DN ranges (Sabins and Lulla 1987, Zhang et al. 2007).

Supervised Classification

Supervised classification is another powerful remote sensing technique for mapping mineral AZs. It involves the selection of sample Regions of Interest (ROIs) and the extraction of their spectral signatures across all bands. These signatures are used to compute statistical parameters that guide classification algorithms. In this study, the Parallelepiped classifier was used to assign each pixel to the most probable class, enabling accurate and detailed thematic mapping (Richards 2022, Lillesand et al. 2015). Supervised classification was applied to false-color composite (FCC) images generated from Sabins BR and from the FOPCS method to identify HA zones.

Sabins Band Ratio FCC Image

The Sabins FCC image was produced by assigning BR of 6/7, 4/6, and 4/2 to the red, green, and blue channels, respectively (Sabins 1999). This combination enhances the spectral expression of alteration minerals. The 6/7 ratio highlights clay-rich zones, since clay minerals show strong reflectance in Band 6 (SWIR1) and low reflectance in Band 7 (SWIR2), which appear reddish in the composite. The 4/2 ratio enhances iron oxide-bearing areas, reflecting the absorption features in the blue region (Band 2) and the high reflectance in the red region (Band 4). These spectral properties allow iron-bearing minerals to be clearly distinguished (Pour and Hashim 2012a, 2012b).

The FOPCS (Feature Oriented Principal Component Selection) process

The FOPCS method, also referred to as the Crosta technique, is a targeted principal component analysis (PCA) approach that uses only a subset of bands selected to emphasize spectral features of interest (Crósta 1989, Loughlin 1991, Crósta et al.

2003). In this study, two band combinations were analyzed: the H-image, designed to enhance hydroxyl-bearing and clay minerals, and the F-image, intended to highlight iron oxide signatures. The eigenvector loadings of the resulting principal components were carefully examined to determine which components best represent the spectral properties of alteration minerals (Zhang et al. 2007).

ASTER Data for Mineral Prospecting

AST data, with their high spatial and spectral resolution, provide valuable coverage for identifying HA minerals and lithological units (Cooley et al. 2002). HA zones such as phyllic, argillic, and propylitic can be distinguished by their characteristic absorption features within AST's spectral range. Specifically, the phyllic alteration zone, dominated by illite and muscovite (sericite), is characterized by a strong Al-OH absorption feature centered at 2.20 μm, which coincides with AST Band 6. The argillic zone, comprising kaolinite and alunite, shows a secondary Al-OH absorption feature at 2.17 μm, corresponding to AST Band 5. The propylitic zone, characterized by chlorite and epidote, exhibits absorption features near 2.35 μm, coinciding with AST Band 8 (Mars and Rowan 2006, Pour et al. 2018, Testa et al. 2018).

In the present study, AST VNIR - SWIR data were analyzed using two methods: mineral indices derived from BR and the SAM classifier. Both approaches were applied to detect (illite, muscovite, kaolinite, alunite, epidote, and chlorite) which are diagnostic minerals of (phyllic, argillic, and propylitic) AZs.

Mineral Indices

Mineral indices were calculated by applying specific BR that target diagnostic absorption features of selected minerals (Rowan and Mars 2003, Rowan et al. 2003). Preprocessing of the AST dataset included radiometric calibration and atmospheric correction of VNIR and SWIR bands. Lithological indices were also derived for the TIR bands, based on the distinct spectral properties of various minerals and rock types (Ninomiya, 2003; Van der Meer et al., 2012).

Three indices were particularly applied in this study:

$$\text{Muscovite Index} = \frac{Band\ 7}{Band\ 6}$$

$$\text{Alunite Index} = \frac{Band\ 7}{Band\ 5} \times \frac{Band\ 7}{Band\ 8}$$

$$Kaolinite\ Index = \frac{Band\ 4}{Band\ 5} \times \frac{Band\ 8}{Band\ 6}$$

Spectral Angle Mapper (SAM) Classifier

The SAM technique classifies pixels based on their spectral similarity to known reference spectra (Rajendran et al. 2013). Each pixel's spectral vector is compared to library spectra of known minerals, and the similarity is quantified by measuring the angle between the vectors. Smaller angles indicate greater similarity. This procedure produces a spectral similarity map, in which each pixel is classified according to its closest match from the spectral library. The SAM output includes a classified image displaying the distribution of alteration minerals and rule images showing the angular

distance (in radians) between pixel spectra and reference spectra (Kruse et al. 1993, Rowan and Mars 2003, Van der Meer et al. 2012).

Figure 18. *Two-dimensional Illustration of Spectral Vectors r (reference spectrum) and n (pixel spectrum), showing the Spectral Angle (a) between them*

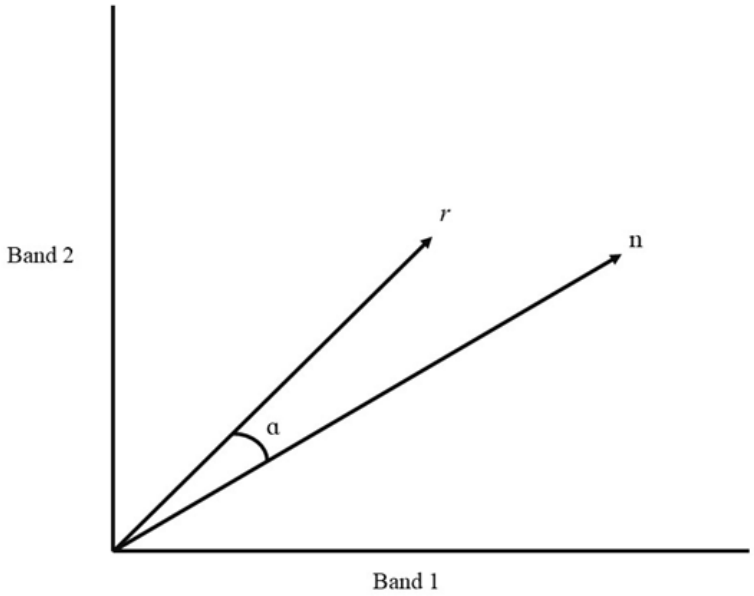

Source: Modified after (Kruse et al., 1993).

Results

Landsat 8 OLI Data Processing for Mineral Prospecting

Multispectral LC8 data were processed to delineate and map AZs associated with mineralization. These zones are defined by the presence of key alteration minerals, including ferric and ferrous iron oxides such as hematite, goethite, and limonite, as well as clay and hydroxyl-bearing minerals such as kaolinite, montmorillonite, illite, and alunite. The diagnostic spectral features of these minerals serve as important indicators for identifying potential mineral deposits within a multispectral remote sensing framework. To avoid misinterpretation, alluvial wadi deposits were masked during the analysis, since they often contain weathered, altered, and fragmented rock material whose spectral signatures can obscure or distort the signals of the targeted alteration minerals.

Band Ratio Images

Selective BR were applied to highlight HA zones. Ratios 4/2, 6/5, and 6/7 were specifically used to identify ferrous iron oxides, ferric iron oxides, and hydroxyl-bearing minerals, respectively. A low-pass filter was first applied to the ratio images to reduce noise. The resulting grayscale images were further enhanced through density slicing, which emphasized the spectral responses associated with the target

minerals. Finally, the density-sliced results were converted into vector classes, allowing the delineation and mapping of distinct AZs.

Ferrous Iron Oxides and Ratio

Ferrous iron oxides are characterized by high reflectance in the red portion of the spectrum (Band 4) and low reflectance in the blue region (Band 2) of LC8 data. For this reason, BR of 4/2 was used to delineate areas enriched in ferrous iron oxides. In the grayscale display, ferrous-rich areas appear in light tones, while in the density-sliced output they are highlighted in red (Figure 3a, b).

Figure 19. *BR 4/2 Image used for mapping Ferrous Oxides: (A) Grayscale Display, where High Values appear as Bright Tones; (B) Density-sliced Display, where High Values are highlighted in Red*

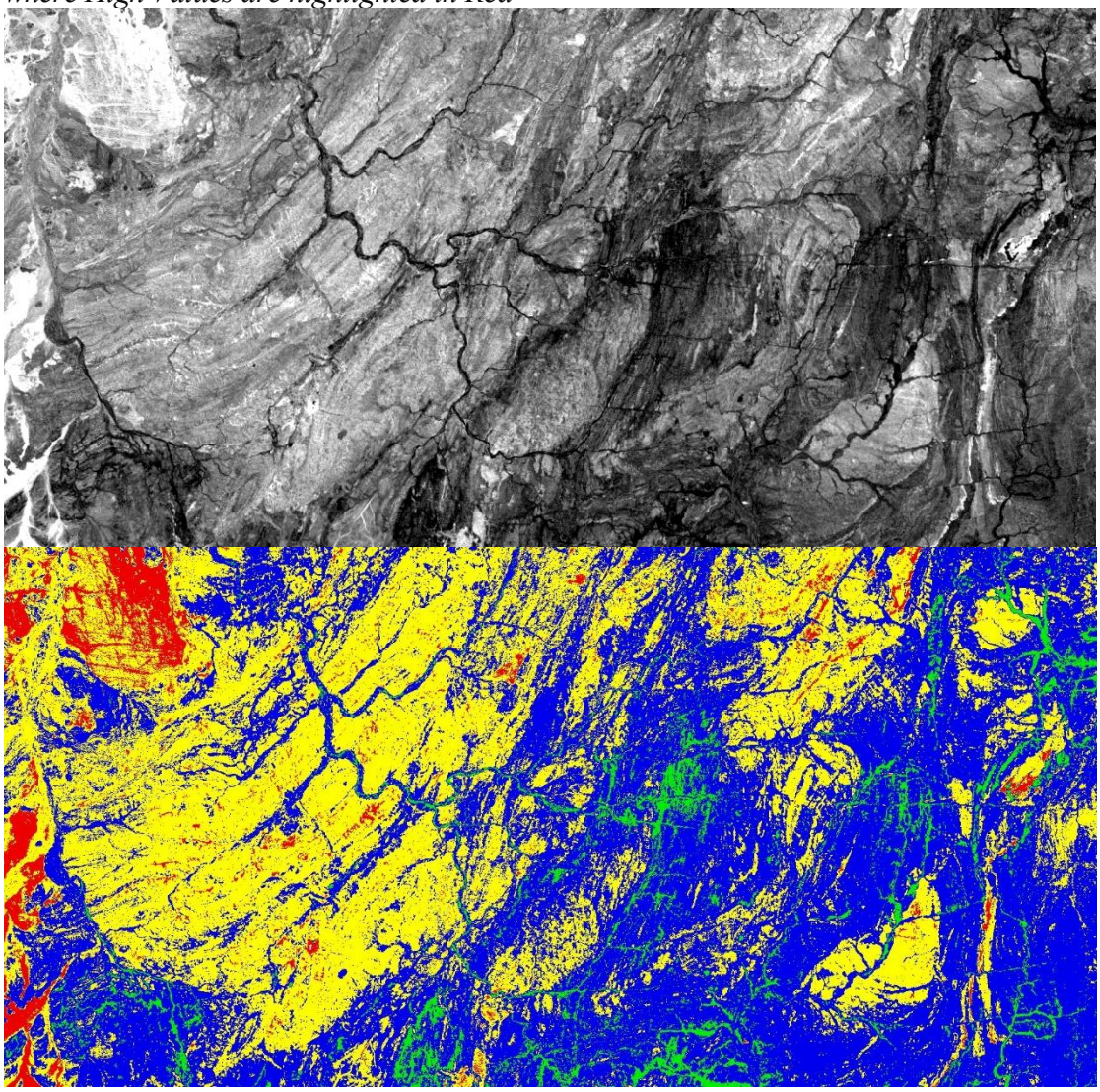

Source: Authors own elaboration

Ferric Iron Oxides Band Ratio

Ferric iron oxides show diagnostic absorption in the near-infrared region (Band 5) and high reflectance in the shortwave infrared region (Band 6). Consequently, the BR 6/5 effectively delineates ferric oxide-rich areas. These appear in light tones in the grayscale image and are displayed in red hues in the density-sliced image (Figure 4a, b).

Figure 20. *BR 6/5 Image used for mapping Ferric Oxides: (A) Grayscale Display, where High Values ap-pear as Bright Tones; (B) Density-sliced Display, where high values are highlighted in Red*

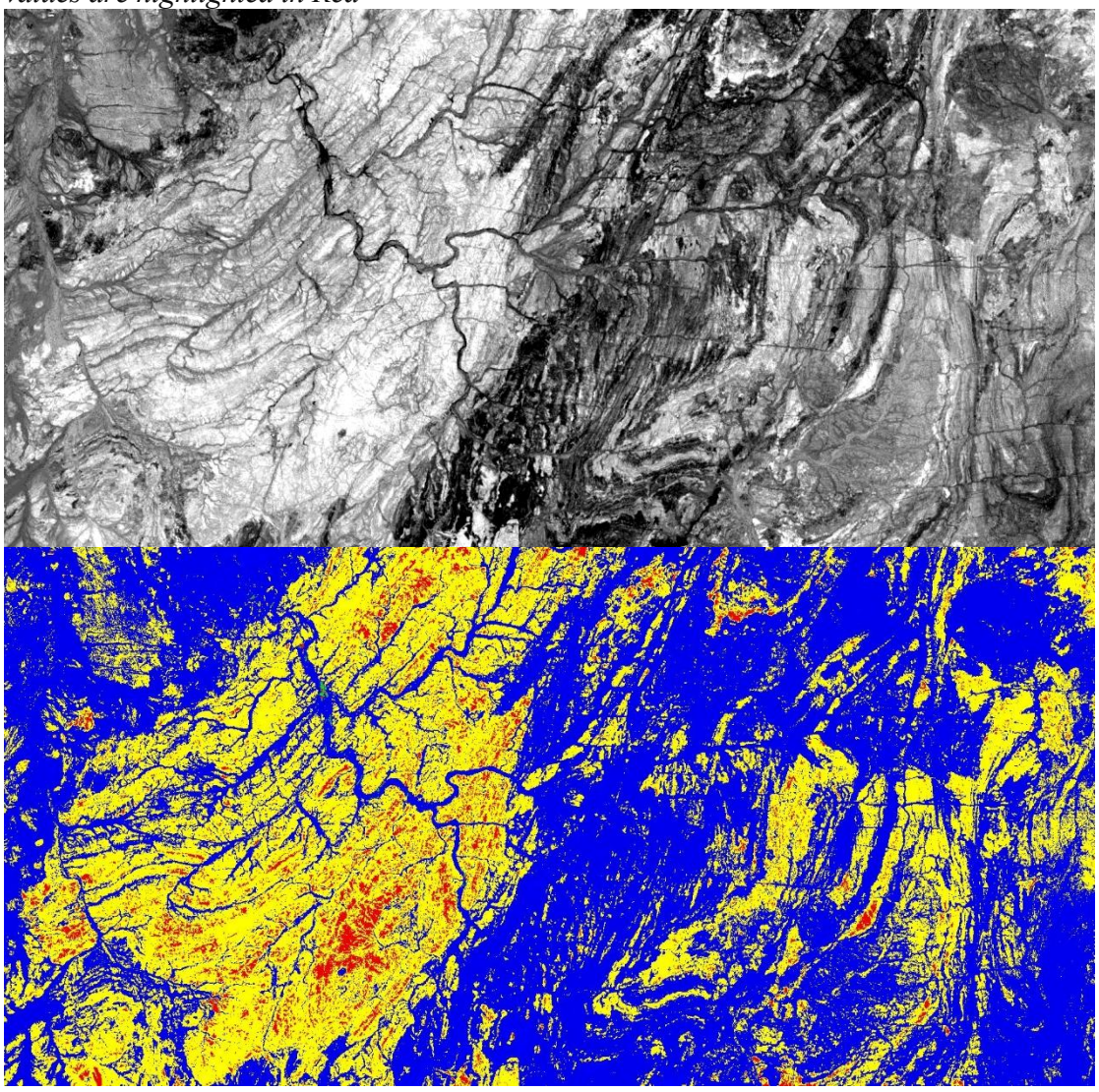

Source: Authors own elaboration

Hydroxyl Bearing Band Ratio

Hydroxyl-bearing alteration minerals, including clays, micas, and amphiboles, exhibit distinct absorption features in the SWIR-2 region (Band 7) due to the strong Al - OH and Mg-OH vibrational absorptions. At the same time, they show high reflectance in the SWIR-1 region (Band 6). Accordingly, BR of 6/7 was used to identify hydroxyl-bearing mineral assemblages. In the outputs, these zones appear in bright tones in the grayscale image and in red hues in the density-sliced version (Figure 5a, b).

Figure 21. *BR 6/7 Image used for Mapping Clay Minerals: (A) Grayscale Display, where High Values appear as Bright Tones; (B) Density-sliced display, where High Values are highlighted in Red*

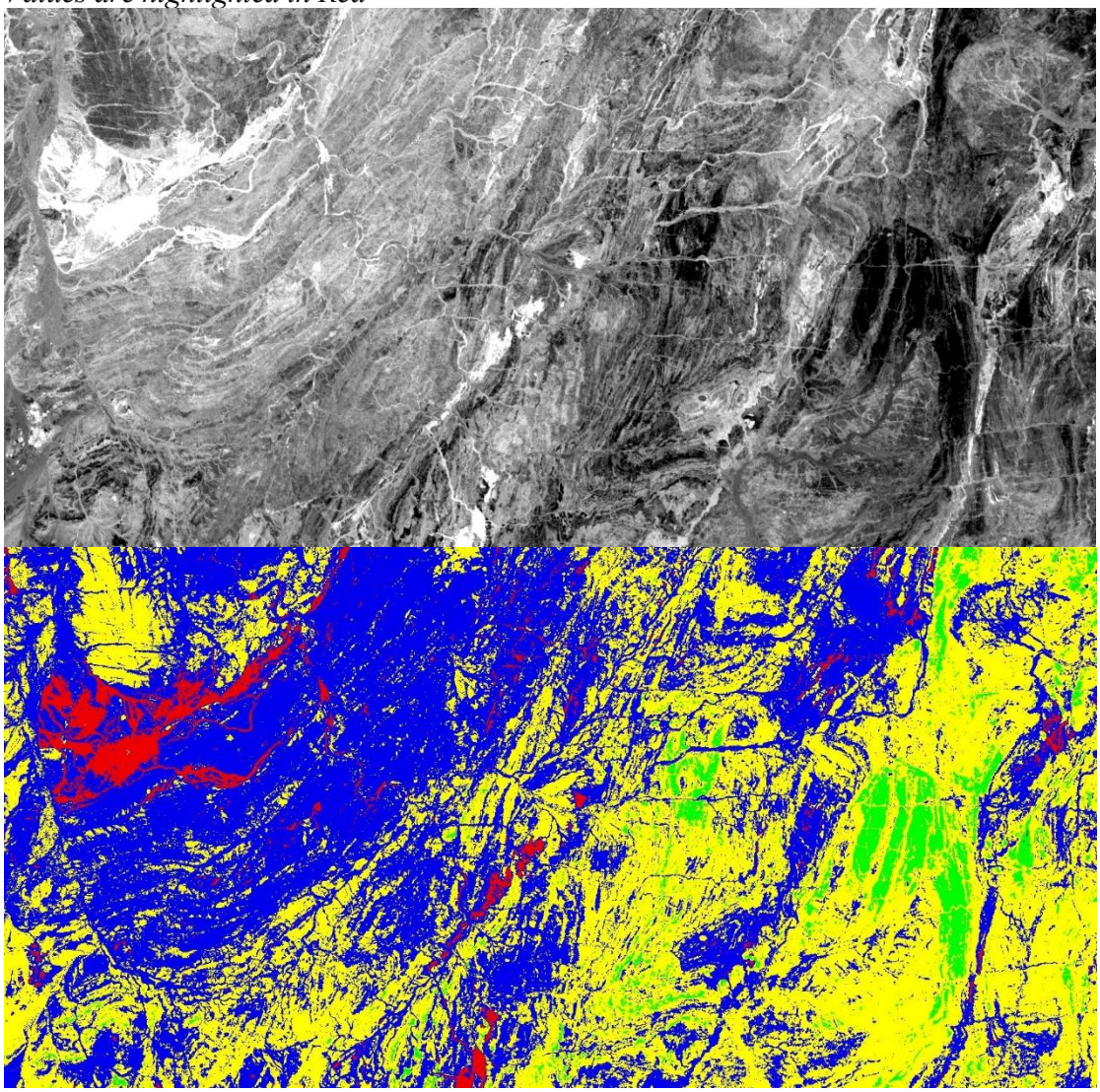

Source: Authors own elaboration

GIS Spatial Analysis

The BR images derived from ratios 4/2, 6/5, and 6/7 revealed three distinct types of potential AZs. Each was extracted as a separate class through density slicing and subsequently converted into vector format within a GIS environment. As shown in Figure 6a, ferrous oxide zones are represented in blue, ferric oxide zones in green, and clay-rich (hydroxyl-bearing) zones in red. To identify the most prospective zones of HA, a spatial intersection analysis was carried out. This procedure highlighted the areas of overlap among the three classes, rep-resenting the zones with the highest probability of being associated with hydrothermal mineralization. These priority targets are displayed in yellow in Figure 6b.

Figure 22. *(a) AZs Overlaid on the Satellite Image, showing High Values of the BR Images: 6/7 for Clay Minerals (red), 4/2 for Ferrous Oxides (blue), and 6/5 for Ferric Oxides (green). (b) Spatial Intersection Analysis of the vectorized Anomalous Values from the BR, highlighting the overlapping AZs in Yellow*

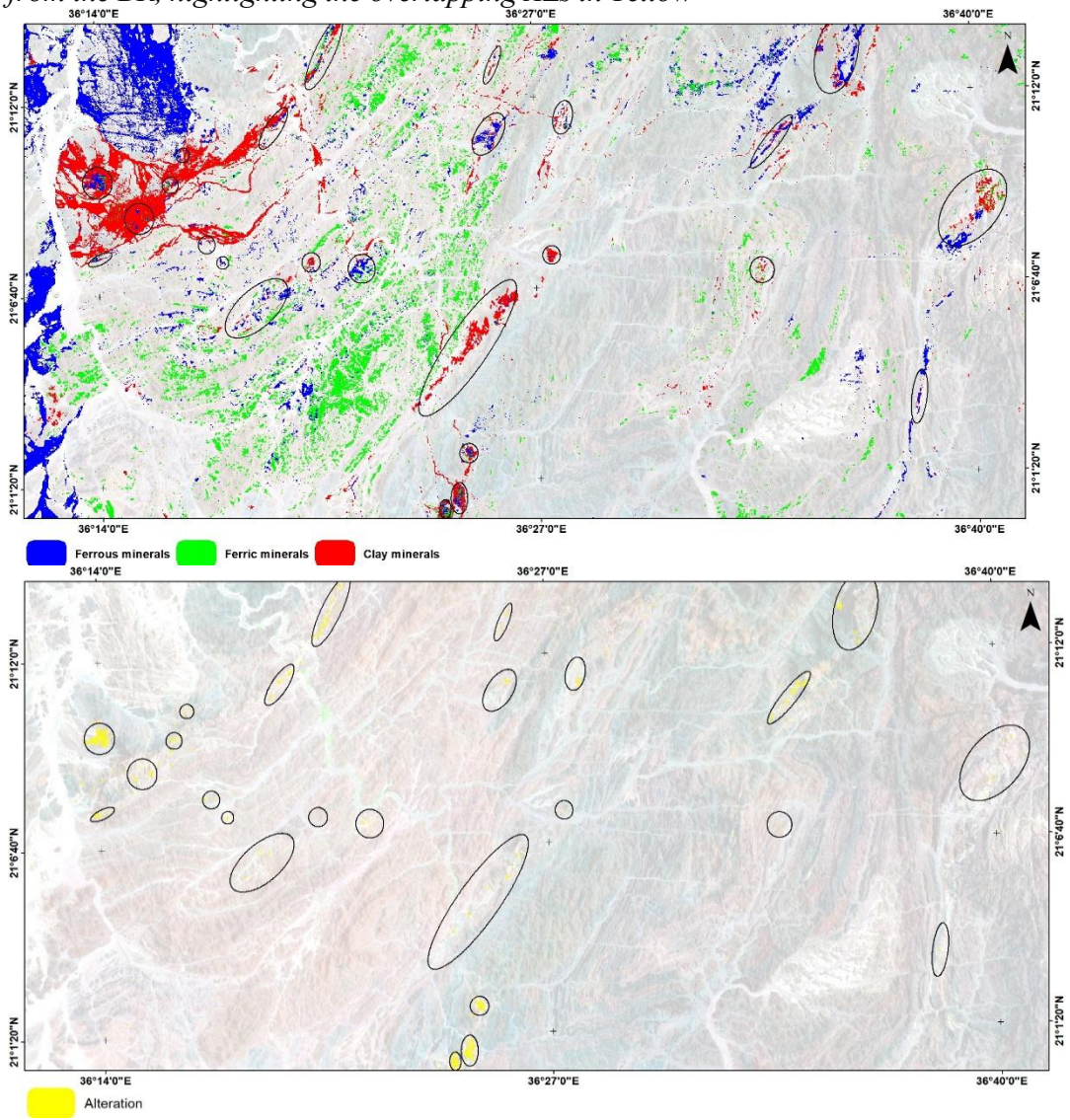

Source: Authors own elaboration

Supervised Classification

In Supervised classification using the Parallelepiped method was applied to identify HA zones in both Sabins and Crosta FCC images.

Sabins Band Ratio FCC Image

The Sabins FCC image was generated by assigning BR of 6/7, 4/6, and 4/2 to the red, green, and blue channels, respectively (Sabins and Lulla 1987). The 6/7 ratio highlights clay-rich minerals, which show high reflectance in Band 6 (SWIR1) and low reflectance in Band 7 (SWIR2), resulting in reddish hues in the composite. Areas enriched in iron oxides are emphasized by the 4/2 ratio, which exploits strong absorption in Band 2 (blue) and high reflectance in Band 4 (red), producing blue hues. The 4/6 ratio is particularly effective for mapping ferrous iron oxides and appears in green hues. Collectively, the Sabins FCC image provides a clear delineation of HA zones associated with mineralization, which are represented by crimson -orange hues (Figure 7).

Figure 23. *Sabins FCC Image showing AZs associated with Mineralization, displayed in Crimson-orange Hues; (b) Classified AZs derived from the Sabins BR Image, displayed in Red*

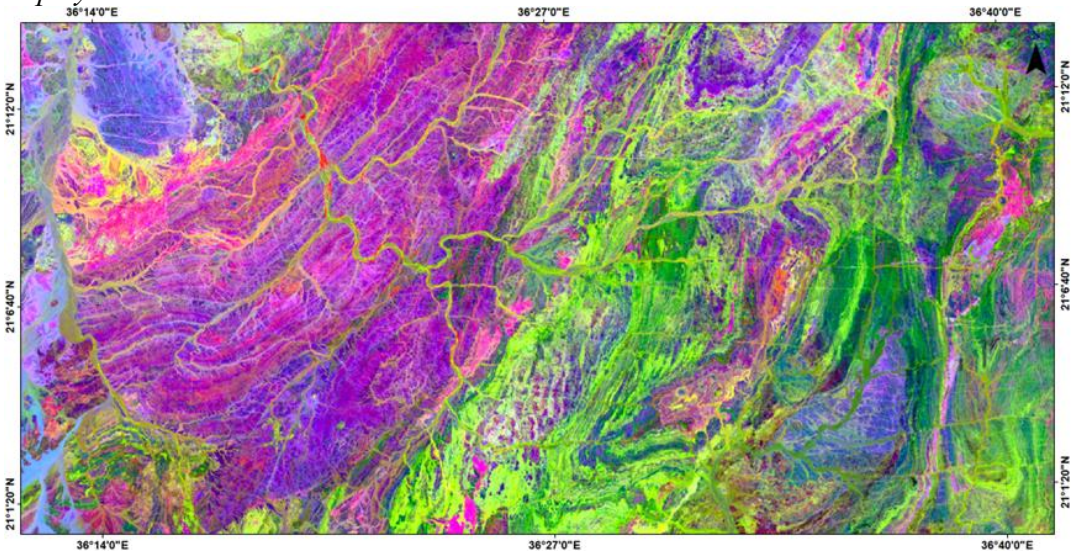

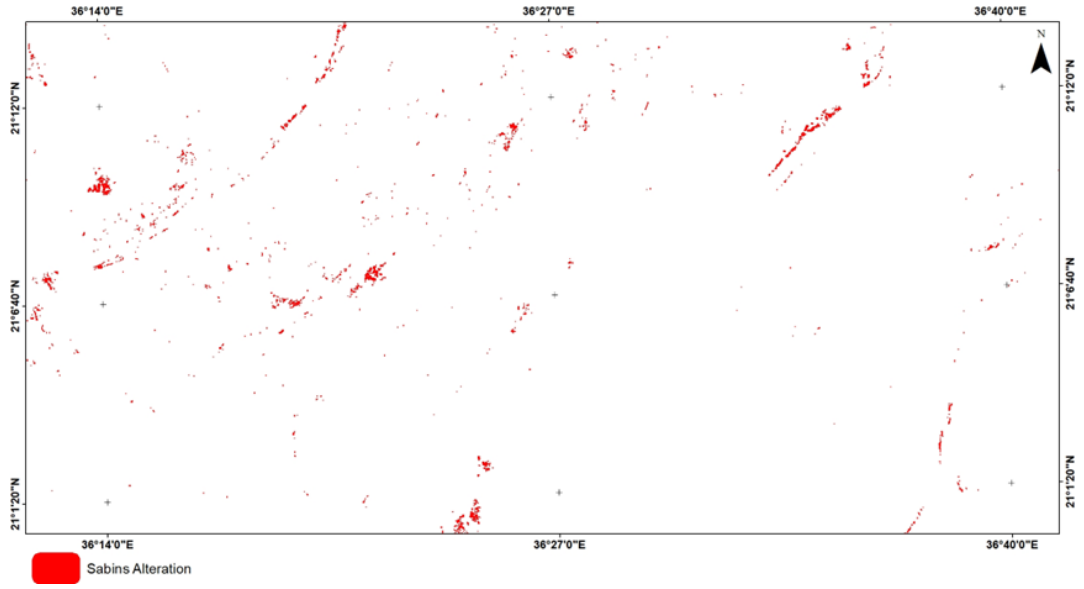

Source: Authors own elaboration

Feature Oriented Principal Component Selection (FOPCS)

FOPCS also known as the Crosta FCC method, is designed to emphasize only those spectral bands that contain diagnostic absorption features of iron oxides and clay-bearing minerals. For LC8 OLI data, the bands selected for mapping clay-bearing minerals were Bands (2, 5, 6, and 7), whereas Bands (2, 4, 5, and 7) were chosen for detecting iron oxides.

H Image (The Hydroxyl bearing and clay minerals)

The H-image is produced from principal component analysis (PCA). In general, PC1 accounts for overall albedo of the selected bands and thus contains minimal spectral variability, while PC2 reflects the contrast between the NIR and SWIR regions. In this study, eigenvector analysis (Table 1) indicated that PC3 and PC4 were the most effective components for delineating zones enriched in clay and hydroxyl-bearing minerals.

Table 2. *Eigenvector Statistics of Principal Components used for Hydroxyl-bearing Mineral mapping (H-image, FOPCS method)*

Eigenvector	Band 2	Band 5	Band 6	Band 7
PC 1	0.168356	0.432960	0.667114	0.582374
PC 2	0.463554	0.725617	-0.169314	-0.479510
PC 3	0.613774	-0.151658	-0.540803	0.554810
PC 4	0.616486	-0.512859	0.483553	-0.350851

Source: Authors own elaboration

In this case, PC4 exhibited the strongest contrast between Bands 6 and 7, with Band 6 showing a strong positive loading and Band 7 a strong negative loading. This contrast makes PC4 particularly sensitive to hydroxyl-bearing minerals. To enhance the mapping of these minerals, which appear as dark pixels in the PC4

image, the image was negated (255 - DN), followed by the application of a low-pass filter to reduce noise. The resulting processed image is referred to as the H-image.

F Image (The iron oxides rich areas)

The FOPCS transformation applied to Bands 2, 4, 5, and 7 produced the F-image. Eigenvector analysis (Table 2) indicated that either PC2 or PC4 effectively isolates iron oxide-rich zones due to the strong contrast observed among the visible bands, which is diagnostic of ferric iron minerals.

Table 3. *Eigenvector Statistics of Principal Components used for Iron Oxide mapping (F-image, FOPCS method)*

Eigenvector	Band 2	Band 4	Band 5	Band 7
PC 1	0.224696	0.476917	0.536085	0.659298
PC 2	0.312708	0.443982	0.389090	-0.744112
PC 3	0.736766	0.214905	-0.632033	0.107361
PC 4	-0.555789	0.727493	-0.402189	-0.009802

Source: Authors own elaboration

PC4 exhibited the greatest contrast in eigenvector loadings between Bands 4 and 2, making it particularly effective for mapping ferric iron oxide minerals. PC4 was therefore selected as the F-image, and a low-pass filter was applied to reduce noise, resulting in the final F-image.

The Crosta composite image (FCC) was then generated by assigning the hydroxyl-sensitive image (H-image) to the red channel, the iron oxide-sensitive image (F-image) to the blue channel, and a mathematically combined image (H-image + F-image) to the green channel. This composite effectively highlights AZs enriched in both iron oxides and clay minerals, which appear in whitish-yellow hues (Figure 8).

Figure 24. *(a) Crosta FCC Image showing AZs associated with Mineralization, displayed in Whitish - Yellow Hues; (b) Classified AZs derived from the Crosta FCC Image, displayed in Red*

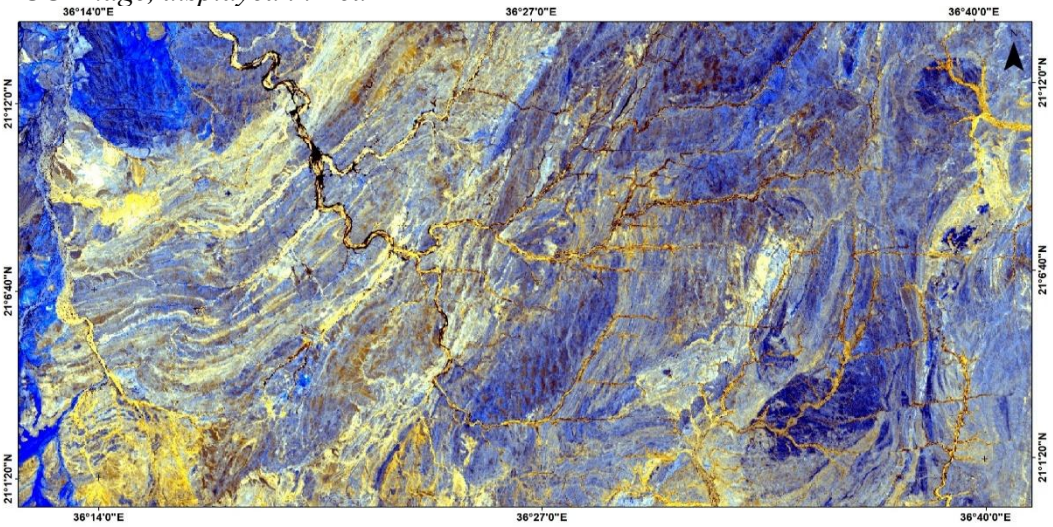

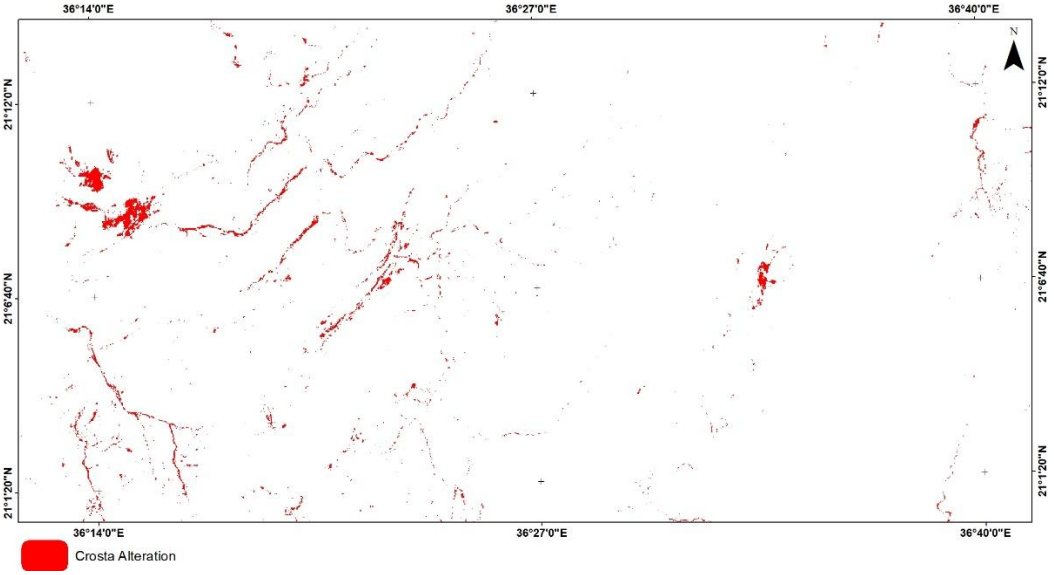

Source: Authors own elaboration

GIS Spatial Analysis

The alteration classes obtained from the supervised classification of both Sabins and Crosta composites were converted into vector format for integration within a GIS environment. A spatial intersection analysis was then performed on the vectorized AZs, enabling the delineation of highly probable AZs. These priority zones are highlighted in red in (Figure 9).

Figure 25. *(a) Classified AZs derived from the Sabins and Crosta Methods Overlaid on the FCC Image; (b) Alteration Map generated through Spatial Intersection of the Sabins and Crosta Composites, with the most probable AZs displayed in Red*

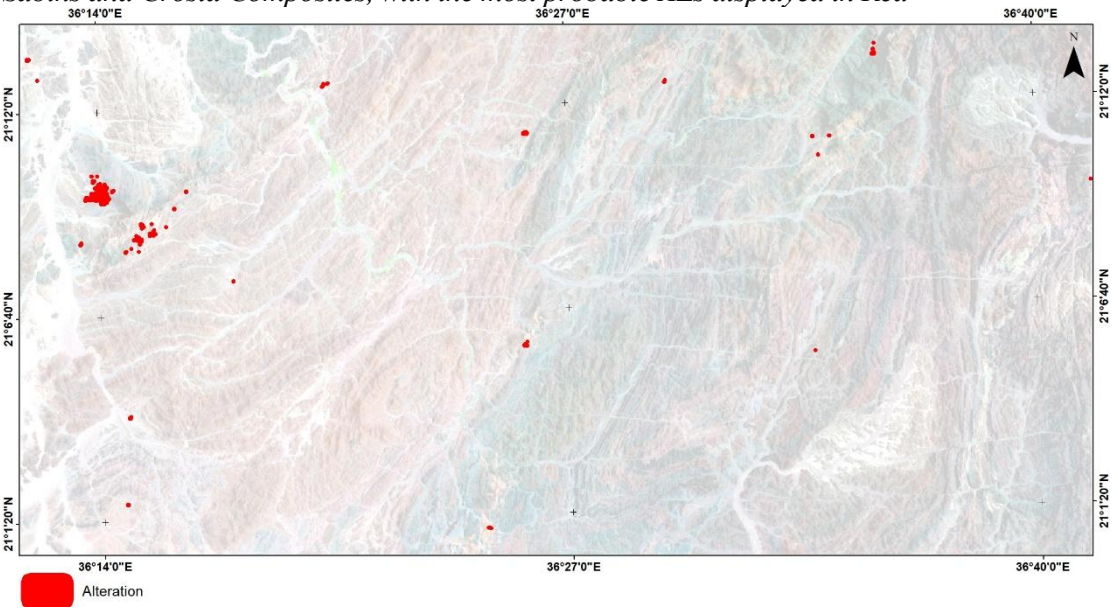

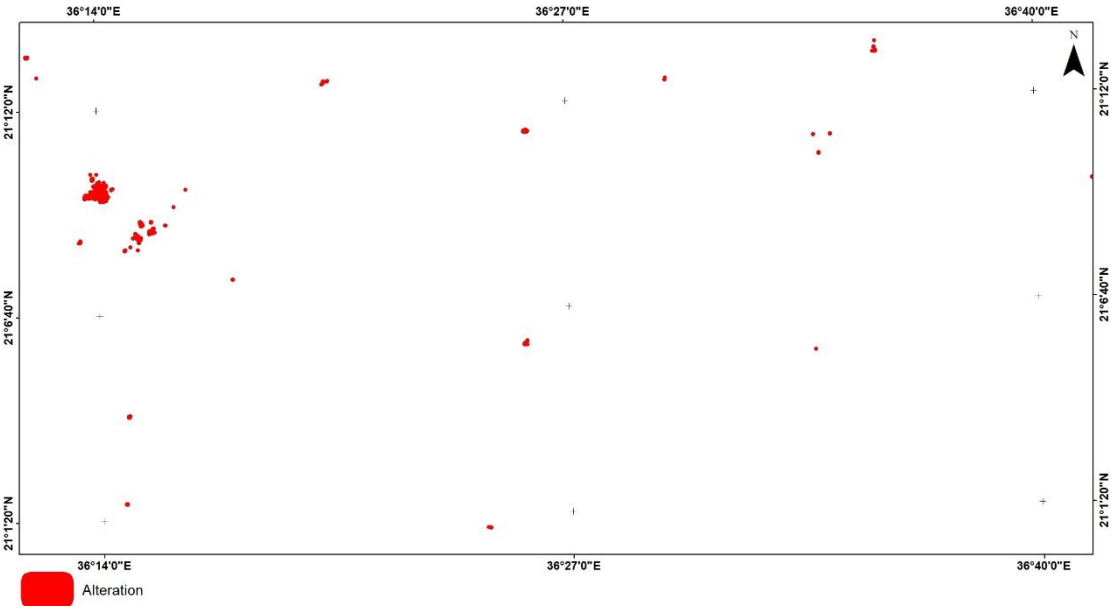

Source: Authors own elaboration

ASTER Data Processing for Mineral Prospecting

This section presents the application of two methods to AST VNIR-SWIR data for mapping hydrothermally altered minerals: (i) spectral BR indices and (ii) spectral analysis using the SAM classifier. These methods target minerals such as illite, muscovite, kaolinite, alunite, epidote, and chlorite, which display distinctive absorption and reflectance features, allowing the identification and delineation of hydro-thermal AZs, including phyllic, argillic, and propylitic zones.

Figure 26. *False Color Composite (FCC) of AST bands 4, 6, and 8 displayed in Red, Green, and Blue Channels, respectively, for the Study Area*

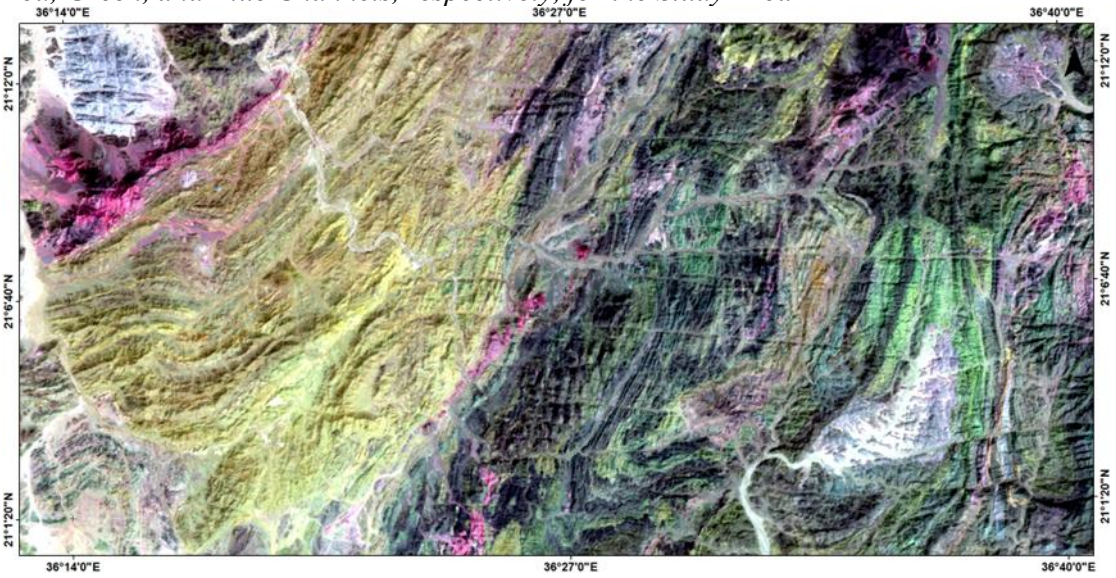

Source: Authors own elaboration

Mineral Indices

Mineral indices were derived by applying spectral BR targeting the diagnostic absorption features of selected minerals. The indices used in this study include the Muscovite Index, the Alunite Index and the Kaolinite Index.

Muscovite Mapping

The Muscovite Index highlights the absorption feature at (2.20 μm, AST Band 6), corresponding to Al-OH bearing minerals that define phyllic AZs. In the grayscale index image, muscovite-rich areas appear as bright tones, concentrated mainly in the upper left part of the study area and extending along a NNE structural trend. Additional occurrences are observed in the central lower region and near the upper right corner, The thresholded, color-coded image and its vectorized results highlight these muscovite-rich zones in red, delineating phyllic AZs (Figure 11a, b).

Alunite Mapping

The Alunite Index delineates the argillic AZs containing alunite and kaolinite minerals, which exhibit AL-O-H absorption features at (2.20 and 2.17 μm, AST band 5), respectively. The Alunite Index image shows brighter tone in the greyscale image distributed in the upper left corner of the image, the rest values are observed in the central lower part with the main NNE trend of the study area see (Figure 12 a). The thresholding high value color coded image and vectorized results appear in blue color mapping the phyllic AZs (Figure 12 b).

Kaolinite Mapping

The Kaolinite Index delineates zones enriched in kaolinite, which define argillic alteration. In the grayscale display, kaolinite-rich zones appear as bright tones, concentrated in the upper left part of the study area and extending along the NNE structural trend. Additional occurrences are observed in the central upper and lower regions and near the upper right corner, all aligned with the same structural trend. In the color-coded and vectorized image, kaolinite-rich zones are mapped in green (Figure 13a, b).

Figure 27. *Muscovite Index derived from AST Data: (a) BR image (Band 7/Band 6), highlighting Muscovite-rich Zones; (b) Vectorized Output of mapped Muscovite, displayed in Red*

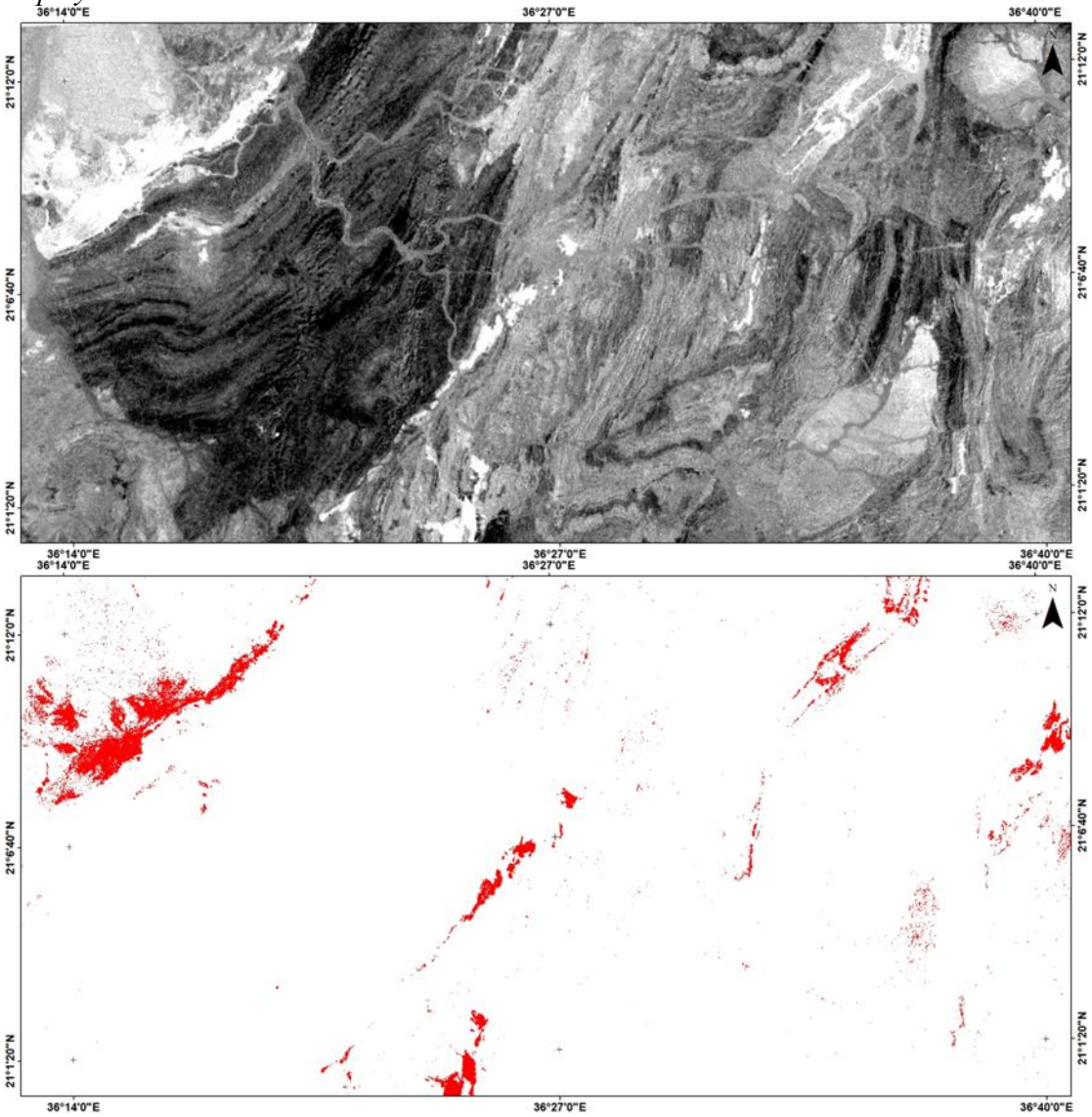

Source: Authors own elaboration

Figure 28. *Alunite Index derived from AST Data: (a) BR Image ((Band 7/Band 5) × (Band 7/Band 8)), highlighting Alunite-rich Zones; (b) Vectorized Output of mapped Alunite, displayed in Blue*

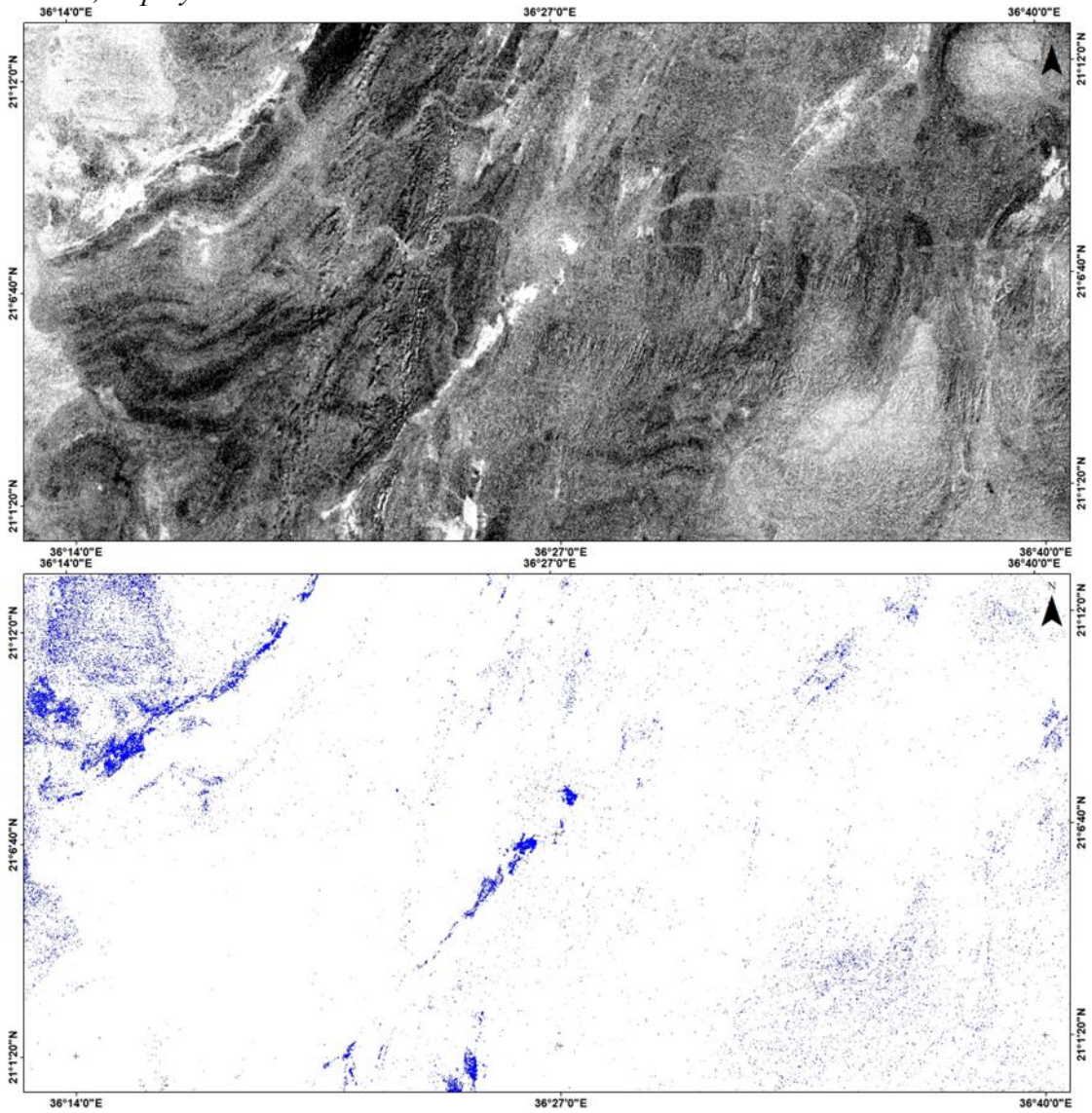

Source: Authors own elaboration

Figure 29. *Kaolinite Index derived from AST Data: (a) BR Image ((Band 4 / Band 5) × (Band 8 / Band 6)), Highlighting Kaolinite-rich Zones; (b) Vectorized Output of mapped Kaolinite, displayed in Green*

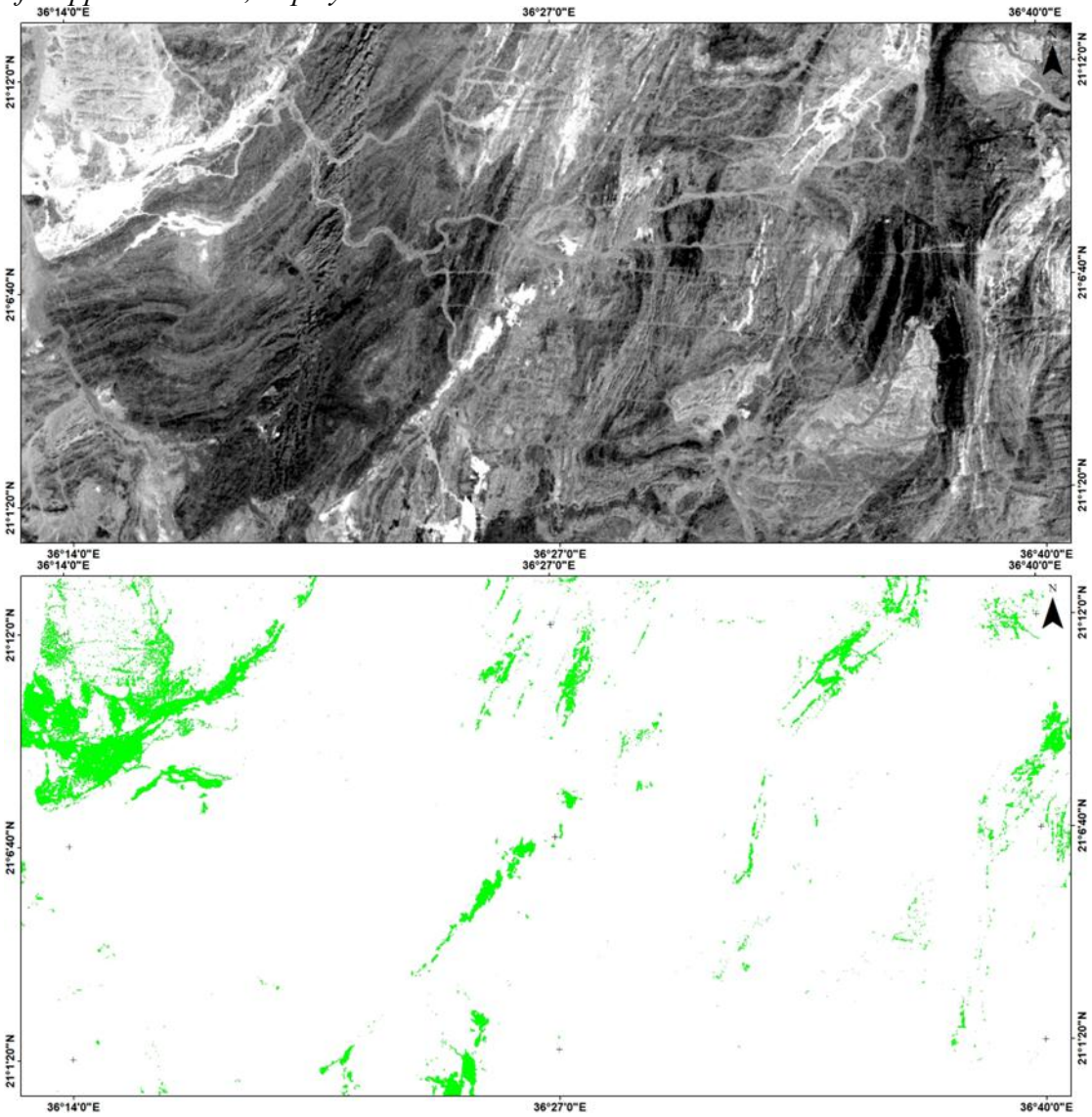

Source: Authors own elaboration

GIS Spatial Analysis

The vectorized results of the mineral indices were integrated within a GIS environment to highlight areas with overlapping phyllic and argillic AZs, which serve as indicators of potential mineralization. The analysis revealed that the upper left corner of the study area represents the most probable zone for mineralization, owing to the strong concentration of alteration signatures. Additional zones of high index values were also identified in the central lower region and near the upper right corner of the study area, all aligned with the dominant NNE structural trend (Figure 14).

Figure 30. *(a) Overlay of combined Phyllic and Argillic AZs on the FCC Image; (b) Integrated Results of Phyllic and ARGILLic AZs derived from Mineral Indices, highlighting the most probable mineralized Zones*

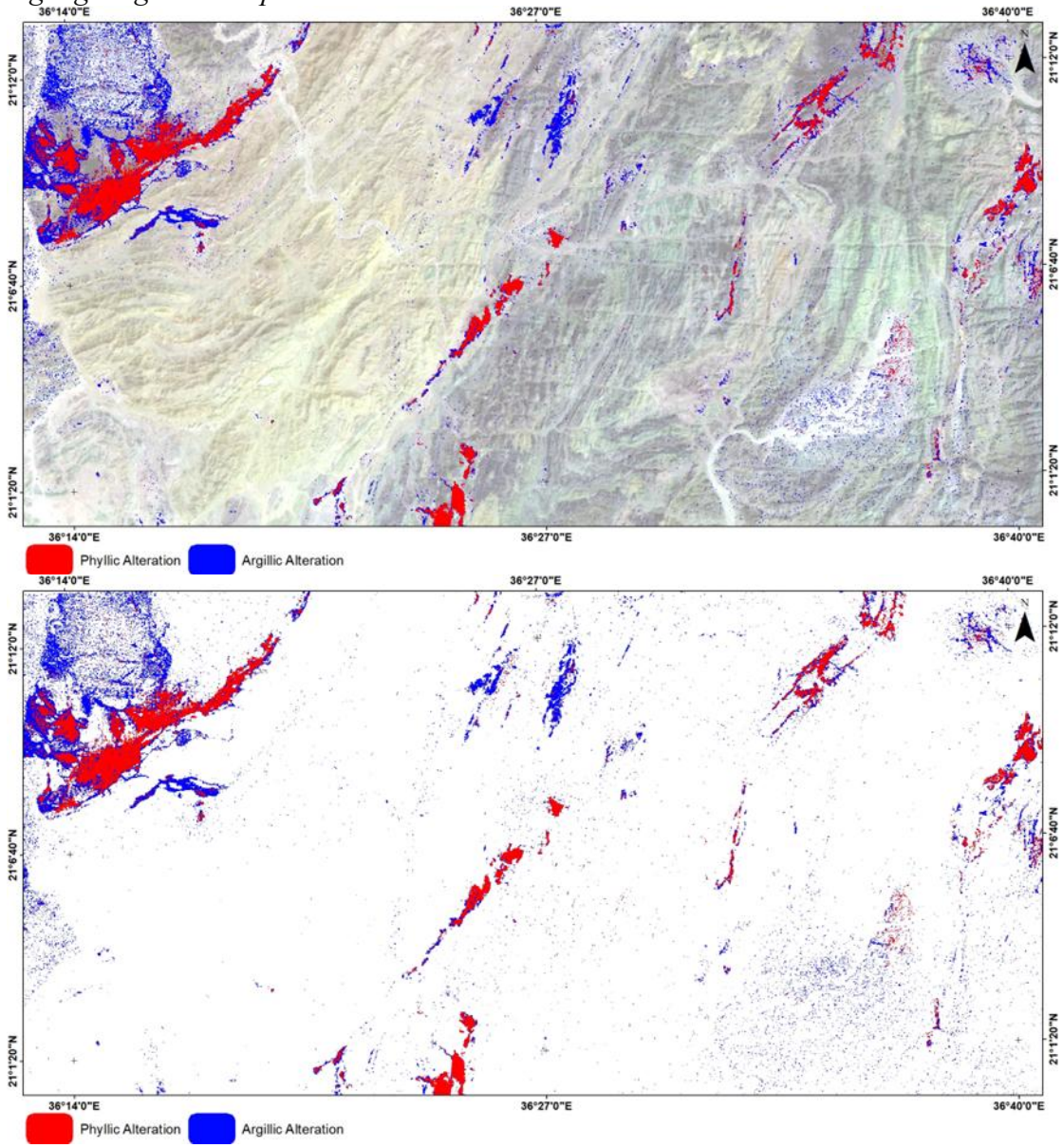

Source: Authors own elaboration

Spectral Angle Mapper Classifier

The SAM algorithm compares the spectral signature of a target object with reference spectra obtained from standardized laboratory spectral libraries, such as those provided by the USGS. In this study, spectra of common HA minerals associated with mineralization, specifically illite, muscovite, kaolinite, alunite, epidote, and chlorite, were selected from the USGS spectral library (Figure 15a). These reference spectra were subsequently resampled to match the spectral resolution and band configuration of the AST sensor (Figure 15b).

Figure 31. *(a) Laboratory Spectra of HA Minerals from the USGS Spectral Library used in this Study; (b) The Same Reference Spectra resampled to match the Spectral Resolution and Band Configuration of AST Bands*

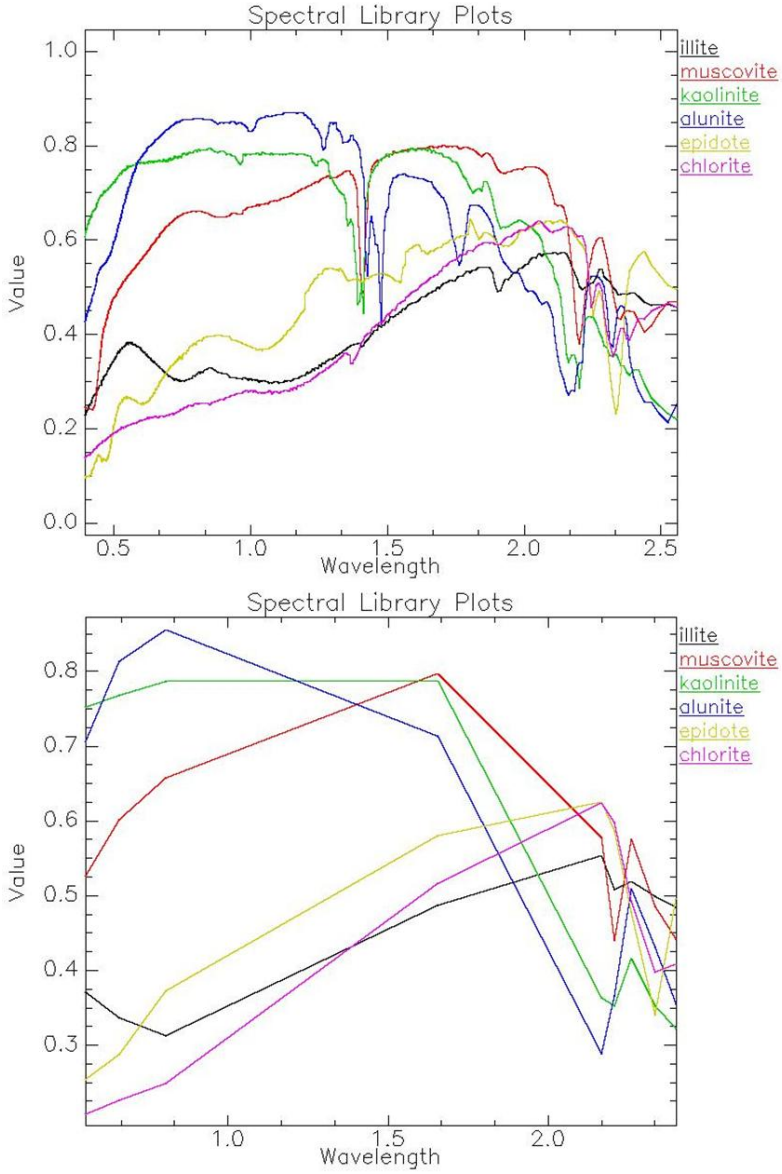

Source: Authors own elaboration

Rule images were generated to highlight the surface distribution of the selected spectra. The SAM algorithm applies a default threshold value, but in this case thresholds behave differently because lower values indicate a higher probability of a pixel belonging to the target class in the SAM rule image. Therefore, manual adjustment of the threshold was performed based on visual interpretation. The SAM-derived illite and muscovite images delineate phyllic AZs, which are represented in red. These zones are concentrated in the upper left corner of the study area and extend into the upper and central parts of the region (Figure 16).

Figure 32. *SAM classifier Results from AST data: (a) Combined Distribution of Illite and Muscovite, displayed in Red; (b) Combined Illite and Muscovite overlaid on the AST FCC Image, Highlighting Phyllic AZs in Red Hues*

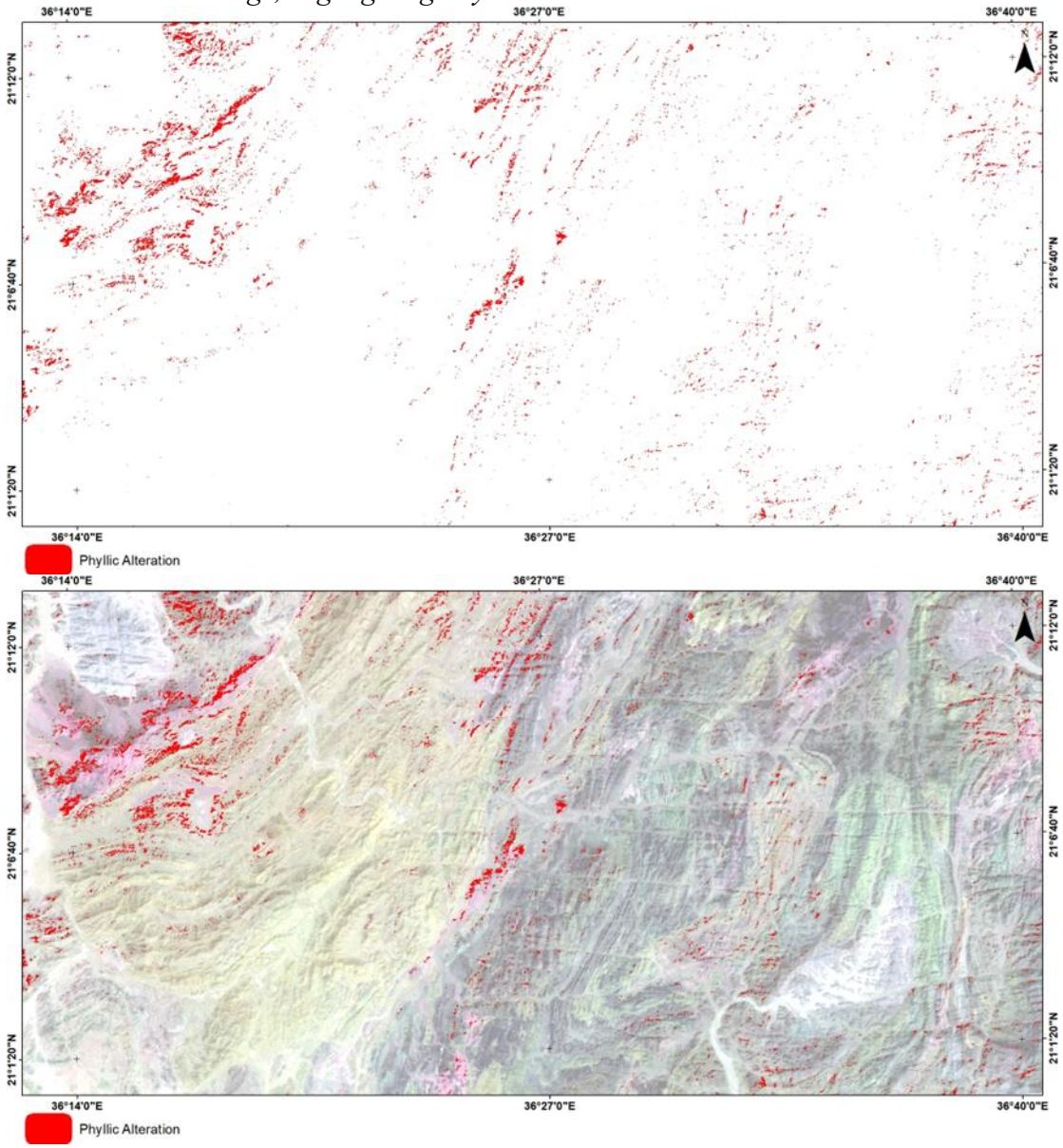

Source: Authors own elaboration

For kaolinite and alunite, the classified image highlights areas of high values corresponding to argillic AZs. These zones are represented in green and are mainly concentrated in the upper left corner of the study area, with more limited occurrences observed in the central region (Figure 17).

Figure 33. *SAM Classifier Results from AST Data: (a) Combined Distribution of Kaolinite and Alunite, Dis-played in Green; (b) Combined Kaolinite and Alunite overlaid on the AST FCC Image, Highlighting Argillic AZs in Green Hues*

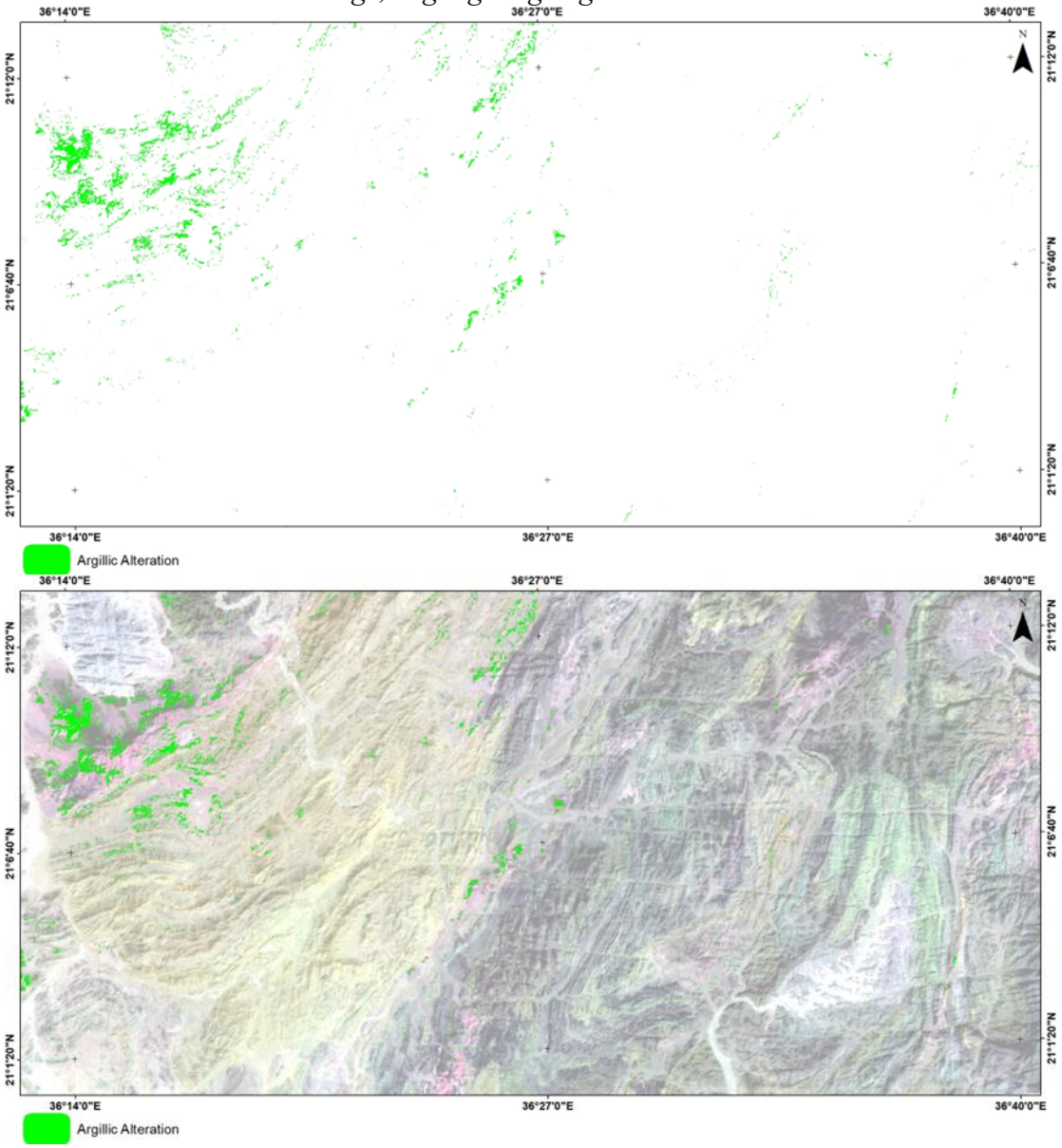

Source: Authors own elaboration

The SAM classification of epidote and chlorite was used to map propylitic AZs. These zones are represented in blue and are primarily concentrated in the left-central part of the study area (Figure 18).

Figure 34. *SAM Classifier Results from AST Data: (a) Combined Distribution of Epidote and Chlorite, displayed in Blue; (b) Combined Epidote and chlorite Overlaid on the AST FCC Image, High Lighting Propylitic AZs in Blue Hues*

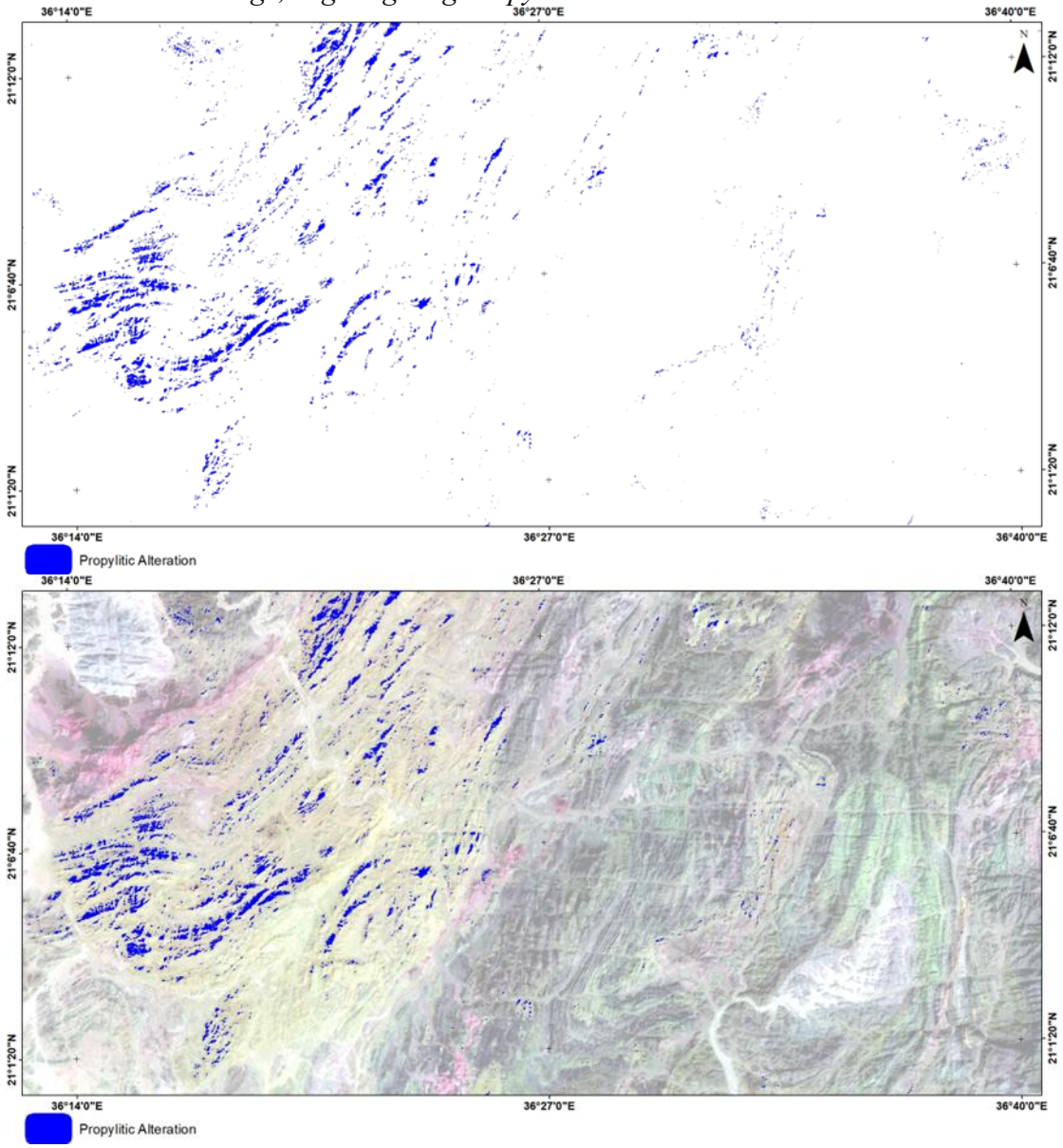

Source: Authors own elaboration

GIS Spatial Analysis

The SAM classification successfully mapped HA minerals, delineating phyllic, argillic, and propylitic zones. The resulting images illustrate the spatial distribution of these zones based on the diagnostic absorption features of their respective endmember minerals. The classified pixels were exported as shapefiles representing the extent of each alteration type. Spatial analysis was then conducted on these shapefiles to extract and delineate the most probable HA zones associated with mineralization (Figure 19a).

The results of the AST SAM spectral analysis revealed several probable AZs within the study area. These zones are primarily concentrated in the upper left

corner, aligned with a NNE structural trend, with additional occurrences in the central region and smaller, scattered zones in the upper middle part of the area (Figure 19b).

Figure 35. *Results of SAM classification applied to AST VNIR-SWIR Data: (a) Alteration Map showing Phyllic (red), Argillic (green), and Propylitic (blue) Zones; (b) AST FCC Image (bands 4, 6, and 8 in RGB) overlaid with SAM-derived AZs*

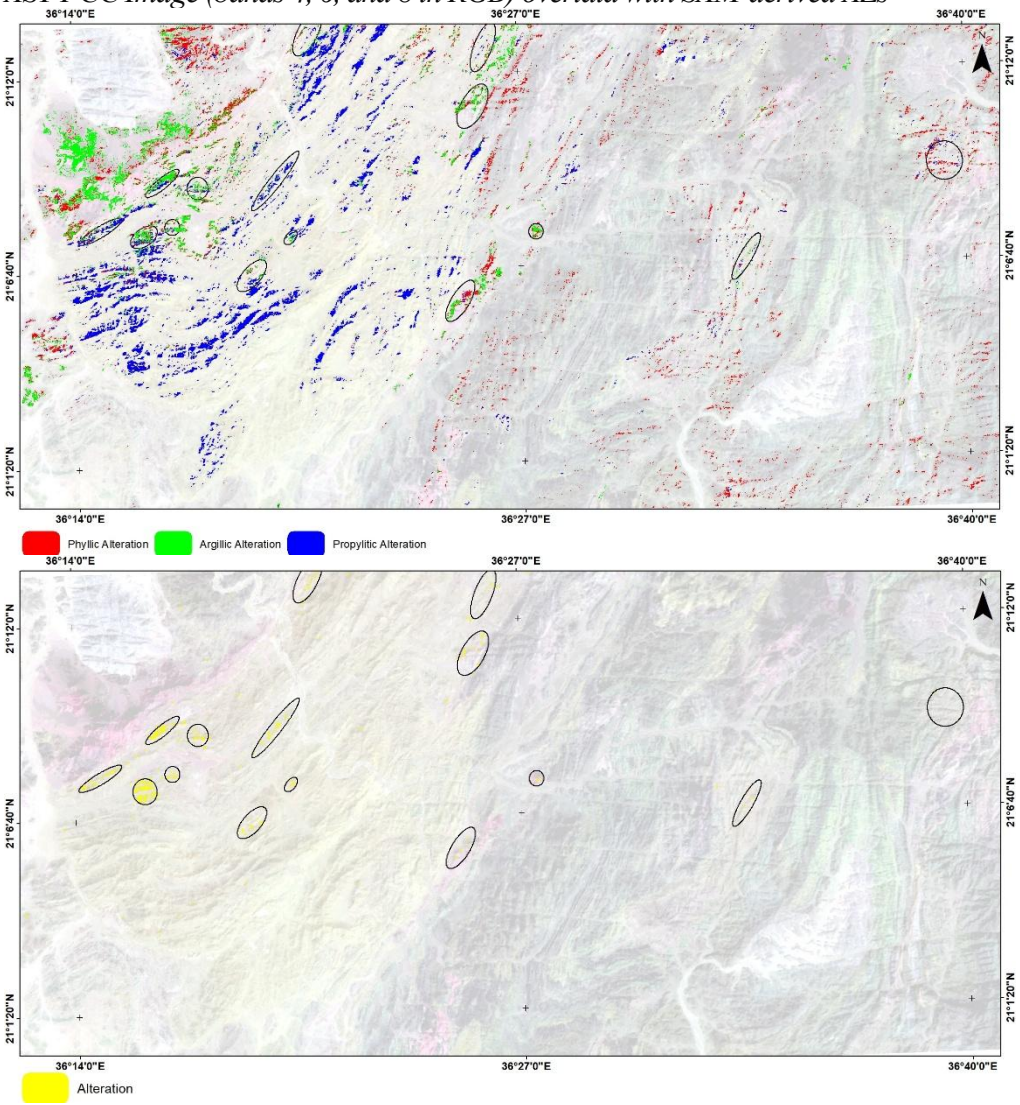

Source: Authors own elaboration

Integration of Landsat 8 and ASTER Mapping Results

LC8 includes two broad SWIR bands (band 6 and band 7) with approximate bandwidths of 0.08 µm and 0.18µm, respectively (Table 4), which limits detailed mineral discrimination. In contrast, AST acquires data in six narrower SWIR bands (bands 4 to band 9) spanning approximately 1.60 - 2.43µm, with individual bandwidths of about 0.04 - 0.10µm (Table 4), therefore, the results demonstrate that AST data provide superior capabilities for hydrothermal mineral prospecting compared to LC8 data (Figure 20).

Table 4. *Quantitative Comparative between LC8 and AST for HA Mapping Results*

Parameter	Landsat 8	ASTER	Overlap
Number of alteration zones	23	15	11
Total alteration area (km²)	53.22	20.78	
Overlap area (km²)			9.25
Percentage of combined area (%)	17.4	44.5	
Mapping scale suitability	Regional mapping	Detailed targeting	High- probable zones
Data availability	Free, frequent	Limited	
SWIR bands	2 bands	6 bands	
SWIR bandwidths	0.08 µm and 0.18µm	From 0.04 to 0.10µm	

Source: Authors own elaboration, bands specifications from USGS and NASA documentation

Quantitative comparison indicates that LC8 delineated 23 AZs covering approximately 53.22 km², whereas AST identified 15 more spatially restricted zones covering about 20.78 km². Spatial intersection analysis reveals 11 overlapping zones with a total area of 9.25 km², corresponding to approximately 44.5 % of the AST-derived alteration area and 17.4 % of the LC8-derived area. These intersected zones served as the most prospective areas (Figure 20b).

Figure 20. *AZs Maps (a) probable AZs related to Mineralization delineated from LC8 and AST Data; (b) The AZs related to Mineralization delineated from the Spatial Intersection*

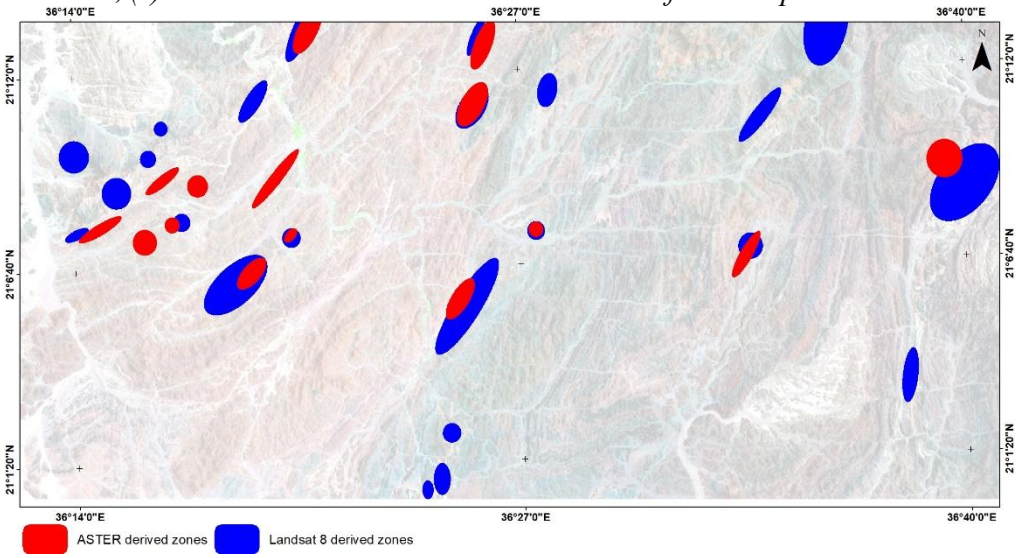

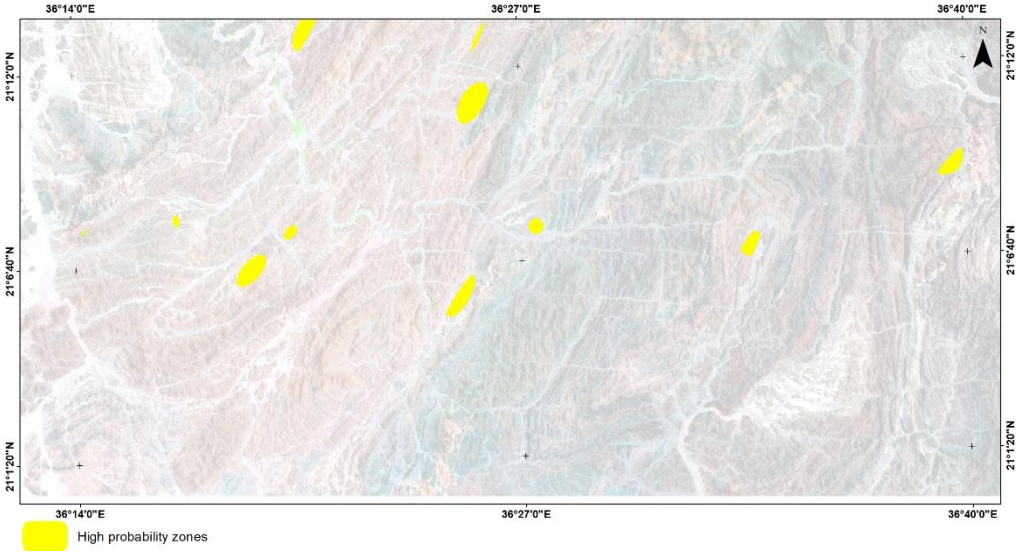

Source: Authors own elaboration

Discussion

The spectral characteristics of HA zones were investigated using integrated LC8 OLI and AST datasets, applying BR analysis, the Crosta technique, supervised classification, mineral indices, and the SAM (SAM) classifier. The integration of these complementary approaches within a GIS framework enabled robust delineation of the most prospective HA zones across the study area.

Overall, the results a quantitative comparison between LC8 and AST datasets (Table 4) indicates that AST-derived AZs overlap approximately 44.5 % of the AST area and 17.4 % of the Landsat area, highlighting the broader reconnaissance capability of Landsat and the more selective mineral discrimination achieved using AST enables the separation of diagnostic absorption minerals such as muscovite, kaolinite, alunite, chlorite, and epidote, resulting in more precise mapping of phyllic, argillic, and propylitic AZs (Figure 19). Accordingly, AST represents a valuable tool for the early stages of mineral exploration, offering a rapid, cost-effective, and reliable approach for identifying prospective zones associated with HA minerals.

Structurally, the mapped AZs which associated with dominant NNE-trending lineaments, fault systems, and shear zones that correspond with regional structural of the ANS. These structures, formed during late Neoproterozoic tectonic events, and recognized for their role in controlling hydrothermal fluid flow. Therefore, AZs that follow these NNE-trending structural were regarded as most probable zones.

Given logistical constraints, limited accessibility in the rugged terrain of the RSHs and the lack of available published geological data in the study area, the interpretation and accuracy assessment of this study relies on the spectral characteristics of satellite imagery, in the absence of field-based validation. Although Landsat-8 and AST data are widely recognized and well documented for HA mapping, future ground verification would substantially improve the reliability of the results. Integrating remote sensing outputs with geophysical data like (magnetic and

radiometric surveys) together with structure and geochemical analyses, would enhance confidence in delineating HA zones and assessing mineralization potential in the study area.

Finally, the differences observed among the applied image processing techniques underscore the importance of using complementary approaches. BR methods emphasize specific spectral contrasts like ferrous oxide, ferric oxide and clay/hydroxyl-bearing (Figure 6a), mineral indices target diagnostic absorption features for muscovite, alunite and kaolinite indices for mapping the altered zones (Figure 14), and SAM classification relies on spectral similarity to reference libraries (Figure 15), to delineating phyllic, argillic, and propylitic zones (Figure 14). Consequently, each method highlights different aspects of HA, and discrepancies among results are expected. However, their integration within a GIS framework provides a more probable and reliable interpretation than dependence on single technique.

Conclusions

This study reveals the effective of the integrated LC8 and AST data for HA mapping around in the RSHs, NE Sudan.

Exploration targets were classified based on the correspond closely with regional structural controls on mineralization within the study area, Gebeit Terrane within the ANS. The results highlight NNE-trending structures as high-priority exploration targets (Figure 19), representing the most prospective zones, whereas the remaining anomalies are considered secondary targets suitable for regional-scale reconnaissance.

Quantitative analysis shows that AST derived AZs overlap approximately 44.5% of the AST area and 17.4 % of the LC8 area, defining high-confidence targets where both sensors agree (Figure 20). These intersected zones represent the most prospective areas for pre-filed exploration stage, confirming that combined use of LC8 and AST offers a robust, cost-effective workflow for mineral exploration in arid and inaccessible.

Future research should focus on integrating alteration mapping with hyperspectral satellite data which offers spectrally narrower bands and very high spatial resolution, together with high-resolution structural data to enable detailed analysis of structure-controlled mineralization. Expanding this methodology through field sampling, and integration with geophysical datasets, including spectroradiometer measurements and magnetic, to enhance resulting accuracy.

References

Abdelsalam MG, Robinson C, El-Baz F, Stern RJ (2000) Applications of orbital imaging radar for geologic studies in arid regions: The Saharan testimony. *Photogrammetric Engineering & Remote Sensing* 66(6): 717–726.

Abdelsalam MG (2010) Quantifying 3D post-accretionary tectonic strain in the Arabian–Nubian Shield: Superimposition of the Oko shear zone on the Nakasib suture, Red Sea Hills, Sudan. *Journal of African Earth Sciences* 56(4–5): 167–178.

Abrams M, Hook S, Ramachandran B (2002) *ASTER user handbook*, version 2. Jet Propulsion Laboratory, Pasadena, CA.

Abrams M (2000) The Advanced Spaceborne Thermal Emission and Reflection Radiometer (ASTER): Data products for the high spatial resolution imager on NASA's Terra platform. *International Journal of Remote Sensing* 21(5): 847–859.

Alimohammadi M, Alirezaei S, Kontak DJ (2015) Application of ASTER data for exploration of porphyry copper deposits: A case study of the Daraloo–Sarmeshk area, southern Kerman copper belt, Iran. *Ore Geology Reviews* 70: 290–304.

Almond DC, Ahmed F (1987) Ductile shear zones in the northern Red Sea Hills, Sudan, and their implication for crustal collision. *Geological Journal* 22(S2): 175–184.

Amer R, El Mezayen A, Hasanein M (2016) ASTER spectral analysis for alteration minerals associated with gold mineralization. *Ore Geology Reviews* 75: 239–251.

Berger BR, Mars JL, Denning P, Phillips JD, Hammarstrom JM, Zientek ML, Dicken CL, Drew LJ, Seltmann R, Herrington RJ (2014) *Porphyry copper assessment of western Central Asia*. U.S. Geological Survey, Reston, VA.

Blondes MS, Gans KD, Thordsen JJ, Reidy ME, Thomas B, Engle MA, Kharaka YK, Rowan EL (2016) *US Geological Survey National Produced Waters Geochemical Database v2.3 (provisional)*. U.S. Geological Survey.

Carrino TA, Crósta AP, Toledo CL, Silva AM, Silva JL (2015) Geology and hydrothermal alteration of the Chapi Chiara prospect and nearby targets, southern Peru, using ASTER data and reflectance spectroscopy. *Economic Geology* 110(1): 73–90.

Cooley T, Anderson GP, Felde GW, Hoke ML, Ratkowski AJ, Chetwynd JH, Gardner JA, Adler-Golden SM, Matthew MW, Berk A, Bernstein LS (2002) FLAASH, a MODTRAN4-based atmospheric correction algorithm: Application and validation. In: *Proceedings of the IEEE International Geoscience and Remote Sensing Symposium*, vol. 3, pp. 1414–1418.

Crósta AP, De Souza Filho CR, Azevedo F, Brodie C (2003) Targeting key alteration minerals in epithermal deposits in Patagonia, Argentina, using ASTER imagery and principal component analysis. *International Journal of Remote Sensing* 24(21): 4233–4240.

Crósta AP, Moore J (1989) *Enhancement of Landsat Thematic Mapper imagery for residual soil mapping in SW Minas Gerais State, Brazil: A prospecting case history in greenstone belt terrain.* In: Proceedings of the Seventh Thematic Conference on Remote Sensing for Exploration Geology, Calgary, Canada, pp. 1173–1187.

Debba P, Van Ruitenbeek FJ, Van der Meer FD, Carranza EJ, Stein A (2005) Optimal field sampling for targeting minerals using hyperspectral data. *Remote Sensing of Environment* 99(4): 373–386.

El Khidir SO, Babikir IA (2013) Digital image processing and geospatial analysis of Landsat 7 ETM+ for mineral exploration, Abidiya area, North Sudan. *International Journal of Geomatics and Geosciences* 3(3): 645–658.

El Khidir SOH (2006) *Remote sensing and GIS applications in geological mapping, prospecting for mineral deposits and groundwater: Berber sheet area, northern Sudan*. PhD dissertation, Al Neelain University.

Fitches WR, Graham RH, Hussein IM, Ries AC, Shackleton RM, Price RC (1983) The late Proterozoic ophiolite of Sol Hamed, NE Sudan. *Precambrian Research* 19(4): 385–411.

Fraser SJ, Green AA (1987) A software defoliant for geological analysis of band ratios. *International Journal of Remote Sensing* 8(3): 525–532.

Gupta RP (2017) *Remote sensing geology*. Springer, Berlin.

Hunt GR, Ashley RP (1979) Spectra of altered rocks in the visible and near infrared. *Economic Geology* 74(7): 1613–1629.

Hunt GR (1979) Near-infrared (1.3–2.4 μm) spectra of alteration minerals: Potential for use in remote sensing. *Geophysics* 44(12): 1974–1986.

Johnson PR, Andresen A, Collins AS, Fowler AR, Fritz H, Ghebreab W, Kusky T, Stern RJ (2011) Late Cryogenian–Ediacaran history of the Arabian–Nubian Shield. *Journal of African Earth Sciences* 61(3): 167–232.

Johnson PR, Kattan FH, Al-Saleh AM (2004) Neoproterozoic ophiolites in the Arabian Shield: Field relations and structure. *Developments in Precambrian Geology* 13: 129–162.

Klemenic PM, Poole S (1988) The geology and geochemistry of Upper Proterozoic granitoids from the Red Sea Hills, Sudan. *Journal of the Geological Society* 145(4): 635–643.

Kröner A, Greiling R, Reischmann T, Hussein IM, Stern RJ, Dürr S, Krüger J, Zimmer M (1987) Pan-African crustal evolution in the Nubian segment of northeast Africa. In: *Proterozoic Lithospheric Evolution*, vol. 17, pp. 235–257.

Kruse FA, Lefkoff AB, Boardman JW, Heidebrecht KB, Shapiro AT, Barloon PJ, Goetz AF (1993) The spectral image processing system (SIPS). *Remote Sensing of Environment* 44(2–3): 145–163.

Lillesand T, Kiefer RW, Chipman J (2015) *Remote sensing and image interpretation*. Wiley, New York.

Loughlin WP (1991) Principal component analysis for alteration mapping. *Photogrammetric Engineering & Remote Sensing* 57(9): 1163–1169.

Mars JC, Rowan LC (2006) Regional mapping of phyllic- and argillic-altered rocks using ASTER data. *Geosphere* 2(3): 161–186.

Mwaniki MW, Möller MS, Schellmann G (2015) A comparison of Landsat 8 and Landsat 7 in mapping geology and visualising lineaments. *ISPRS Archives* 40: 897–903.

Ninomiya Y (2003) A stabilized vegetation index and mineralogic indices for ASTER data. In: *IGARSS 2003 Proceedings*, vol. 3, pp. 1552–1554.

Pour AB, Hashim M (2012) Identifying areas of high economic-potential copper mineralization using ASTER data. *Advances in Space Research* 49(4): 753–769.

Pour AB, Hashim M (2012) The application of ASTER data to porphyry copper and epithermal gold deposits. *Ore Geology Reviews* 44: 1–9.

Pour AB, Hashim M, Park Y, Hong JK (2018) Mapping alteration mineral zones using ASTER data. *Geocarto International* 33(12): 1281–1306.

Pour AB, Hashim M, Hong JK, Park Y (2019) Lithological and alteration mineral mapping using Landsat-8 and ASTER data. *Ore Geology Reviews* 108: 112–133.

Rajendran S, Nasir S, Kusky TM, Ghulam A, Gabr S, El-Ghali MA (2013) Detection of hydrothermal mineralized zones using ASTER data. *Ore Geology Reviews* 53: 470–488.

Richards JA (2022) *Remote sensing digital image analysis*. Springer, Berlin.

Rowan LC, Hook SJ, Abrams MJ, Mars JC (2003) Mapping hydrothermally altered rocks using ASTER. *Economic Geology* 98(5): 1019–1027.

Rowan LC, Mars JC (2003) Lithologic mapping using ASTER data. *Remote Sensing of Environment* 84(3): 350–366.

Roy DP, Wulder MA, Loveland TR et al. (2014) Landsat-8: Science and product vision. *Remote Sensing of Environment* 145: 154–172.

Sabins FF (1999) Remote sensing for mineral exploration. *Ore Geology Reviews* 14(3–4): 157–183.

Sabins FF Jr, Lulla K (1987) *Remote sensing: Principles and interpretation*. W.H. Freeman, New York.

Safari M, Maghsoudi A, Pour AB (2018) Application of Landsat-8 and ASTER data for porphyry copper exploration. *Geocarto International* 33(11): 1186–1201.

Seedorff E, Dilles JH, Proffett JM, Einaudi MT, Zurcher L, Stavast WJ, Johnson DA, Barton MD (2005) *Porphyry deposits: Characteristics and origin of hypogene features.* Economic Geology 100th Anniversary Volume: 251–298.

Shnain SK, Najm MN, Taher NA, Abdalrazzaq AS, Rashit B, Lishchyna V (2024) *Classification of Landsat 8 images using CNN based on MNF transform.* In: Proceedings of the 35th FRUCT Conference, pp. 692–698.

Spatz DM, Wilson RT, Pierce FW, Bolm JG (1995) Remote sensing characteristics of porphyry copper systems. *Arizona Geological Society Digest* 20: 94–108.

Stern RJ (1994) Arc assembly and continental collision in the Neoproterozoic African Orogen. *Annual Review of Earth and Planetary Sciences* 22: 319–351.

Stern RJ (2002) Crustal evolution in the East African Orogen. *Journal of African Earth Sciences* 34(3–4): 109–117.

Testa FJ, Villanueva C, Cooke DR, Zhang L (2018) Lithological and hydrothermal alteration mapping using ASTER imagery. *Remote Sensing* 10(2): 203.

Vail JR (1985) Alkaline ring complexes in Sudan. *Journal of African Earth Sciences* 3(1–2): 51–59.

Van der Meer FD, Van der Werff HM, Van Ruitenbeek FJ et al. (2012) Multi-and hyperspectral geologic remote sensing: A review. *International Journal of Applied Earth Observation and Geoinformation* 14(1): 112–128.

Wulder MA, White JC, Goward SN et al. (2008) Landsat continuity: Issues and opportunities. *Remote Sensing of Environment* 112(3): 955–969.

Yamaguchi Y, Fujisada H, Kahle AB et al. (2001) ASTER instrument performance and applications. In: *IGARSS 2001 Proceedings*, vol. 3, pp. 1215–1216.

Yamaguchi Y, Fujisada H, Kudoh M et al. (1999) ASTER instrument characterization. *Advances in Space Research* 23(8): 1415–1425.

Zeinelabdein KE, Albiely A (2008) Ratio image processing techniques for mineral prospecting. *ISPRS Archives* 37: 1295–1298.

Zhang X, Pazner M, Duke N (2007) Lithologic and mineral information extraction using ASTER data. *ISPRS Journal of Photogrammetry and Remote Sensing* 62(4): 271–282.

Abbreviations

Abbreviations used in this paper include:

OLI	Operational Land Imager
Landsat 8	LC8
ASTER	AST
Red Sea Hills	RSHs
ANS	Arabian Nubian Shield
VNIR	Visible / Near Infrared
SWIR	Shortwave Infrared
TIR	Thermal Infrared
TIRS	Thermal Infrared Sensor
USGS	United State Geological Survey
UTM	Universal Transverse Mercator
Band Ratio	BR
Hydrothermal Alteration	HA
Alteration Zones	AZs
WGS	World Geodetic System
ENVI	Environment for Visualizing Images
FLAASH	Fast Line of sight Atmospheric Analysis of Spectral Hypercube
MNF	Minimum Noise Fraction
FOPCS	Feature Oriented Principal Component Selection
PCA	Principal Component Analysis
DN	Digital Number
ROI	Regions Of Interest
FCC	False Color Composite
NNE	North Northeast
SSW	South Southwest
SAM	Spectral Angle Mapper